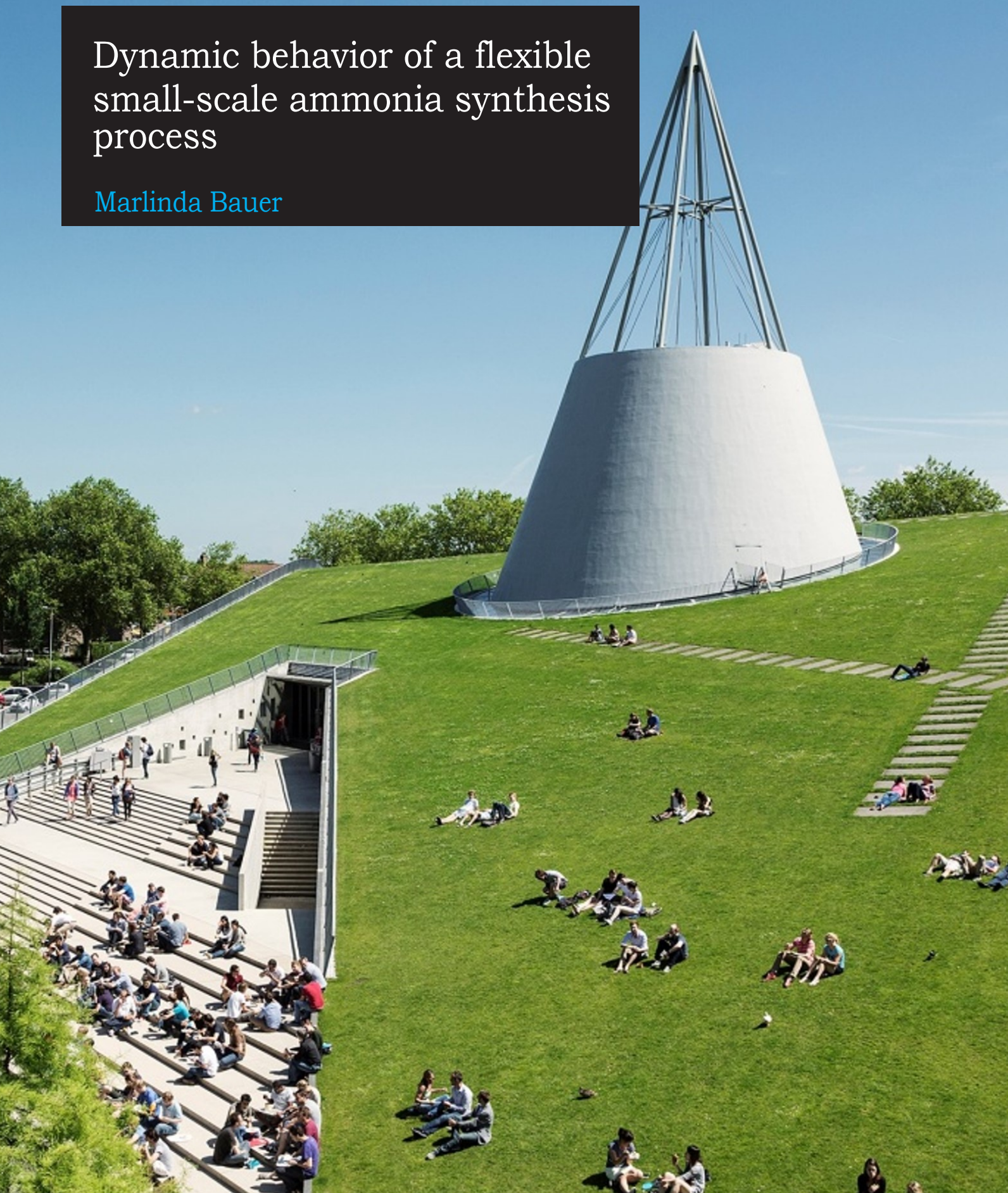


Dynamic behavior of a flexible small-scale ammonia synthesis process

Marlinda Bauer



Dynamic behavior of a flexible small-scale ammonia synthesis process

by

Marlinda Bauer

in partial fulfillment of the requirements for the degree of

Master of Science
in Mechanical Engineering

at the Delft University of Technology,
to be defended publicly on Monday, 7th November, 2022 at 9:00 PM.

Thesis committee:	Prof. dr. ir. E.L.V. Goetheer,	TU Delft
	Prof. dr. ir. W. de Jong,	TU Delft
	Dr. ir. M. Ramdin,	TU Delft
	Dr. ir. G. van Zee,	Proton Ventures

An electronic version of this thesis is available at <http://repository.tudelft.nl/>.

Preface

This master thesis, as it lies before you, marks the end of my time as a student at Delft University of Technology. This fulfills the final requirement in order to receive my Master of Science degree in Mechanical Engineering, with a specialization in Energy, Flow and Process Technology.

I would like to thank Proton Ventures B.V. for giving me the opportunity to collaborate with them on this graduation project. It was a joy to meet everyone and to experience such a close-knit and welcoming company. My expressions of gratitude to Dr. ir. Gerard van Zee for guiding me through the project. Thank you for your help, feedback and expertise during this research.

I want to thank my supervisor Prof. dr. ir. Earl Goetheer for his insightful feedback and advice throughout the thesis project. Furthermore, I'd like to thank Prof. dr. ir. Wiebren de Jong and Dr. ir. Mahinder Ramdin for being part of my graduation committee.

Finally, I would like to express my gratitude to family and friends for their support. And last, but definitely not least, thank you Siddharth for providing me with help and feedback on my report, and keeping me motivated throughout the whole project.

*Marlinda Bauer
Schiedam, October 2022*

Abstract

Due to climate change, the growth in renewable energy is still accelerating and reaching new records each year. Not everything can be electrified, hence, the production of green hydrogen as an energy vector is gaining momentum. However, lowest cost hydrogen will not always be produced at the demand centres, necessitating transport of hydrogen which is nascent. In this, it has been realised that due to its easy liquefaction, proven transport at scales and matured production process, ammonia can be an excellent energy carrier. Currently, ammonia production accounts for more emissions than any other chemical and to achieve net-zero targets these emissions must be reduced ~ 25 -fold. Therefore, ammonia synthesis with renewable energy will be imperative. Operating with variable hydrogen feed rates will be part of the challenge.

In this work, the dynamics of a small-scale ammonia synthesis plant with a capacity of 60 *tons/day* was studied. The application of chemisorption as replacement for the traditional condensation step for ammonia recovery was adopted in the study. In the system, the hydrogen feed was sourced from an electrolyser powered by renewable energy. Hence, it was imperative to study the sensitivity and the response of the synthesis loop to the fluctuations in hydrogen feed. For the dynamics model, different scenarios of ramp-up and ramp-down were tested for two control structures to evaluate the response of various system parameters to these deviations. Therefore, the feasibility of these control structures was assessed and some of their potential limitations were identified.

The objective of this work was achieved with three simulation models. A steady-state model was employed to study the equilibrium conditions of the ammonia synthesis loop. A second more extensive model included reaction kinetics, heat integration and a chemisorption operation. The widely applied Temkin-Pyzhev rate equation was modified into LHHW form to fit this application. With the selected ZA-5 iron-based catalyst the operating pressure was established at 130 *bar* to avoid overheating the catalyst. The simulation resulted in the reactor dimensions to attain the maximum possible conversion of 22.1% under these conditions. For the third model, the inputs from the two models were translated into the a dynamic model. The latter was used to study the behavior of the system parameters when subjected to fluctuations in the hydrogen feed flow.

Three scenarios were tested with respect to the hydrogen variations: a (step and linear) reduction in the hydrogen feed of 10%, 25% and 50% of the initial value. With the default control system, the pressure varied by 16 *bar* with only a 10% step reduction of the hydrogen feed. This necessitated the development of control strategies to control the pressure deviations in order to eliminate metal fatigue in the equipment. The first control structure compensated the lack of hydrogen by adding more nitrogen into the system. The second control structure reduced the recycle flow rate to decrease the ammonia production rate in the reactor.

Both control philosophies were successfully applied to control the system pressure for the 10% and 25% H_2 ramp-down/up scenarios. The greatest pressure range measured during transient state in a linear 25% H_2 reduction scenario for *control philosophy 1* and 2 were 3.8% and 4.5%, respectively. The effects of the variations and the control strategies have also been studied. In this research the nitrogen supply was assumed to be infinite, therefore a nitrogen buffer must be present. In addition, the use of a hydrogen buffer is required for a gradual decrease and dampens rapid changes in the hydrogen supply in order to minimize pressure variations.

Contents

Acknowledgements	i
Abstract	iii
List of Figures	vii
List of Tables	ix
Nomenclature	xi
1 Introduction	1
1.1 Ammonia as an energy carrier	1
1.2 Flexible small-scale ammonia production	1
1.3 Research questions	3
1.4 Thesis outline	4
2 Literature study	5
2.1 Ammonia.	5
2.1.1 Equilibrium	5
2.2 The Haber-Bosch process	6
2.3 Industrial State-of-the-art	7
2.4 Catalyst	8
2.4.1 Principles	9
2.4.2 Catalysts for Ammonia Synthesis	10
2.4.3 Developments in Ammonia Synthesis Catalysts.	11
2.5 Reaction Kinetics	14
2.6 Absorption for Ammonia Recovery.	16
2.6.1 Strontium Chloride.	16
2.6.2 Determining the absorption temperature.	16
2.7 Control theory.	18
3 Scope & approach	21
3.1 Objective	21
3.2 Scope	21
3.3 Approach	22
3.3.1 Assumptions	23
3.3.2 Scenarios	23
3.3.3 Thermodynamic Equation of State	24
4 Simple Steady state simulation (MODEL 1)	25
4.1 System components	25
4.2 Exploring the Dependency of Conversion on Pressure and Temperature	26
4.3 Model validation	27
4.4 Key takeaways	28
5 Detailed Steady state simulation (MODEL 2)	29
5.1 Reactor kinetics.	29
5.1.1 Selection of rate equation	29
5.1.2 Modified Temkin LHHW equation	31
5.2 Reactor configuration	36
5.2.1 Isothermal vs. Adiabatic Reactor Behaviour	36
5.2.2 Reactor inlet temperature (Adiabatic reactor)	38
5.2.3 Reactor Dimensions	39
5.3 Absorption.	40
5.3.1 Modelling of absorption	40
5.3.2 Absorber Design	41

5.4	Pressure drops	41
5.5	Reactor heat exchanger	42
5.6	Results	43
5.6.1	Reactor hierarchy	44
5.6.2	Absorber hierarchy	45
5.7	Model validation	46
5.8	Heat integration	47
6	Dynamic Simulation (MODEL 3)	49
6.1	Scenario & assumptions	49
6.2	Prepare the Dynamic Simulation	49
6.2.1	Additional steps for pressure-driven simulations	50
6.3	Specification of Dynamic data	50
6.4	Run the Simulation	52
6.5	Add a Control strategy	52
6.5.1	Base control structure	53
6.5.2	Additional information	54
6.5.3	Control Philosophy 1	54
6.5.4	Control Philosophy 2	55
7	Results & discussion of dynamic simulation	57
7.1	Abrupt change in hydrogen feed	57
7.2	Gradual change in hydrogen feed (with H ₂ buffer)	60
7.2.1	Control Philosophy 1	61
7.2.2	Control Philosophy 2	67
7.2.3	Summary & comparison	72
8	Conclusions & recommendations	75
8.1	Summary of Steady-state simulations	75
8.1.1	Kinetics	75
8.1.2	Simulation results	75
8.2	Conclusions of Dynamic simulations	76
8.3	Recommendations	78
A	Reaction kinetics	79
A.1	Validation LHHW rate equation	79
A.2	Experimental Data Fit to Haber & Le Rossignol Correlation	80
A.3	Haber & Le Rossignol vs. Gillespie & Beattie equilibrium correlations	80
A.4	Derivation of simplified equilibrium correlation from Haber & Le Rossignol	81
A.5	MATLAB® codes	82
A.5.1	Comparison of kinetic rate equations	82
A.5.2	Validation of Modified LHHW	84
B	Model 2: Input specifications & additional results	87
B.1	Summary table input specifications	87
B.2	Flow sheet and stream tables	88
C	Model 3: Simulation information & input specifications	91
C.1	Pressure-driven simulation additional information	91
C.2	Control parameter recommendations from Aspen	92
C.3	Summary table input specifications	93
D	Model 3: Problem solving Control Structure 1	95
E	Model 3: Additional results ramp-down 25% scenario	99
E.1	Control Structure 1	99
E.1.1	System pressures & temperatures	99
E.1.2	Reactor loop heat duties	101
E.1.3	Heat-exchanger (HEX-01) specifics	102
E.2	Control Structure 2	103
E.2.1	System pressures & temperatures	103
F	Model 3: Additional results	105
F.1	Control Philosophy 1 - Gradual reduction in hydrogen feed flow	105
F.2	Control Philosophy 2 - Gradual reduction in hydrogen feed flow	108
	Bibliography	115

List of Figures

1.1	Current technology readiness level (TRL) of green ammonia synthesis process	2
1.2	Schematic diagram of conventional methane fed vs. electrically driven Haber Bosch process	3
1.3	Value chain of ammonia production from renewables	4
1.4	Thesis outline	4
2.1	Mole fraction of ammonia at equilibrium as a function of temperature and pressure (initial mixture of 1:3 N ₂ / H ₂ gas)	6
2.2	Traditional Haber-Bosch Process	7
2.3	Linde vs. Conventional Ammonia Plant	8
2.4	Potential Energy Diagram for Ammonia Synthesis	9
2.5	Reduction of nitrogen in the Haber-Bosch reaction through a dissociative mechanism .	10
2.6	Turnover frequencies for ammonia synthesis as a function of the adsorption energy of nitrogen	10
2.7	Saturation Vapor Pressure of NH ₃ above liquid NH ₃ & above Absorbent	17
2.8	Varying the control parameters of a PID controller	18
2.9	Difference between the control types (P, PI, PID) (source: Getting Started with Aspen Dynamics)	19
3.1	Flow Sheet of the Proposed Small-scale Ammonia Plant	22
3.2	Workflow Models Ammonia Synthesis Loop	23
4.1	<i>MODEL 1</i> : Simple Steady-state simulation	25
4.2	<i>MODEL 1</i> : Dependency of conversion on pressure and reactor temperature for an isothermal GIBBS reactor	26
4.3	<i>MODEL 1</i> : Dependency of conversion on pressure and feed temperature for an adiabatic GIBBS Reactor	27
4.4	Validation <i>MODEL 1</i> (Literature data from Max Appl)	27
5.1	Reaction rate of ammonia synthesis plotted versus conversion for various equations . .	30
5.2	Reaction rate of ammonia synthesis plotted versus conversion for various equations at 200 bar	31
5.3	Reaction Rate (p,T) vs. Conversion at 400 °C & 200 bar	32
5.4	Reaction Rate (p,T) vs. Conversion at 400 °C & 200 bar	34
5.5	Validation Modified LHHW at 50 bar	35
5.6	Validation Modified LHHW at 200 bar	35
5.7	Activity vs. Space Velocity of ZA-5, A301, ICI74-I and A110-2 Catalyst (P = 150 bar, T = 425 °C)	36
5.8	Space Velocity of 25,000 hr ⁻¹	37
5.9	Space Velocity of 50,000 hr ⁻¹	37
5.10	Influence of Reactor Inlet Temperature on the Conversion, p = 200 bar	38
5.11	Adiabatic reactor profiles at inlet temperature of 250 °C vs. 500 °C	38
5.12	Steady-state simulation of Absorber section (Absorber Hierarchy)	40
5.13	Steady State Simulation of Reactor Section (Reactor Hierarchy)	42
5.14	<i>MODEL 2</i> : Detailed Steady State Simulation	43
5.15	Hierarchies <i>MODEL 2</i>	44
5.16	The adiabatic plug flow reactor profile in model 2	45
5.17	Decomposed Absorption Reaction and Cooling with Heat Exchanger in Absorption Hierarchy	46
6.1	Step approach to a Dynamic simulation	49
6.2	FLASH2 Vessel Dimensions (Absorber)	51
6.3	<i>MODEL 3</i> : Dynamic simulation	52
6.4	Dynamic model with a base control structure	53
6.5	System response to a 10% ramp-down in hydrogen feed with base control structure . .	54
6.6	Concept Visualization of Control Philosophy 1	55
6.7	Concept Visualization of Control Philosophy 2	56

7.1	10 % Step-down scenario Control Philosophy 1	58
7.2	10 % Step-down scenario Control Philosophy 2	59
7.3	Aspen Dynamics flowsheet with Control Philosophy 1	61
7.4	Time series for 25% Ramp-down/up scenario - <i>Control Structure 1</i>	62
7.5	Time series for 25% Ramp-down/up scenario - <i>Control Structure 1</i>	63
7.6	Time series for 25% Ramp-down/up scenario - <i>Control Structure 1</i>	64
7.7	Compressor map of a typical centrifugal compressor (source: Turbomachinery International)	66
7.8	Dynamic Model with Control Philosophy 2	67
7.9	Time series for 25% Ramp-down/up scenario - <i>Control Structure 2</i>	68
7.10	Residence time vs. inlet flow rate reactor (25% Ramp-down/up scenario - <i>Control Structure 2</i>)	69
7.11	Time series for 25% Ramp-down/up scenario - <i>Control Structure 2</i>	70
7.12	Time series for 25% Ramp-down/up scenario - <i>Control Structure 2</i>	71
7.13	Heat duties and temperature differences in the reactor loop	73
A.1	Conversion vs. Pressure ($T_{feed} = 600 K$) Adiabatic Plug Flow Reactor with LHHW Temkin Kinetics	79
A.2	Conversion vs. Feed Temperature ($p = 200 bar$) Adiabatic Plug Flow Reactor with LHHW Temkin Kinetics	79
A.3	Experimental Data Points According to Haber Compared to the Haber & Le Rossignol Equilibrium Correlation	80
A.4	Haber & Le Rossignol vs. Gillespie & Beattie equilibrium correlation at 50 bar	80
A.5	Haber & Le Rossignol vs. Gillespie & Beattie equilibrium correlation at 200 bar	81
B.1	<i>MODEL 2</i>	88
B.2	<i>MODEL 2</i> : Absorber Hierarchy	89
B.3	<i>MODEL 2</i> : Reactor Hierarchy	90
C.1	Additional Information for Pressure Driven Simulations (source: Getting Started with Aspen Dynamics)	92
C.2	Recommendations for PID controller stability (source: Getting Started with Aspen Dynamics)	92
C.3	Recommendations for Controller Tuning (source: Getting Started with Aspen Dynamics)	93
D.1	Result of a 90% drop of the N_2 feed flow	95
D.2	Isolation of the compressor	96
D.3	Removal of the heat-exchanger from the simulation	96
D.4	Isolation of the reactor	97
D.5	Isolation of the reactor & absorber	97
D.6	Reduction of the absorber volume	98
E.1	Control Structure 1 - initial state	99
E.2	Control Structure 1 - steady state after 25% H_2 ramp-down	100
E.3	Reactor loop heat duties (<i>Control structure 1</i>)	101
E.4	Specific heat capacity of the in-going hot and cold streams	102
E.5	temperatures around the heat-exchanger (HEX-01) - 25% ramp-down/up scenario	102
E.6	Control Structure 2 - initial state	103
E.7	Control Structure 2 - steady state after 25% H_2 ramp-down	103
E.8	Reactor loop heat duties (<i>Control structure 2</i>)	104
F.1	Time series for 10% Ramp-down/up scenario - <i>Control Structure 1</i>	105
F.2	Time series for 10% Ramp-down/up scenario - <i>Control Structure 1</i>	106
F.3	Time series for 10% Ramp-down/up scenario - <i>Control Structure 1</i>	107
F.4	Time series for 10% Ramp-down/up scenario - <i>Control Structure 2</i>	108
F.5	Residence time vs. inlet flow rate reactor (10% Ramp-down/up scenario - <i>Control Structure 2</i>)	109
F.6	Time series for 10% Ramp-down/up scenario - <i>Control Structure 2</i>	109
F.7	Time series for 10% Ramp-down/up scenario - <i>Control Structure 2</i>	110
F.8	Time series for 50% Ramp-down/up scenario - <i>Control Structure 2</i>	111
F.9	Residence time vs. inlet flow rate reactor (50% Ramp-down/up scenario - <i>Control Structure 2</i>)	112
F.10	Time series for 50% Ramp-down/up scenario - <i>Control Structure 2</i>	113
F.11	Time series for 50% Ramp-down/up scenario - <i>Control Structure 2</i>	114

List of Tables

2.1	Novel Ammonia Synthesis Catalysts	12
2.2	Rate Equations for the Ammonia Synthesis Reaction	15
3.1	Decentralized Mini Ammonia Plant	21
5.1	Selected rate equations and parameters	30
5.2	Plant Data from Various Industrial Haber-Bosch Plants	36
5.3	Operating Temperatures of Various Iron Ammonia Catalysts	39
5.4	Absorber Specifications (Shell & Tube type)	41
5.5	Results Reactor Hierarchy	44
5.6	Results Absorption Hierarchy	45
5.7	Absorber HEX Simulation Details	46
6.1	Controller Parameters for Control Structure 1	55
6.2	Controller Parameters for Control Structure 2	56
7.1	Timeline simulation	60
7.2	Summary table comparing the two control philosophies	72
7.3	Range of Pressure fluctuations at the reactor outlet for each ramp-down/up scenario	72
A.1	Simulation information for LHHW validation	79
B.1	Equipment specifications for model 2	87
B.2	Summary Table for <i>MODEL 2</i>	88
B.3	Summary Table for Absorber Hierarchy	89
B.4	Summary Table for reactor hierarchy	90
C.1	Pressure-driven vs. flow-driven simulations	91
C.2	Equipment specifications for <i>MODEL 3</i>	93

Nomenclature

Abbreviations

DV	Disturbance Variable
EOS	Equation of State
LCOH	Levelised Cost of Hydrogen
LHHW	Langmuir-Hinselwood-Hougen-Watson
Mtpa	million tonnes per annum
MV	Manipulated Variable
PI	Proportional Integral
PID	Proportional-Integral-Derivative
PR	Peng-Robinson
PV	Process Variable
SMR	Steam Methane Reforming
SP	Setpoint
SRK	Soave-Redlich-Kwong
SV	Space Velocity
TRL	Technology Readiness Level

Symbols

R, r	Reaction rate
f	Catalyst Activity Factor
P_x	Partial Pressure of component X
k_1	Forward kinetic constant
k_2	Reverse kinetic constant
A	Arrhenius constant/ frequency factor
X	Conversion percentage
n	Number of moles
α	Transfer coefficient
AK	Specific rate constant
K_{ad}	Adsorption equilibrium constant
ρ	Density
δS	Reaction entropy
δH	Reaction enthalpy
p_0	Reference pressure
R	Gas constant
E_a	Activation Energy
h	Heat transfer coefficient
Q	Heat Duty

1

Introduction

1.1. Ammonia as an energy carrier

Driven by ambitious CO₂ reduction goals (Paris agreement) to combat climate change, there is a rapid uptake of renewable power generation sources, such as solar and wind [1]. As per IEA, achieving net zero would require that 90% of the total electricity generation comes from renewables and 70% of this will be attributable to solar PV and wind [2]. The availability of most of these energy sources is variable by nature. Therefore, stabilizing the grid will become more and more challenging. In some economies, gas-based power plants (“peaker plants”) already play a key role in stabilizing the electricity grid [3] [4]. Consequently, the electricity system will have to improve its flexibility and thus organize adequate seasonal and short-term energy storage. Not everything can be electrified or produced on-site [5]. As a result, it can be expected that there will be a demand for energy carriers.

Hydrogen’s potential as energy vector has been discussed at least since the 1980s [6]. Green hydrogen, produced from renewable electricity by electrolysis, presents a cleaner alternative. However, not all locations are made equal in terms of economic viability for energy carrier production. Most of the times, these places are also not necessarily close to the demand centres. For example: Chile, Morocco, Colombia, Oceania are amongst the top 10 places with the lowest Levelised Cost of Hydrogen (LCOH) for green hydrogen production [7]. Further, due to its low volumetric energy density, it is essential to either liquefy or compress to high pressures for any meaningful utilization [8]. Hence, transport of large quantities of H₂ over sea-routes appears to be unlikely.

Unlike hydrogen transport which is still nascent, ammonia’s transport has been proven for decades [9] and at scales ¹. Ammonia is a widely used key industrial chemical feedstock and fertilizer. The current market for ammonia is around 180 Mtpa with seaborne trade of 20 Mtpa [10] and this is expected to reach approximately 350 Mtpa [9]. There are some key advantages [11] for ammonia as an energy carrier:

- Matured production process
- Industrial experience in safely handling of ammonia
- Smallest footprint and CAPEX (in terms of storage capacity)
- Easy liquefaction by compression or cooling

Therefore, ammonia is often positioned as a stable energy carrier to achieve Net-zero targets [12].

1.2. Flexible small-scale ammonia production

Ammonia is currently manufactured through Haber-Bosch process in a high-pressure reactor and with an iron-based catalyst. Accounting for over 1.4% of the global carbon dioxide emissions, ammonia production emits more CO₂ than production of any other chemical [13]. This is because the source of hydrogen atoms for ammonia production is SMR which uses natural gas. As per International Energy Agency’s Net zero scenario, the direct CO₂ emissions from ammonia production needs to be reduced from 450 Mtpa to 17 Mtpa [14]. This is a ~ 25-fold reduction from current emissions. Therefore, to

¹Current seaborne trade for ammonia amounts to about 20 million tonnes per annum (Mtpa) [10]

achieve this emissions reduction, running ammonia synthesis plants on renewables will be imperative.

The Haber-Bosch process favours large scale ammonia production (up to 3,300 *tonnes/day*) mainly due to the steam reforming step, and is operated under elevated temperatures (400 - 500 °C) and pressures (200 *bar*), all of which hamper flexible operations. Therefore, running an ammonia plant on renewable electricity requires a different production system than the current industrial plants.

Figure 1.1 shows the Technology Readiness Level (TRL) of some of the possible green ammonia synthesis processes. Electrochemical synthesis of ammonia is promising. However, several challenges have been identified [15] [16] and the process is far from commercialisation. Alternatively, an easier and feasible pathway would be the replacement of CO₂ intensive methane-fed process by generation of hydrogen through electrolysis using renewable electricity [17].

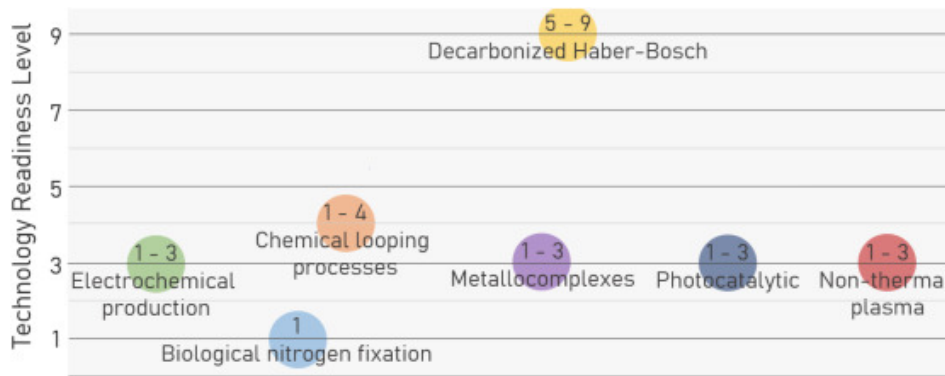


Figure 1.1: Current technology readiness level (TRL) of green ammonia synthesis process

Source: [18]

Ammonia production today is concentrated in a few countries/regions around the world². More than 120 countries don't have any ammonia production infrastructure. This is largely due to the size of the Haber-Bosch based ammonia production plants. Some of the reasons why such a huge majority of countries don't have ammonia production based on these large Haber-Bosch based plants are [19] [20]:

- Requirement of high investment sums
- Production capacity far exceeds domestic demand
- Resource requirements
 - Infrastructure for handling natural gas
 - Infrastructure for H₂ production
 - Energy for the plant

A small-scale ammonia plant can enable smaller players³ and countries and countries where production costs are lower⁴ to establish NH₃ production. This gives them more control over their supply chain (reducing lead times and costs) [21].

The feasibility of an electrically driven Haber-Bosch process lies in the development of a small-scale, decentralized and flexible process that can line up to the geographically isolated and intermittent renewable energy sources [23]. Figure 1.2 presents the schematics of the Haber-Bosch with the conventional methane-fed vs. electrically driven process.

To achieve agile operation for coping with the intermittency of renewables, a small-scale (capacity of < 100 *tons/day*) ammonia synthesis plant operating under milder conditions (< 50 *bar*) is proposed. In addition, these conditions reduce the energy requirements significantly. This demands the development of a novel catalyst that allows for these milder operating conditions.

²Top 5 producer countries are responsible for production of more than 50% of the total ammonia produced IEAsustnitr.

³Reliable and economic procurement for businesses reliant on ammonia is regarded as difficult [21].

⁴For example : Canada, Chile, Argentina or Morocco are regarded as being the places to produce low cost green ammonia for import to Europe [22].

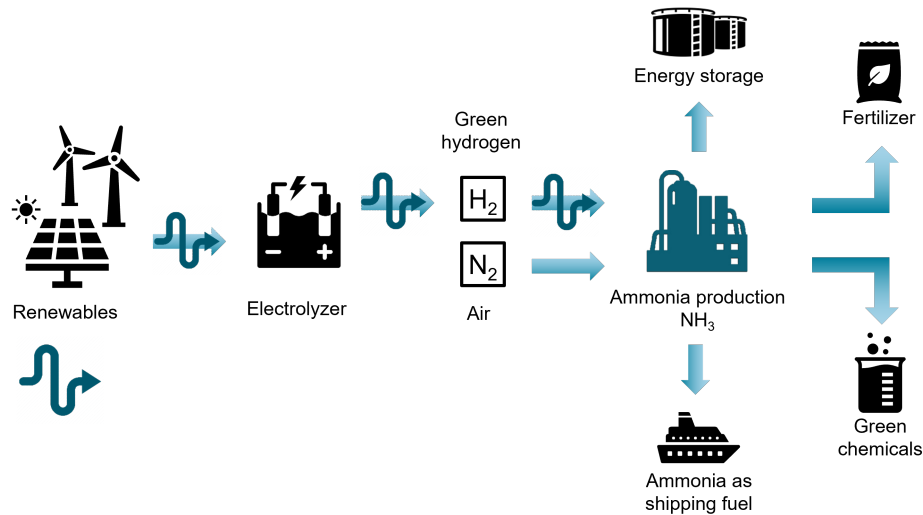


Figure 1.3: Value chain of ammonia production from renewables

1.4. Thesis outline

The following summarises the topics that are covered in each of the chapters:

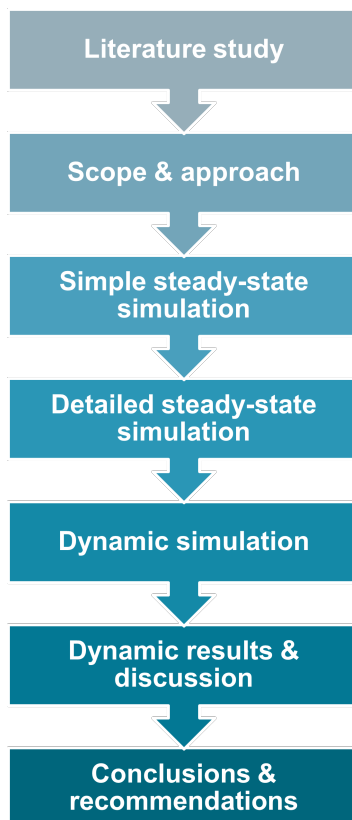


Figure 1.4: Thesis outline

Chapter 2 consists of a literature study involving catalyst, reaction kinetics, absorption for ammonia separation and control theory.

Chapter 3 discusses the most important conclusions from the literature study and details the scope and approach of the work. It features the process to be modelled and explains the need for different simulation models. Assumptions and proposed scenarios for variations in the hydrogen feed are presented.

Chapter 4 contains a steady-state simulation model to study the equilibrium of ammonia synthesis.

Chapter 5 results in a steady-state simulation model with reaction kinetics, heat integration and absorption enthalpy. The chapter discusses the selection and modification of a kinetic rate expression. This is followed by motivation for decisions on the reactor configuration and modelling of the absorption step.

Chapter 6 describes the development of the dynamic simulation model (using Aspen Plus Dynamics) from the steady-state model of Chapter 5. It also explains the development of control strategies.

Chapter 7 discusses the results of the different control structures for the dynamic simulation model when subjected to various hydrogen reduction scenarios.

Chapter 8 summarizes the conclusions of this work and provides recommendations for future research.

2

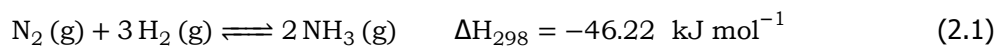
Literature study

In preparation for modelling of the ammonia synthesis loop, the Haber-Bosch process, state-of-the-art synthesis, catalysts for this application and reaction kinetics must be studied. Additionally, research was done on chemisorption for ammonia separation. Lastly, control theory for proper design of a control system is covered.

2.1. Ammonia

Ammonia is widely used in the manufacture of fertilizers and is a resource for the production for both organic and non-organic compounds [25]. Hence, the synthesis of ammonia has an important position in the economy as it is a key raw material for both agriculture and industry. Earlier, it was retrieved from coal or acquired from saltpeter. However, in order to keep up with the increase in demand for fertilizer at the beginning of the 20th century, ammonia synthesis from N_2 and H_2 was developed by Fritz Haber. This process was later applied to industrial production by Carl Bosch. Today, Ammonia is still produced on industrial scale using the Haber-Bosch process.

Ammonia is produced from nitrogen and hydrogen according to equation 2.1, a simple chemical reaction without the formation of any by-products.



In theory, since ammonia synthesis is an exothermic reaction, it will form ammonia at ambient conditions [26]. However, in practice the reaction is difficult to achieve since rate of formation is too slow to be detected. As the rate of formation is a function of the temperature, speeding up of the reaction can be achieved by increasing the temperature. This, however, effects the equilibrium which favors the reaction towards ammonia at lower temperatures due to the exothermic nature of the reaction. Therefore, in order to push the reaction towards ammonia production (product side), a high pressure must be applied to achieve sufficient conversion.

2.1.1. Equilibrium

A reaction is in equilibrium when the forward and backward reaction rates are equal, which means there are no net changes in the concentrations of reactants and products. The equilibrium of ammonia synthesis reaction can quantitatively be described using the equilibrium constant [27]:

$$K_p = \frac{(P_{NH_3})^2}{(P_{H_2})^3(P_{N_2})} \quad (2.2)$$

The standard equilibrium constant of ammonia synthesis reaction at 25 °C is 6.8×10^5 .

In 1930, Gillespie and Beattie established a basis for an analytical expression of the equilibrium constant based on experimental data from Haber [28], Larson & Dodge [29] and Larson [30]. The treated data extends from 10 – 1000 atm and from 325 °C – 500 °C and results in the following correlation for the equilibrium constant [31]:

$$\log_{10} \frac{K_p}{K_p^*} = \left[\frac{0.1191849}{T} + \frac{25122730}{T^4} + \frac{38.76816}{T^2} \sum (x_i A_{0i}^{1/2}) + \frac{64.49429}{T^2} (\sum x_i A_{0i}^{1/2})^2 \right] p \quad (2.3)$$

$$\log_{10}K_p^* = -2.691122\log_{10}T - 5.519265 \times 10^{-5}T + 1.848863 \times 10^{-7}T^2 + \frac{2001.6}{T} + 2.6899 \quad (2.4)$$

The values for the equation of state constant A_{oi} of H_2 , N_2 and NH_3 have been determined by Gillespie and Beattie to be 0.1975, 1.3445 and 2.3930 atmospheric litres per mole respectively [31]. A visual representation of these relations is shown in Figure 2.1.

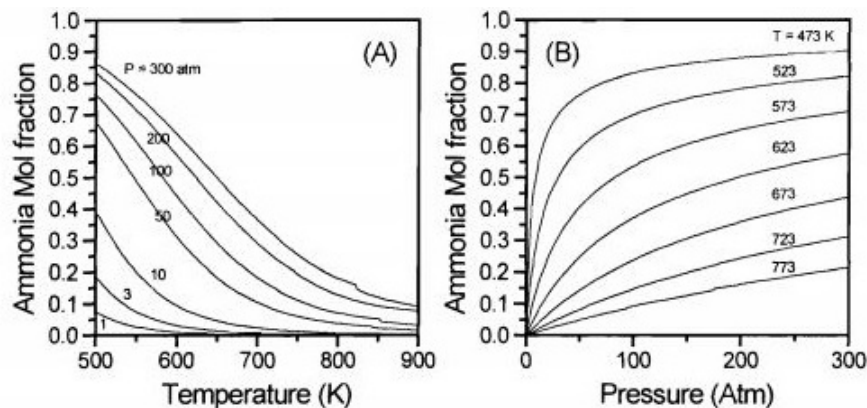


Figure 2.1: Mole fraction of ammonia at equilibrium as a function of temperature and pressure (initial mixture of 1:3 N_2/H_2 gas)

Source: [32]

The Le Chatelier principle is used to predict the behaviour of a system due to changes in temperature, pressure and concentration. The reaction equilibrium as described by Le Chatelier principle states that reversible changes in a system are self-correcting [33]; a reaction in equilibrium will return to a balanced state when disturbed. The following illustrates the effect of different "disturbances" on the reaction equilibrium:

- **Pressure:** a change in pressure/volume will induce a response to restore the equilibrium by creating fewer or more moles. Increasing the pressure will shift the equilibrium towards the side with fewer molecules.
- **Temperature:** Temperature's effect on the equilibrium depends on whether a reaction is exothermic or endothermic. For an exothermic case, a temperature increment will cause the reaction to shift to the reactant side to compensate this. In this case, a lower temperature is needed to shift the reaction to the product side.
- **Partial pressure:** the conversion can be enhanced by removal of the products. This forces the reaction to keep on forming products until equilibrium is achieved.

All of these can be applied to shift the equilibrium in the favor of the ammonia product. Figure 2.1 supports this by showing the effect of temperature and pressure on the ammonia equilibrium.

2.2. The Haber-Bosch process

From the Le Chatelier principle described in the previous section, it is clear that due to the volume reducing and exothermic nature of the ammonia reaction, a higher ammonia concentration can be realized at higher pressure and lower temperature. Yet, Fritz Haber implemented high temperatures in order to reach fast kinetics. However, this led to the reverse reaction inhibiting the NH_3 synthesis. To reduce this effect, Haber introduced increased pressures to enhance the conversion [34]. The process, however, was difficult to realize on an industrial scale. Haber realized that the conversion in a single pass converter was too low to be commercially interesting. Therefore, he proposed the idea of a more dynamic approach by using a recycle system. This recycle system resulted in a higher ammonia production from the make-up gas. Additionally, Haber directed efforts on the space time yield in the recycle loop rather than on the simple yield in a single pass. Therefore, Haber's focus was on the product yield per unit volume of catalyst and per unit time.

These innovations have provided the base for the development of experimental equipment that realized the first pressurized catalytic process to produce ammonia in industrial history [35]. This was a

breakthrough in the evolution of the catalytic process on an industrial scale.

In February 1908, Carl Bosch was assigned the task to develop this process for commercial application on industrial scale by Baden Aniline and Soda (BASF). Bosch instantly realized that he had to focus on three primary challenges: find an efficient and stable catalyst, develop equipment and materials to manufacture ammonia at high pressure and design economical methods to produce hydrogen and nitrogen. The first industrial Haber-Bosch plant was built by BASF in 1913 capable of producing 9000 *tonne/year* at Oppau, Germany [36].

The Haber-Bosch process which is one of the most important innovations of the 20th century [37], is carried out at elevated pressures (15-35 *MPa*) and temperatures (350-500 °C) in the presence of a heterogeneous catalyst and with a H₂ to N₂ ratio of 3:1 [38] [39]. This process has been completely optimized at large scale for industrial use, but the requirement of these extreme process conditions make ammonia production incredibly energy- and capital intensive.

Even though the process has achieved significant technological progress, it is still based on the original principles developed by Haber and Bosch over a century ago [40]. The simplified flow diagram of the typical methane-fed ammonia synthesis process is shown in Figure 2.2. A modern ammonia production process can be divided into two principal parts: obtaining hydrogen from methane (Steam reforming, CO Shift, CO₂ removal) and the Haber-Bosch reaction (Reactor) to produce ammonia from nitrogen and hydrogen.

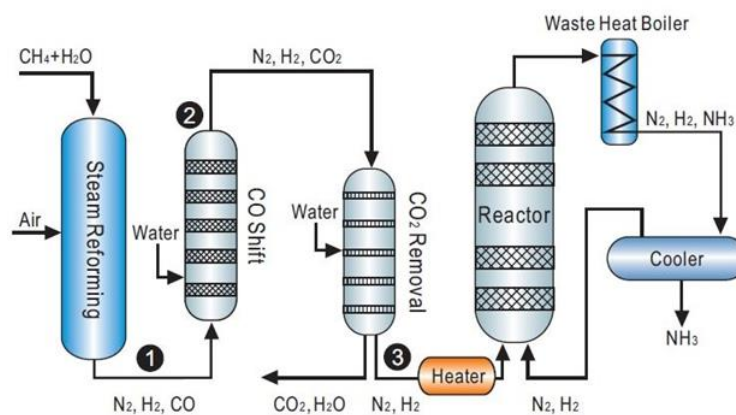


Figure 2.2: Traditional Haber-Bosch Process

Source: [41]

2.3. Industrial State-of-the-art

In the 20th century, numerous alterations have been made in the ammonia plant technology in order to improve manufacturing rates and for new processes to be built accommodating for greater capacities. There is a strong competition by the four main technology licensors: Haldor Topsøe, Thyssenkrupp Industrial Solutions (TKIS), Kellogg Brown and Root (KBR) and Ammonia Casale.

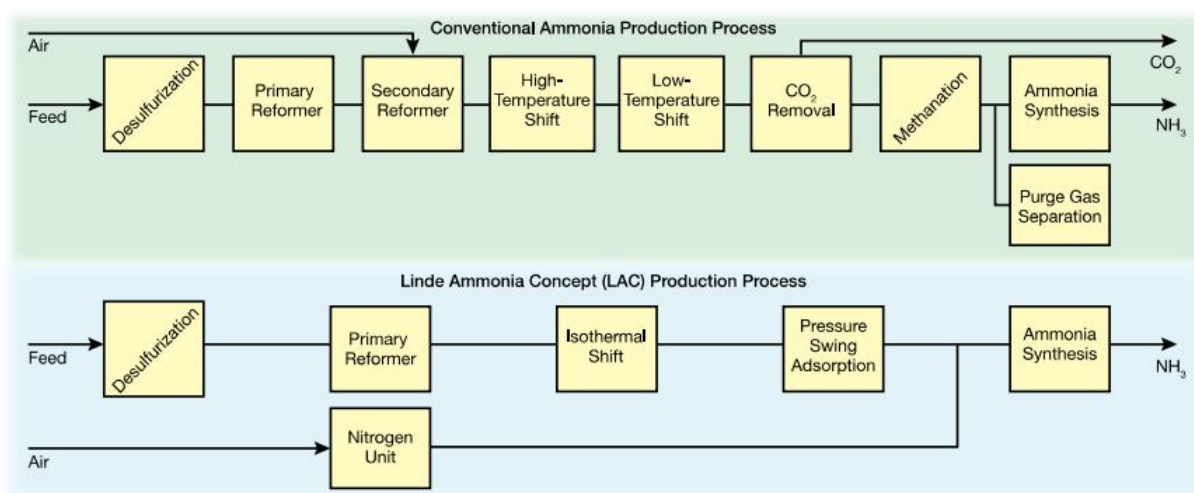


Figure 2.3: Linde vs. Conventional Ammonia Plant

Source: [42]

The Linde Ammonia Concept (LAC) is a process at the forefront of innovation for the production of ammonia from natural gas, based on Casale's technology [42]. LAC is an established design with 40 years of operating knowledge for processes with volumes from 200 to 2,000 *mt/day* [43]. The plant mainly consists of a combination of production technologies: a standard nitrogen process, a modern hydrogen plant and high-productivity ammonia synthesis. As seen in the process scheme, Figure 2.3, LAC substitutes the expensive and complicated front compared to a conventional ammonia plant. It does so by employing two well-demonstrated process technologies: a Pressure Swing Adsorption (PSA) purification unit to obtain high-purity hydrogen from a steam-methane reformer, and a cryogenic nitrogen production unit for high-purity nitrogen from air.

2.4. Catalyst

To realize a more sustainable process for ammonia synthesis, it is essential to reduce the extreme conditions required for the Haber-Bosch process. This has led to a rise in the demand for novel or enhanced catalysts.

For over a century, research has been done on the catalytic NH_3 reaction from nitrogen and hydrogen. Since then, these studies have resulted in great progress and innovation in the industry and academics. Catalytic novelty has even been awarded Nobel Prizes for the contribution to the field. During the 20th century, methods for the catalytic ammonia reaction have played an essential role in the evolution of the chemical industry. This led to the great interest in improving and understanding of the ammonia catalyst and the establishment of novel concepts and foundations such as structure sensitivity, promoting and poisoning. Attempts to improve traditional catalysts or develop entirely new compositions from different metals are still taking place.

Following the purchase of Haber's patents in 1908, BASF began the development of a commercial process which drove Carl Bosch, Alvin Mittasch and others to investigate more than 2,500 various catalysts [25]. Subsequently, they established a multi-component iron based catalyst for the manufacturing of ammonia, indicating a turning point in industrial catalysis. Just several years after that, methanol through catalytic synthesis was accomplished and high pressure operation became a key method in organic chemistry. Ammonia synthesis catalyst has been the base for numerous scientists on fundamental concepts and approaches in researching heterogeneous catalysis. The achievements in the ammonia industry and its catalyst created the groundwork for heterogeneous catalysis.

To date, it still appeals to many researchers. Currently, improvements to the catalyst are still being made and many novel concepts can be acquired.

In this chapter, important characteristics of catalysts are identified along with their influence on the reaction kinetics. Subsequently, recent innovations in the field of catalysts for ammonia synthesis are highlighted, proposing novel catalyst materials and compositions to function under milder process conditions.

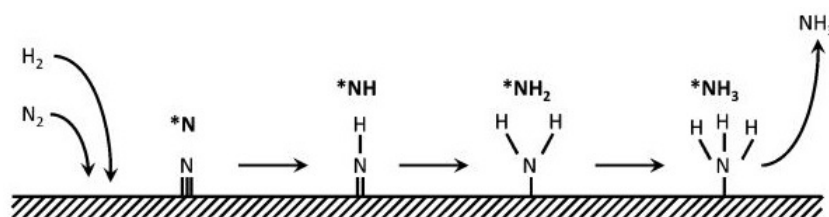
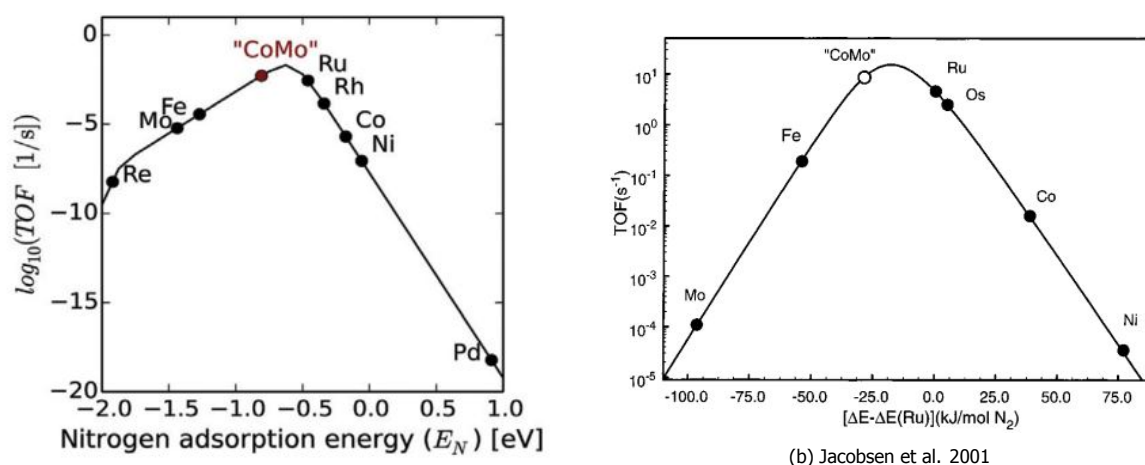


Figure 2.5: Reduction of nitrogen in the Haber-Bosch reaction through a dissociative mechanism

Source: [44]

Active catalysts are mainly governed by the activation energy of the dissociation reaction [47]. Swift NH_3 synthesis demands a catalyst that strongly activates the reactants, but at the same time creates a comparatively weak binding of the transitional species and products [48]. Transition metals have the ability to donate and admit electrons efficiently to form chemical bonds, making them good catalysts. The best catalyst should form bonds with intermediate strength, not too weak to dissociate nitrogen, but not so strong that it will inhibit the desorption of products. To accomplish high activity, a balance needs to be struck between two conflicting measures: a low barrier for N_2 dissociation and little coverage of the catalyst surface with adsorbed nitrogen atoms during the ammonia reaction. The Sabatier optimum reflects this compromise in a volcano plot showing the relation between activity and bond strength [48] as depicted in Figure 2.6. The turn-over frequency (TOF) is a measure of the catalyst activity ($\text{molNH}_3/\text{molcatalyst/s}$).



(a) Medford et al. 2015

(b) Jacobsen et al. 2001

Source: [49]

Figure 2.6: Turnover frequencies for ammonia synthesis as a function of the adsorption energy of nitrogen

Source: [48]

On metals, this association between the nitrogen binding energy E_N and the transition-state energy $E_{N=N}$ (equal to activation energy ΔE_a), is a linear energy scaling (or Brønsted–Evans–Polanyi)[50] [51]. Therefore, it's not possible to vary $E_{N=N}$ and E_N independently for this group of catalysts.

At industrial conditions, Ruthenium (Ru) and Osmium (Os) reach closest to the peak of the volcano-plot. Despite that, the third-best transition metal is more economically appealing compared to these metals, Iron (Fe). A resolution could be to combine two metals to create a surface with the necessary intermediate N_2 interaction: one with poor and one with strong adsorption energy. A combination between Molybdenum and Cobalt was experimentally found to be close to the optimum. A Co-Mo catalyst was acquired with the use of this proposition and it showed to have a greater activity than the other elements, much higher even than Ru and Fe at low NH_3 concentrations [52].

2.4.2. Catalysts for Ammonia Synthesis

Iron-Based Catalysts The iron-based catalysts have been examined for almost a century and were the first ones to be used as functioning ammonia synthesis catalysts. These catalysts can be categorized according to either magnetite-based and wüstite-based catalysts.

- **Magnetite-Based Catalysts**

When BASF was testing catalysts to commercialize ammonia production, they discovered that fusing few percent of alumina, some calcium oxide and potassium alkali into pure iron, a suitable catalyst can be obtained. These promoters, or activators, when added to a solid catalyst improve the efficiency of the catalyst (by increasing the activity or selectivity). The most effective catalyst was shown to be a magnetite-based iron catalyst with a small amount of promoter which is still used today. This multi-component mixture has proven to be so successful that even now ammonia catalysts are produced founded on this concept. This Magnetite Fe_3O_4 -based catalyst was discovered in 1913, and is presently manufactured by Haldor Tøpsoe under the name KM1. KM1 consists of 91-95 Wt% of iron oxides with 5-9wt% of K_2O , Al_2O_3 , CaO and SiO_2 as promoters and is used in the industrial range.

- **Wüstite-Based Catalysts**

A similar catalyst was developed by Zhejiang University of Technology, China in 1986 based on FeO . This Wüstite catalyst is the most active iron-based catalyst and is widely used in the industry all around the world [35]. Catalysts of type A-301 and ZA-5 were developed successfully have turned into the leading catalyst in the industry for nearly 30 years.

Both of these conventional iron-based catalysts are still widely applied for the manufacture of ammonia because of its proven effectiveness and their economical cost.

Iron-Cobalt-Based Catalysts The AMV process was developed corresponding to the 74-1 Fe-Co catalyst developed by the Imperial Chemical Industries (ICI) Corporation, which made the operating pressure decline to 10–12 MPa .

Ruthenium-Based 40 years ago, Ozaki et al. suggested that the volcano-shaped curve (Figure 2.6) could be utilized to depict catalytic efficiency in relation to chemical adsorption of nitrogen for metal elements. This curve shows ruthenium closest to the optimum, making it the most active metal. This opposes the result obtained by Mittasch et al. [53], concluding that ruthenium is less active than iron. Later research posed that this disagreement is caused by different reaction conditions, as the initial results were under elevated temperature and pressure (100 bar , 550 $^\circ\text{C}$) while the latter significantly lower conditions [54]. In 1972, Ozaki et al. [55] discovered that a catalyst comprised of ruthenium as active component, carbon as support and potassium as promoter presented high activity for NH_3 synthesis. This discovery led to subsequent studies on the development of ruthenium catalysts.

After collective effort between British Petroleum (BP), which was behind the invention of a ruthenium compound loaded on a graphite carbon carrier, and Kellogg, that established the corresponding NH_3 production process with this Ru/C catalyst. In 1992, they successfully achieved industrial application of this catalyst in a new process, KAAP (Kellogg Advanced Ammonia Process). This process applicable to the Ru–K–Ba/AC catalyst managed to reduce the synthetic pressure to under 10 MPa .

The KAAP catalyst is 10-20 more active than the iron magnetite catalyst [56]. The KAAP catalyst enhances the speed of reaction, and therefore a lower temperature is required. Consequently the catalyst allows for lower operating pressures to achieve a similar conversion. Another advantage is that it is not hindered by ammonia, meaning it can enhance the conversion after the ammonia equilibrium has been reached with an iron catalyst. However, Ru/C catalysts are hindered by hydrogen and are quite costly. Another downside is susceptibility to corrosion of the support causing deactivation [57]. KAAP cleverly utilizes the advantages of both catalyst systems (Fe and Ru/C) by combining them in a separated multi-bed arrangement with intercooling [58].

Even though the cost of Ruthenium is higher than iron, it still poses an attractive option due to its high activity under lower pressure and temperature conditions. It presents benefits in terms of reducing equipment cost, saving energy and enhanced equipment reliability. Due to this potential Ruthenium based catalyst have been widely investigated, and research is still going on to improve this catalyst.

2.4.3. Developments in Ammonia Synthesis Catalysts

A non-extensive list of catalysts found in literature, that could allow for milder operating process conditions, can be found in Table 2.1. The industrially used iron-based and ruthenium-based catalysts have been depicted to serve as reference for comparison.

Table 2.1: Novel Ammonia Synthesis Catalysts

Inventor/Source	Catalyst (T,p)	Production rate (mmol NH ₃ /g/h)
Conventional/Industrial		
Haldor¹ (KM1) Magnetite	Fe ₃ O ₄ /Promoter (400°C, 90 bar)	13.51
Zhejiang University (A301, ZA-5) Wüstite	FeO ₄ /Promoter (400°C, 100 bar)	14.91 ¹
	FeO ₄ /Promoter (325/400°C, 100 bar)	14.1/22.3 ²
UK-BP (KAAP)	Ru–K–Ba/AC (400°C, 100 bar)	58.41 ¹
	Ru–K–Ba/AC (325°C, 100 bar)	38.4 ²
Tokyo Institute of Technology³	Fe–K ₂ O–Al ₂ O ₃ (315°C, 20 bar)	1.45
Novel		
Tokyo Institute of Technology³	3wt%Ru/CeO ₂ (315°C, 20 bar)	2.25
Tokyo Institute of Technology⁴	0.5wt%Ru/C ₁₂ A ₇ e ²¹ (400°C, 1 bar)	0.969
	2wt%Ru/C ₁₂ A ₇ e ²¹ (400°C, 1 bar)	2.684
	9.1 wt%Ru–Ba/AC (400 °C, 1 bar)	2.417
	6 wt%Ru–Cs/MgO ref	3.107
AIST^{5,6}	6.4 wt%Cs–2 wt%Ru/MgO (400°C, 25 bar)	4.2
	1wt%Ru/CeO ₂ (440°C, 30 bar)	11.5
	1wt%Ru/CeO ₂ (420°C, 30 bar)	8.5
	1wt%Ru/CeO ₂ (400°C, 30 bar)	5.9
Tokyo Institute of Technology⁷	LaCoSi (400°C, 1 bar)	1.25
	LaCoSi (400°C, 9 bar)	5
Oita University⁸	Ru/La _{0.5} Ce _{0.5} O _{1.75} (350°C, 10 bar)	31.3
	Ru/La _{0.5} Ce _{0.5} O _{1.75} (400°C, 10 bar)	65
	Ru/La _{0.5} Ce _{0.5} O _{1.75} (350°C, 30 bar)	44.4
RTI International⁹	Ru/MOF (350°C, 95 bar)	64.6
Warwick Ventures¹⁰	Fe/Promoter (450°C, 10 bar)	25
	Fe/Promoter (450°C, 30 bar)	39
Dalian Institute¹¹	Cr–LiH (300°C, 10 bar)	3.5
Tokyo Institute of Technology¹²	10wt% Ru/Ba–Ca(NH ₂) ₂ (300°C, 1 bar)	9
	10wt% Ru/Ba–Ca(NH ₂) ₂ (300°C, 9 bar)	23.3
	10wt% Ru/Ba–Ca(NH ₂) ₂ (375°C, 9 bar)	60
Liang et al.¹³	24.8 wt%Ba–4 wt%Ru/AC (400°C, 30 bar)	25.88
	4 Ba–4 Ru/AC (400 °C, 30 bar)	28.36
Zhong and Aika¹⁴	3 Ba–2 Ru/AC (312 °C, 1 bar)	2.43
Seetharamulu et al.¹⁵	Cs–Ru/HT (450 °C, 1 bar)	3.125

Continued on next page

Table 2.1 – Continued from previous page

Inventor/Source	Catalyst (T,p)	Production rate (mmol NH ₃ /g/h)
Yang et al. 2010 ¹⁷	5Ru/MgO (350°C, 30 bar)	7.39
Xialong et al. ¹⁸	Ru/BaCe _{0.9} Y _{0.1} O _{3-λ} (425°C, 30 bar)	19.3
Tokyo Institute of Technology ¹⁹ Kojima and Aika	Co ₃ Mo ₃ N – 2 wt%Cs (400°C, 1 bar) Co ₃ Mo ₃ N – 10 wt%Cs (400°C, 31 bar)	0.986 15.0

¹ Liu, H. (2013). Ammonia synthesis catalysts: innovation and practice. World Scientific.

² Chonggen, P. A. N., Ying, L. I., Jiang, W., & Huazhang, L. I. U. (2011). Effects of reaction conditions on performance of Ru catalyst and iron catalyst for ammonia synthesis. Chinese Journal of Chemical Engineering, 19(2), 273-277.

³ Aika, K. I., & Niwa, Y. (1999). Basic concepts and properties of new generation ammonia synthesis catalysts for industrial use. In Studies in Surface Science and Catalysis (Vol. 121, pp. 327-332). Elsevier.

⁴ Tokyo Institute of Technology. EP 2650047A1 (2011) H. HOSONO, M. HARA, M. KITANO

⁵ Javaid, R., Matsumoto, H., & Nanba, T. (2019). Influence of Reaction Conditions and Promoting Role of Ammonia Produced at Higher Temperature Conditions in Its Synthesis Process over Cs□Ru/MgO Catalyst. ChemistrySelect, 4(7), 2218-2224.

⁶ Tetsuya NANBA, Keisuke KOBAYASHI, Yuki NAGATA, Rahat JAVAID, Hideyuki MATSUMOTO. (2019). Effect of preparation condition on ammonia synthesis over Ru/CeO₂.

⁷ Tokyo Institute of Technology, Y. GONG, M. KITANO, H. HOSONO

⁸ Oita University. (2018) Y; OGURA, K. NAGAOKA

⁹ RTI International (2019) C. BALL

¹⁰ Warwick Ventures. UK. (2019) J. LAPWORTH GB1806687.8

¹¹ Dalian Institute of chemical physics. CHINA. (2016) P. CHEN. P. WANG. DOI: 10.1038/NCHEM.2595 EP3081294A1

¹² Self-organized Ruthenium-Barium Core-Shell Nanoparticles on a Mesoporous Calcium Amide Matrix for Efficient Low-Temperature Ammonia Synthesis, M. KITANO, H. HOSONO, M. HARA

¹³ Liang, C., Wei, Z., Luo, M., Ying, P., Xin, Q., & Li, C. (2001). Hydrogen spillover effect in the reduction of barium nitrate of Ru-Ba (NO₃)₂/AC catalysts for ammonia synthesis. In Studies in Surface Science and Catalysis (Vol. 138, pp. 283-290). Elsevier.

¹⁴ Zhong, Z. H., & Aika, K. I. (1998). Effect of ruthenium precursor on hydrogen-treated active carbon supported ruthenium catalysts for ammonia synthesis. Inorganica chimica acta, 280(1-2), 183-188.

¹⁵ Seetharamulu, P., Reddy, K. H. P., Padmasri, A. H., Rao, K. R., & Raju, B. D. (2009). Role of promoters on highly active nano-Ru catalyst supported on Mg-Al hydrotalcite precursor for the synthesis of ammonia. Catalysis Today, 141(1-2), 94-98.

¹⁶ Chen, H. B., Lin, J. D., Cai, Y., Wang, X. Y., Yi, J., Wang, J., ... & Liao, D. W. (2001). Novel multi-walled nanotubes-supported and alkali-promoted Ru catalysts for ammonia synthesis under atmospheric pressure. Applied surface science, 180(3-4), 328-335.

¹⁷ Yang, X. L., Zhang, W. Q., Xia, C. G., Xiong, X. M., Mu, X. Y., & Hu, B. (2010). Low temperature ruthenium catalyst for ammonia synthesis supported on BaCeO₃ nanocrystals. Catalysis Communications, 11(10), 867-870.

¹⁸ Xiaolong, Y. A. N. G., Chungu, X. I. A., XIONG, X., Xinyuan, M. U., & Bin, H. U. (2010). Preparation and catalytic properties of barium cerate and yttrium-doped barium cerate supported ruthenium for ammonia synthesis. Chinese Journal of Catalysis, 31(4), 377-379.

¹⁹ Kojima, R., & Aika, K. I. (2001). Cobalt molybdenum bimetallic nitride catalysts for ammonia synthesis: Part 2. Kinetic study. Applied Catalysis A: General, 218(1-2), 121-128.

2.5. Reaction Kinetics

It's essential to have information on the reaction kinetics to determine the best operating conditions, for the design of a reactor, and to perform the control of a plant. This is done by predicting the relation between the rate of formation of ammonia and the operating variables [46].

The synthesis rate (r) can be expressed as a function of the concentration of reactions (N_2 and H_2) and a product (NH_3) in the form of a power law rate expression $r = kP_{N_2}^n P_{H_2} P_{NH_3}^{\alpha}$. Another form, the most widely used rate expression for ammonia synthesis for iron catalysts, known as the Temkin-Pyzhev equation, was first proposed in 1940 [59]:

$$r = k_1 P_{N_2} \left(\frac{(P_{H_2})^3}{(P_{NH_3})^2} \right)^{\alpha} - k_2 \left(\frac{(P_{NH_3})^2}{(P_{H_2})^3} \right)^{1-\alpha} \quad (2.6)$$

k_1 and k_2 are forward and reverse reaction rate constants and P_{N_2} , P_{H_2} , and P_{NH_3} are partial pressures of nitrogen, hydrogen and ammonia. α is the transfer coefficient. The kinetic constants k_1 and k_2 can be calculated using the Arrhenius equation[60]:

$$k_1 = A_f \exp\left(-\frac{E_{syn.}}{RT}\right) \quad (2.7)$$

$$k_2 = A_b \exp\left(-\frac{E_{dec.}}{RT}\right) \quad (2.8)$$

The Temkin-Pyzhev rate equation is suitable for the range of 370-495 °C and 150-310 atm [61]. This expression was derived with the assumptions that nitrogen dissociative adsorption is rate-determining and that the surface coverage by atomic nitrogen is high [62].

The Temkin-Pyzhev rate equation is still the commonly used expression to date. However, several other rate equation have been developed by various scientists, of which many are based on the Temkin-Pyzhev equation. Some tried to achieve a better accuracy of the equation using experimental data, or aimed to find an expression for different operation conditions or catalysts.

For all catalyst materials the dissociative adsorption of N_2 is the rate determining step. However, it was found that on ruthenium catalysts the synthesis reaction is kinetically inhibited by H_2 adsorption on the catalyst surface[63]. Therefore, the Temkin-Pyzhev rate expression cannot directly be applied to reactions with a ruthenium catalyst. Instead some works propose to alter the Temkin equation by adding a denominator to account for the strong hydrogen adsorption. Resulting, in the development of a combination between the Temkin and Langmuir-Hinselwood-Hougen-Watson (LHHW) model to express the characteristics of ruthenium more accurately [57].

A non-extensive list of rate equations found in literature have been summarized in Table 5.1 along with their application. The top part of the table present iron-based catalyst, while the bottom expressions are for ruthenium catalysts. Some equations use the activity of the components instead of partial pressures. Others replace the need for both the forward and backward rate term by including and equilibrium constant (K_{eq}).

Table 2.2: Rate Equations for the Ammonia Synthesis Reaction

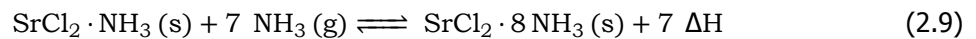
Author/Name	Rate equation	Range	Catalyst	Note
Temkin-Pyzhev (1940) [64]	$r = k_1 P_{N_2} \left(\frac{(P_{H_2})^3}{(P_{NH_3})^2} \right)^\alpha - k_2 \left(\frac{(P_{NH_3})^2}{(P_{H_2})^3} \right)^{1-\alpha}$	370-495 °C 150-310 atm	Fe-K ₂ O-Al ₂ O ₃	$\alpha = 0.5$
Langmuir-Hinshelwood [62]	$r_{-2} = k_{-2} \theta_N^2 \left(K_{eq} \frac{P_{N_2} (P_{H_2})}{(P_{NH_3}) (P_O)^2} - 1 \right)$	Industrial Range	Iron-based	r_{-2} is reverse reaction rate of the N ₂ dissociation step (Equation 2.5.2 [1/s])
Ozaki, Taylor & Boudart (1960) [65]	$r = \frac{k P_{N_2}}{(1 + K P_{NH_3} / P_{H_2}^{1.5})^2}$	~ 218-302 °C 1/3 – 1 bar	Doubly promoted Iron (Two types)	Uniform surface N main species on surface
Nielsen et al. from Haldor Topsøe (1964) [61]	$r = \frac{k \left(P_{N_2} K_{eq}^2 - \frac{P_{NH_3}^2}{P_{H_2}^3} \right)}{\left(1 + \frac{K_{NH_3} P_{NH_3}}{P_{H_2}^0} \right) \alpha}$	370-495°C 149-309 atm	KM1-R (Promoted Iron)	Reduces to original Temkin with $\alpha = 0.75$, $\omega=1.5$
Dyson & Simon (1968) [66]	$r = k_2 \left(K_{eq}^2 a_{N_2} \left(\frac{a_{H_2}^3}{a_{NH_3}} \right)^\alpha - \left(\frac{a_{NH_3}^2}{a_{H_2}} \right)^{1-\alpha} \right)$	Industrial Range	Iron-based	
Buzzi Ferraris et al. (1974) [67]	$r = \frac{a_{N_2} a_{H_2}^2 - \frac{1}{K^2} \left(\frac{a_{NH_3}}{a_{H_2}} \right)}{C_1 a_{N_2}^2 + C_2 \frac{a_{NH_3}^2}{a_{H_2}} + C_3 a_{H_2} a_{NH_3}}$	370-495°C 149-309 atm	Iron-based	Best fit to Nielsen et al. data with only 0.08% error
Rossetti et al. (2006) [68] Modified Temkin	$\frac{d\eta}{dt} = k\lambda(q) \frac{(a_{N_2})^{0.5} \left(\frac{a_{H_2}}{a_{NH_3}} \right)^{0.375} - \frac{1}{K_{eq}} \left(\frac{a_{NH_3}}{a_{H_2}} \right)^{1.125}}{1 + K_{H_2} (a_{H_2})^{0.3} + K_{NH_3} (a_{NH_3})^{0.2}}$	370-460°C 50-100 bar	Promoted Ru/C	H ₂ & NH ₃ adsorption terms $\lambda = 1.5$ or 3 (H ₂ :N ₂ Ratio) Data fit experimental test (error < 5%)
Modified Temkin from [68] with different parameters [25]	$r = k_1 (1 + \gamma_{NH_3})^2 \frac{f_{N_2} \left(\frac{f_{H_2}^{0.45}}{f_{NH_3}^{0.3}} \right) - \frac{1}{K_a} \left(\frac{f_{NH_3}^2}{f_{H_2}^3} \right)}{1 + K_{H_2} f_{H_2}^{1.5} + K_{NH_3} f_{NH_3}^{2.8}}$	350-450°C, 100 bar H ₂ /N ₂ = 1-3	Ba-Ru-K/AC	Parameters from Zhang et al. $\alpha = 0.15$ error < 5%
Aika & Ozaki (1969) [69]	$r = k P_{N_2} P_{H_2}^0 P_{NH_3}$	346-410 °C	Ruthenium	Reduced pressures (very low activity)
Aika (2017) [63]	$r = \frac{k_1 P_{N_2}}{(1 + K_d P_{NH_3} / P_{H_2}^{1.5} + K_c P_{H_2}^{0.5})^2}$	Low pressures	Ruthenium	

2.6. Absorption for Ammonia Recovery

Chemisorption by metal halides has been researched to replace the conventional condensation step in the ammonia synthesis process to remove the ammonia product from the recycle stream. Metal halide salts, such as magnesium chloride or strontium chloride, have been shown to be promising contenders for NH_3 storage materials because of their capacity to contain several moles of ammonia per mole of salt. The ammonia take-up from the recycle stream can be more complete and at higher temperatures with such an absorption than ammonia separation through condensation [70]. Metal halides have been studied for over 15 years as an indirect storage for hydrogen due to their high hydrogen capacities [71] [72] [73]. Working pairs of sorption metal chloride and ammonia have been described to have a high energy density and adequate cyclability [74]. A drawback however in comparison to condensation, is that it requires a cyclic operation for the uptake and release of ammonia from the absorbent. Therefore, switching between absorption and desorption beds to regenerate the ammonia is required.

2.6.1. Strontium Chloride

For the separation of ammonia from the recycle stream, Strontium Chloride amine $\text{Sr}(\text{NH}_3)_8\text{Cl}_2$ was suggested by the partners of the project, from Technical University of Denmark (DTU). $\text{Sr}(\text{NH}_3)_8\text{Cl}_2$ provides high volumetric and gravimetric ammonia densities. It is known that SrCl_2 absorbs most NH_3 molecules with low binding energy (1-7: 41.4 kJ/mol, 8: 48.1 kJ/mol ammonia) [75]. During desorption, the last ammonia atom requires either extremely low pressure or high temperature to be released due to its higher binding enthalpy. Hence, only the absorption/desorption of the first seven molecules is considered in the simulation. The binding of the seven ammonia molecules with mono-amine that form octa-amine is described according to the following reaction:



The reaction in Equation 2.9 is exothermic. At 1 atm and 25 °C, this reaction enthalpy (ΔH) = -41.432 kJ/(mol of NH_3) [76]. This is almost twice as much as the condensation enthalpy of ammonia (-23.3 kJ/mol [77]). Because absorption in an equilibrium reaction and binding of ammonia has a strong exothermal effect, the absorber requires continuous heat removal.

2.6.2. Determining the absorption temperature

The equilibrium gas pressure over the salt p_{eq} (Pa) can be expressed by the van 't Hoff equation:

$$p_{eq} = p_0 e^{-\frac{\Delta H}{RT} + \frac{\Delta S}{R}} \quad (2.10)$$

where

p_0 = a reference pressure equal to 1 Pa;

ΔH = the reaction enthalpy J/mol;

ΔS = the reaction entropy J/(molK);

T = the reaction temperature K;

R = the ideal gas constant 8.314 J/(molK)

Based on Gunasekara, Saman Nimali, et al. [78], the equilibrium pressure-temperature curve of the NH_3 - SrCl_2 for the conversion between $\text{Sr}(\text{NH}_3)\text{Cl}_2$ and $\text{Sr}(\text{NH}_3)_8\text{Cl}_2$ was plotted. This is done based by filling in the Van't Hoff equation 2.10 for various temperatures and pressures [79], see Figure 2.7. In the same Figure the phase diagram of NH_3 is shown based on data [77]. The lines represent the condensation and absorption vapor pressures for ammonia as a function of temperature. The grey line in Figure 2.7 represents the equilibrium absorption temperature as function of partial NH_3 pressure above the absorbent material. The red line shows the vapor saturation pressure of NH_3 above liquid NH_3 (as in a vapor-liquid phase diagram).

The operating temperatures and pressure for absorption and desorption can be found using the grey line. Above the grey line is the absorption region, absorption will occur here. For a certain partial ammonia pressure in the system, the reaction must happen below a certain temperature. If the temperature is too high desorption occurs and operation happens in the desorption region (below the grey line).

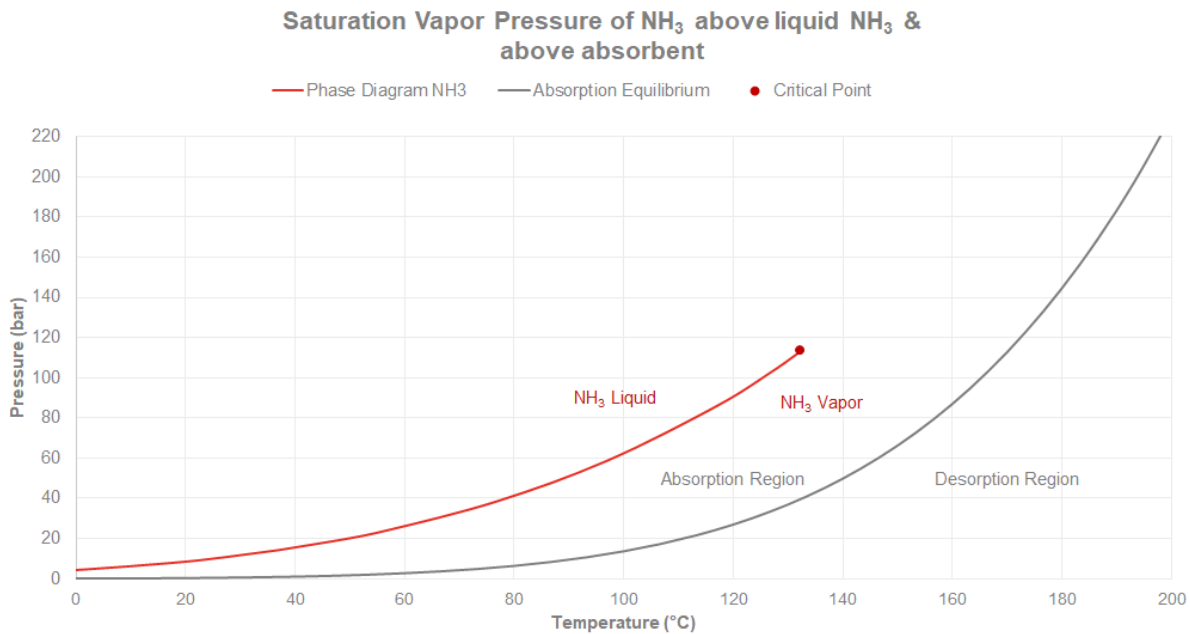


Figure 2.7: Saturation Vapor Pressure of NH₃ above liquid NH₃ & above Absorbent

Source: [78]

Take-aways There are a few key differences in ammonia separation via condensation and through absorption.

1. Equilibrium:
For the same partial NH₃ vapor saturation pressure, the absorption temperature is higher than the condensation temperature.
2. Separation Method:
Fixed-bed operation with breakthrough curve can lead to practically complete removal of NH₃ from the recycle stream. For condensation, very low temperatures or very high pressures are required to avoid high concentrations of H₂ and N₂ in the liquid ammonia. This is not the case for absorption.

Hence, for the same pressure, absorption can be performed at a considerably higher temperature than condensation (much closer to the reactor temperature). This is one of the main advantages of the absorption method. Another advantage is that absorption allows for a higher ammonia recovery from the gas mixture resulting in almost no ammonia presence in the recycle stream. These characteristics result in a reduced pressure in the system and a higher reaction conversion, which offer advantages for dynamic operation.

2.7. Control theory

To design a control structure for the dynamic simulation of the ammonia synthesis loop, knowledge about system control is required. Therefore, this section entails a short background on control theory. The purpose of a control system is to maintain stable process operations by compensating for disturbances. Some important terms used in process control are:

- PV: Process variable that you want to maintain at a given operating point (= setpoint).
- MV: Process variable that is changed by the controller.
- DV: A process variable which perturbs a process and causes the control variables to deviate from the desired setpoints.

Basics of a PID Controller

A commonly used type of control used in the process industries, is the proportional–integral–derivative controller (PID). This method applies feedback in a control loop and constantly computes an error value $e(t)$ as the difference between a desired setpoint (PV) and a measured process variable (MV). It will then carry out an adjustment based on proportional, integral, and derivative terms. Below, the influence of these terms is described.

- Proportional term (P) = proportional to the current value of the error.
- Integral Term (I) = accounts for past values of the error and integrates them over time to produce the I term.
- Derivative Term (D) = best estimate of future trend of the error based on its current rate of change. The faster the change, the greater the controlling effect and the other way around. This is referred to as 'anticipatory control'.

These terms appear in the following equation for the output value of the controller in reaction to the measured error value:

$$u(t) = MV(t) = \underbrace{K_p e(t)}_{P\text{-proportional}} + \underbrace{K_p / \tau_i \int_0^t e(t) dt}_{I\text{-Integral}} + \underbrace{K_p \tau_d \frac{de(t)}{dt}}_{D\text{-Derivative}} \quad (2.11)$$

with

$$\text{error } e(t) = \text{Process variable (PV)} - \text{Setpoint (SP)} \quad (2.12)$$

The tuning parameters K_p , K_i , K_d represent the controller gain, controller integral reset and controller derivative term, respectively. These tuning parameters of a PID controller can have significant impact on the controller stability. Figure 2.8 depicts the effects of varying each control parameters have on the control response subjected to a step change. Loop tuning is required for an optimal control function. Tuning balances the effects from the proportional, integral and derivative terms.

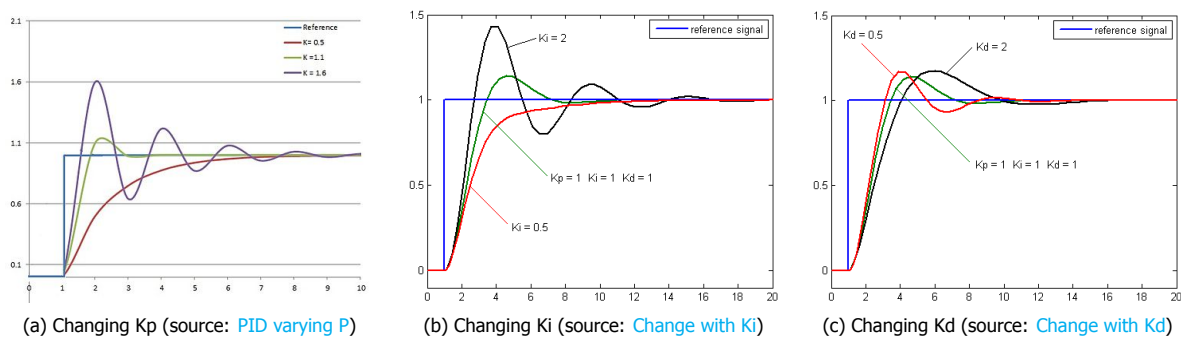


Figure 2.8: Varying the control parameters of a PID controller

Instead of using PID control, it is also possible to implement either Proportional (P) or PI control. Figure 2.9 depicts the differences in dynamic response between these three types of control.

A proportional control can dampen out the oscillations from disturbances and stop the cycling of the process variable, however, a retained offset between the process variable and its SP will always be present. A PI control can dampen out oscillations and return the process variable to the setpoint. Decreasing the controller integral action gives a more aggressive dynamic response, but can lead to an unstable controller. A PID controller can anticipate the direction of the error and thus respond more quickly, by measuring the rate of change in error. Increasing the derivative constant can give a better dynamic response but must be done with caution in real plants with 'noisy' process data inputs.

The majority of controllers in chemical processes are under PI or PID control. Figure C.2 in Appendix C presents stability recommendations for these three control types.

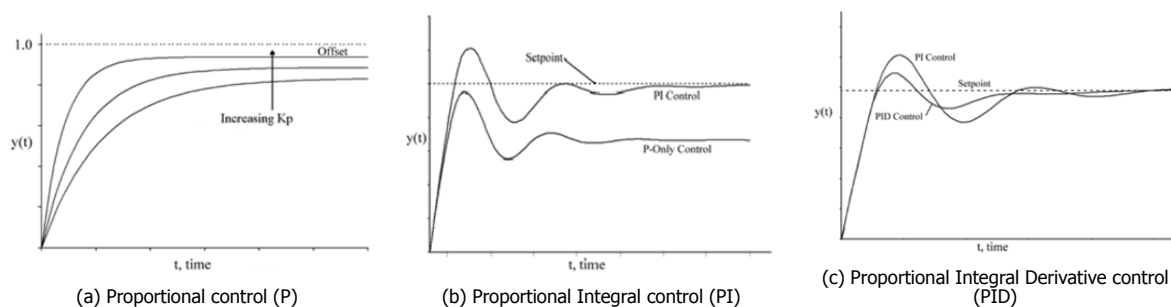


Figure 2.9: Difference between the control types (P, PI, PID) (source: [Getting Started with Aspen Dynamics](#))

Control Action

Another important expression in control theory is control action, which can be direct acting or reverse acting.

- **Direct acting** means that the process has a negative steady state gain. An example is the temperature control of a reactor with a cooling fluid. In case the reactor temperature rises above the set point (positive error), the flow rate of the cooling fluid must be increased by opening the valve more (positive controller output). Therefore, a positive error results in a positive control output.
- The opposite is a **reverse acting** controller, this process has a positive steady state gain. Which means a negative correction must be employed to create the correct controller output. For example, the pressure in a reactor surpassed the setpoint and must be reduced (the error is positive). This means the flow to the reactor must be lowered, this is done by decreasing the valve opening (the controller output is negative). Therefore, the control action must be reversed.

3

Scope & approach

3.1. Objective

The primary objective of this study is the analysis of the dynamic response of an ammonia synthesis process subjected to variations in the hydrogen feed flow rate. The cause for these perturbations is fluctuation of the electricity delivered to the electrolyzers due to the use of renewable energy sources, such as solar and wind power. More specifically, the goal was to develop a suitable control structure that helps the system cope with these variations. Subsequently, the feasibility of this control structure was tested and the effects of this control on the process was studied.

3.2. Scope

The initial scope of the present work was to support the design of a lab-scale ammonia synthesis loop as part of a collaborative project between Proton Ventures B.V. and other partners. This project aimed to develop a ammonia synthesis demonstration plant (10 *kg/day*) employing a novel catalyst suitable for operation at mild conditions (< 50 *bar*).

During the course of this work, unexpected delays were encountered in the progress of the collaborative research project. Therefore, the application focus was shifted towards Proton Ventures's small-scale NFUEL[®]-units for decentralized production of ammonia, using a conventional iron-based catalyst instead. With the application of a iron catalyst, the operating pressure has to be elevated to the industrial range (100-350 *bar*).

The largest capacity of the NFUEL[®] range at 60 *tons/day* was selected as the size reference for present study. This capacity is considered more relevant considering future industrial implementation. The application of chemisorption as replacement for the traditional condensation step for ammonia recovery was adopted as the principal technological innovation element of the study. The use of metal halides as absorbers allows for the possibility of solid ammonia storage (like a cartridge). The absorption process step consists of a fixed-bed (based on breakthrough curve). When the bed is fully loaded it is switched with an empty bed. The metal halide, Strontium Chloride (SrCl₂) has been selected as the absorbent (see Section 2.6).

Table 3.1: Decentralized Mini Ammonia Plant

	Decentralized Mini NH₃ Unit
Capacity	60 <i>tons/day</i>
Catalyst	Iron-based
Operating Pressure	Industrial
Feed Conditions	Ambient
NH₃ separation	Fixed bed chemisorption with SrCl ₂

Table 3.1 summarizes the main characteristics of the ammonia synthesis unit selected for the current work.

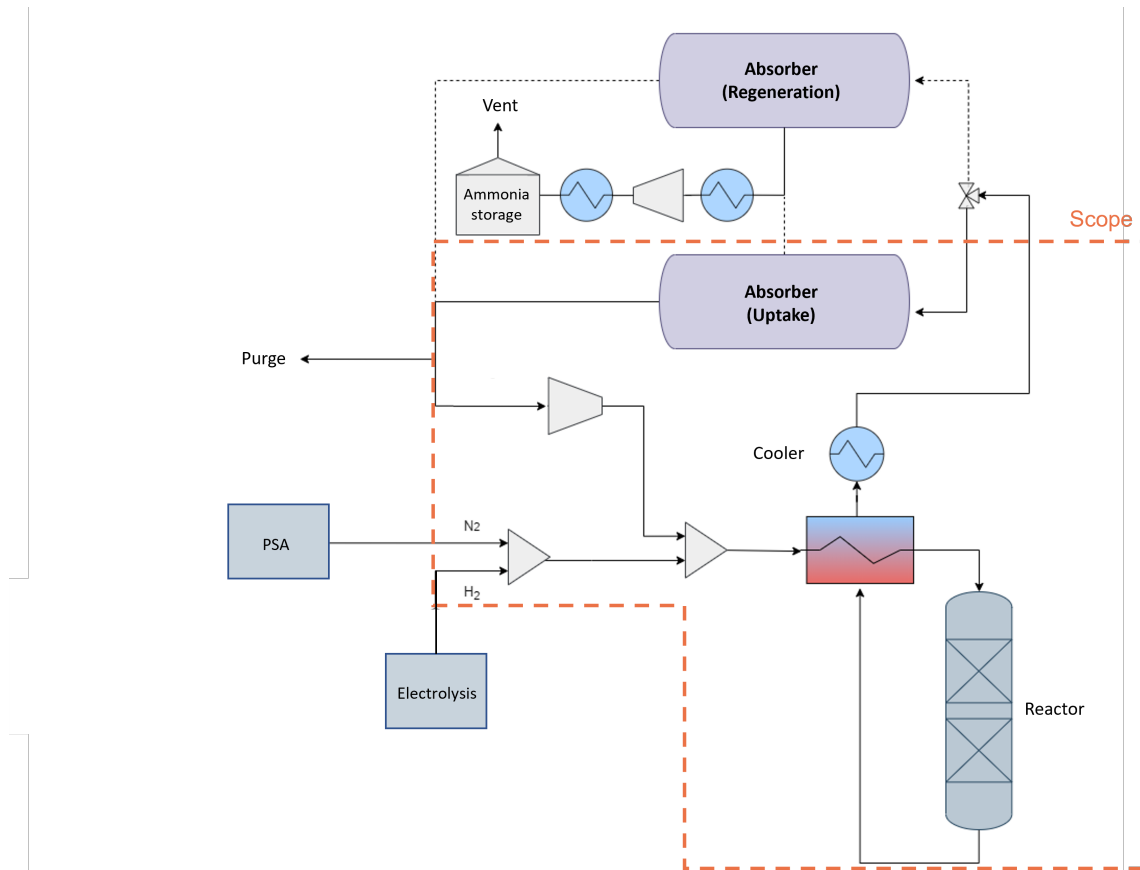


Figure 3.1: Flow Sheet of the Proposed Small-scale Ammonia Plant

Figure 3.1 shows the conceptual process design of the proposed small-scale ammonia plant, including the preparation of reactants and storage of liquid ammonia product. The scope of this thesis work is limited to the ammonia synthesis loop. Therefore, not all components of this flow sheet are included in the simulation models, the orange line represents the scope boundaries for the to-be modelled components.

3.3. Approach

The objective of this work was achieved in three consecutive steps. Figure 3.2 describes each step together with the required inputs and the desired outputs. The first step was creation of a simple steady-state model to determine the thermodynamic limitations and maximum attainable reaction conversion. Next, a more detailed model that incorporates reactor kinetics was composed. The key outputs of the second step is reactor design, absorber design, operating conditions and identification of possibilities for heat integration. Finally, a dynamic model was made for studying the dynamic behavior of the synthesis loop. In this step, two control strategies were developed to aid the synthesis loop in coping with changes in the hydrogen feed streams. The key deliverables of the three models are:

1. Simple Steady-State Simulation

(Gibbs reactor)

- ⇒ Thermodynamic Limitations
- ⇒ Maximum conversion & Productivity reactor

2. Detailed Steady-State Simulation

(Plug-flow reactor with kinetics, absorption enthalpy and heat integration)

- ⇒ Process Conditions
- ⇒ Actual conversion & productivity reactor
- ⇒ Reactor & Absorber Sizing
- ⇒ Cooling Requirements

3. Dynamic Simulation

- ⇒ Control Structure
- ⇒ Dynamic System Behaviour
- ⇒ Response Time

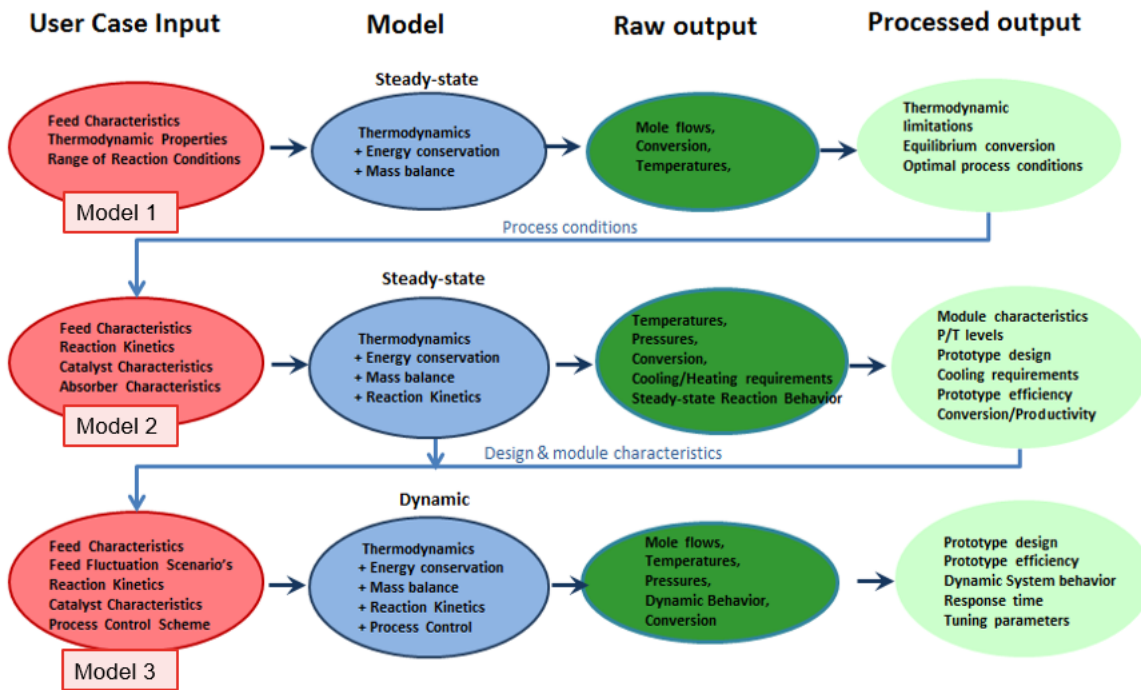


Figure 3.2: Workflow Models Ammonia Synthesis Loop

3.3.1. Assumptions

The following assumptions were made for development of the models:

- The feed streams are assumed to be pure hydrogen and nitrogen.
- The simulation models do not include the production and storage of the reactants or their compression.
- The models only consist of an absorber which separates the ammonia from the recycle continuously. Regeneration of absorber unit was not simulated.
- The storage and liquefaction of ammonia are not included in the simulation.

3.3.2. Scenarios

The control strategies and the effects of variations in the hydrogen feed stream on the synthesis loop were tested under certain scenarios. The hydrogen production by electrolysis is subjected to variations in renewable energy generation. Drops in solar/wind energy generation were expected due to their natural variability. For this work, these variations are assumed to be a one-time reduction for a certain period of time. The hydrogen production is assumed to be directly linked to the reduction in renewable energy. Three such different scenarios with a maximum reduction in the hydrogen feed of 10%, 25% or 50% are anticipated ¹.

¹The mean hourly variation in wind power production depends on the physical location of the site, the time of the year, size of the asset. ~ 25% has been reported as the mean hourly deviation (on an annual basis) in wind power production in the Nordic region [80]. The variability (in terms of magnitude and frequency) in PV output is far greater than for wind turbines. Under broken cloud conditions, ramps as high as 80%/min can occur [81]. Hence, PV-only based ammonia production is not possible unless there's enough molecular and electrical buffer.

3.3.3. Thermodynamic Equation of State

The basis for computation of density as a function of temperature and pressure is presented by an Equation of State (EOS) relation. The Aspen Plus properties database contains several EOS relations, including Peng-Robinson (PR) and Soave-Redlich-Kwong (SRK). Both of these provide a good match for ammonia synthesis at high-pressure conditions for both the vapor and liquid phases [82]. From industrial experience, it has been established that PR and SRK suit oil and gas processing systems very well [83]. The Soave-Redlich-Kwong EOS is also known to perform well in systems with polar components such as ammonia. Further, the SRK-EOS results have been compared to plant data published in Ullmann's Encyclopedia of industrial chemistry" [46]. Satisfactory fit to the data has been reported [84]. The SRK-EOS has also been successfully implemented by Aspen in an ammonia synthesis model [85]. For the present study, SRK has been chosen as Equation of State for the simulation models.

4

Simple Steady state simulation (MODEL 1)

The aim of the first model is to find the thermodynamic limitations and maximum attainable conversion for the synthesis process. This simulation model consists of a GIBBS reactor and a simple species separation block to represent the recycle loop with absorption. The implementation of *MODEL 1* in Aspen Plus is presented in Figure 4.1. A brief description of each of the components is given below.

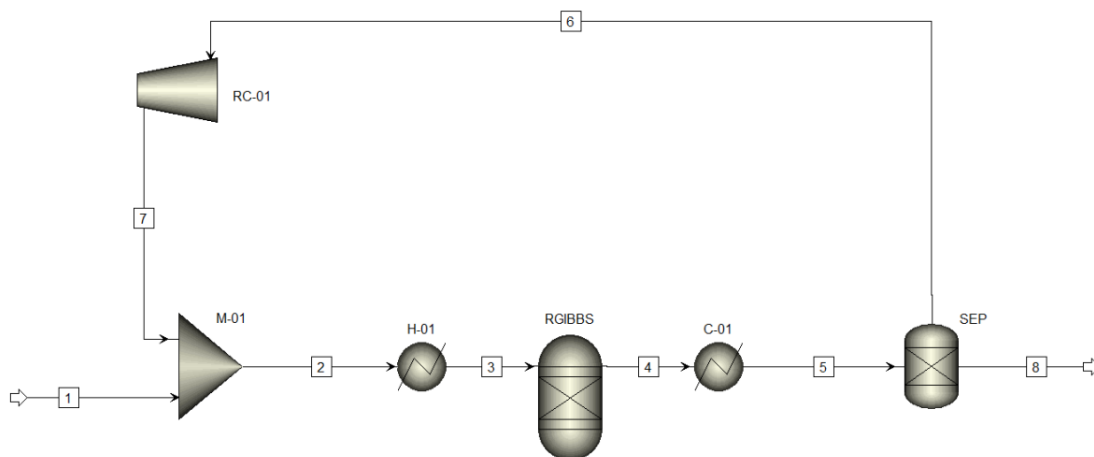


Figure 4.1: *MODEL 1*: Simple Steady-state simulation

4.1. System components

Feed (Stream 1) The feed consists of a mixture of pure streams of H_2 and N_2 in stoichiometric ratio (3:1). The feed stream has a pressure of 200 *bar*, and a temperature of 150 °C. The temperature of 150 °C is used as this is assumed to be the upper limit of the discharge temperature permitted for reciprocal compression equipment.

Mixer (M-01) This is a simple unit operation utilized to combine the make-up/feed stream (stream 1) and recycle stream (stream 7) together to form the feed for the reactor (stream 2).

Heater & Cooler (H-01 & C-01) A heater was implemented to warm up the feed stream before entering the reactor. After the reaction, the outgoing stream needs to be cooled back down to a temperature at which the absorption takes place. In industrial applications, heat between the ingoing and outgoing reactor streams is exchanged, using a heat exchanger device. In this configuration, however, a separate heater and cooler was chosen, as at this phase the focus was on the determination of the thermodynamic equilibrium conditions. As an initial estimate, a 0.5 *bar* pressure drop was assumed for both units.

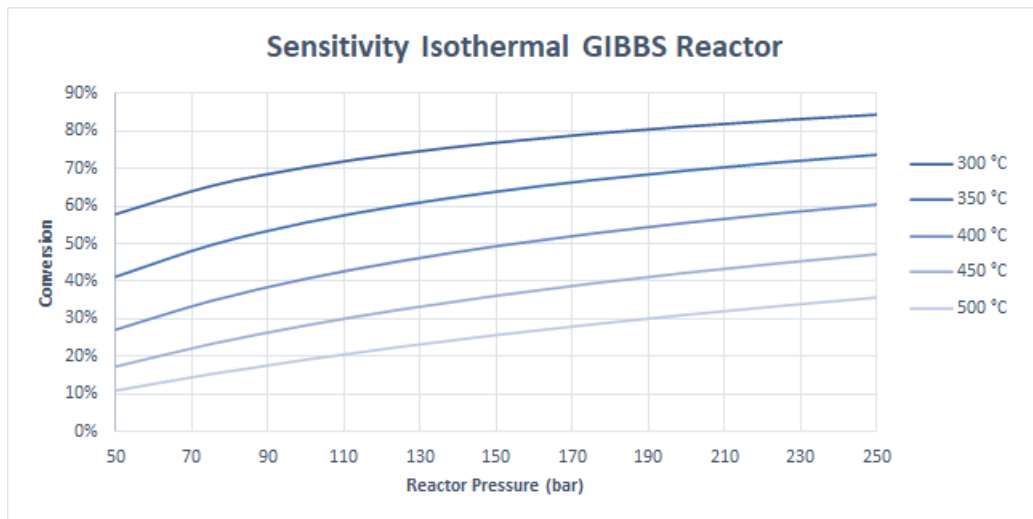


Figure 4.2: MODEL 1: Dependency of conversion on pressure and reactor temperature for an isothermal GIBBS reactor

GIBBS reactor (RGIBBS) A GIBBS reactor solves several equations to find the thermal and chemical equilibrium of the components by minimizing the Gibbs Free Energy [86], depending on temperature and pressure conditions. This unit type does not take into account the reaction kinetics. Both adiabatic and isothermal operation were selected for the reactor resulting in two different simulation scenarios.

Separation block (SEP) To represent the absorber, a separation block was adopted. This block implements a split between components and requires only the recycled components (H_2 , N_2) and component(s) that leave the system (NH_3) to be specified. This type of logical operation is not a physically realistic but is useful to simplify the simulation for the separation step.

Recycle compressor (RC-01) The unreacted nitrogen and hydrogen are recycled back and combined with the feed. An isentropic compressor with a discharge pressure of 200 bar has been implemented to bring the recycle flow up to the required feed pressure.

4.2. Exploring the Dependency of Conversion on Pressure and Temperature

Following the finalization of the simulation model, a sensitivity analysis was carried out to evaluate the conversion as function of the pressure and temperature in the reactor. This sensitivity has been performed for both adiabatic as isothermal reaction conditions. Reaction conversion is referred to as the amount of reactants that have converted into products, divided by the amount of reactants before reaction, as given by:

$$X_A = \frac{n_A(t=0) - n_A(t)}{n_A(t=0)} \quad (4.1)$$

For ammonia synthesis, the conversion percentage defined on the basis of nitrogen is given by:

$$X_{N_2} = \frac{\text{Amount of } N_2 \text{ consumed}}{\text{Initial amount of } N_2} \times 100\% \quad (4.2)$$

The relationship between the calculated conversion and the temperature or pressure of the reactor is given in Figure 4.2 for an isothermal reactor and in Figure 4.3 for an adiabatic reactor.

An isothermal reactor is maintained at a constant temperature whereas, an adiabatic reactor does not transfer heat across the system boundary. Ammonia synthesis is an exothermic process. The conversion of the adiabatic reactor is stronger limited by the reaction equilibrium than the isothermal reactor because of the temperature rise.

It is clear from figures 4.2 and 4.3 that high pressure and low temperature are preferred if the ammonia synthesis reaction is limited by equilibrium. However, a trade-off exists between the selection of a suitable temperature and pressure for a desired conversion, as discussed in literature (Section 2.1). Selecting a temperature too low will lead to slow kinetics of the reaction, while at high temperatures

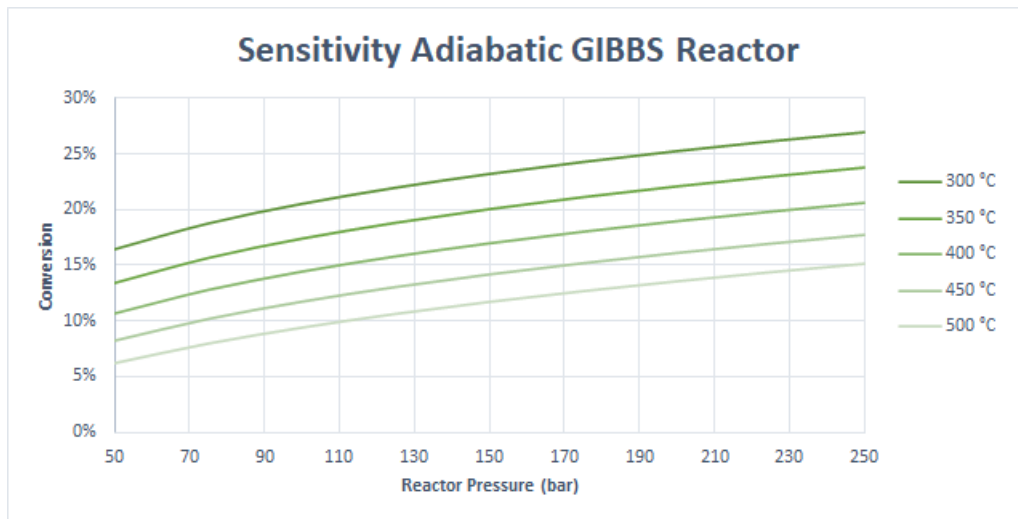


Figure 4.3: *MODEL 1*: Dependency of conversion on pressure and feed temperature for an adiabatic GIBBS Reactor

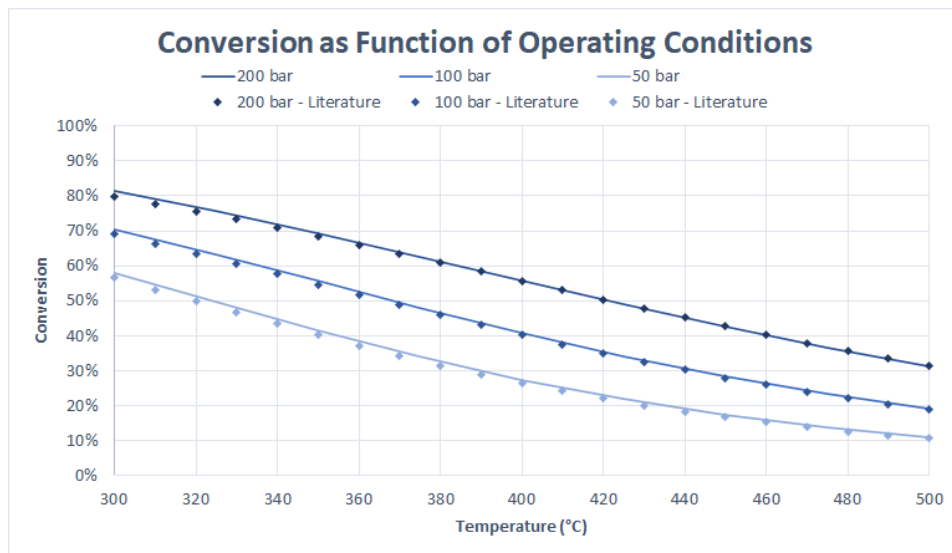


Figure 4.4: Validation *MODEL 1* (Literature data from Max Appl)

Source: [46]

the reaction will proceed quickly but is constrained by thermodynamic equilibrium. Similarly, choosing an insufficient or large system pressure can have repercussions as well. A low pressure will inhibit the NH_3 production and a high pressure will cause high power consumption rates and equipment costs. In general, the optimal operating conditions will be different for an adiabatic and an isothermal reactor.

4.3. Model validation

Literature data [46] for the Ammonia content in equilibrium with reactants for a reactant ratio $\text{H}_2:\text{N}_2$ of 3:1 was compared with simulation results obtained with the model with isothermal GIBBS reactor. This data, calculated from the Gillespie & Beattie equilibrium correlation [31], was converted to a conversion % as follows:

$$\text{Conversion} = \frac{2 \times \text{Mole fraction } \text{NH}_3}{(1 + \text{Mole fraction } \text{NH}_3)} \quad (4.3)$$

Figure 4.4 is a plot of the reaction conversion as a function of temperature for the simulation results with isothermal reactor and literature data. A close resemblance is observed, by which the simulation model is considered to be validated.

4.4. Key takeaways

- ⇒ **Takeaway:** For ammonia synthesis, the reaction in an adiabatic GIBBS reactor is strongly limited by the exothermic heat of reaction. Therefore, the conversion for an isothermal GIBBS reactor is significantly higher for a given operating pressure.
- ⇒ **Takeaway:** For a desired ammonia production capacity, a balance exists between the operating conditions (temperature and pressure) and the economics of the system. This balance also depends on the type of reactor (adiabatic or isothermal) type.
- ⇒ **Takeaway:** In order to determine a suitable set of operating conditions of the system and selection of reactor type, reaction kinetics have to be included. It is also important to consider other aspects affected by design decisions, such as power consumption, equipment costs and required reactor/catalyst volume.

5

Detailed Steady state simulation (*MODEL 2*)

The second model, including reactor kinetics, was used to attain the operating conditions and reactor design parameters. Additionally, this simulation model provided cooling requirements, heat integration possibilities and absorber design. At the end of this chapter these mentioned results were taken from the simulation models. To achieve these results the following steps were undertaken:

- The kinetic equation was established
- The reactor configuration was determined
- A heat-exchanger was implemented
- The absorber was simulated

This model is based on *MODEL 1* but with three major differences. Simulation *MODEL 2* has a reactor that incorporates a rate equation, heat integration and an absorption unit that represents reality more closely. The reactor was simulated as a fixed-bed ammonia reactor with catalyst which requires the implementation of the rate equation for the reaction. To simulate this type of reactor, a PLUG FLOW reactor was selected in Aspen Plus. For a better comparison with industrial plants, a heat-exchanger is included to improve heat integration by exchange of heat between the inlet and outlet streams of the reactor. For the absorber, the enthalpy of the chemisorption reaction was incorporated using a stoichiometry reactor to account for heat released in the absorption process.

5.1. Reactor kinetics

5.1.1. Selection of rate equation

In a PLUG FLOW reactor, a rate equation expresses the kinetics of the ammonia reaction. Literature study has shown that there are three commonly used rate equations. These are: Temkin-Pyzhev, Dyson & Simon and Nielsen et al. The Temkin-Pyzhev equation is broadly assumed to represent the ammonia reaction at regular industrial conditions [87] with reasonable accuracy. The other two relations are essentially improvements of the Temkin-Pyzhev equation. The selection of these three equations is supported by application reported by various authors [88] [89] [90], as well as Aspen Plus's internal ammonia synthesis simulation [85].

The three selected equations and their respective parameters are summarized in Table 5.1.

The relations have a forward and a backward reaction rate term. These terms are dependent on partial pressures, catalyst activity factors and reaction rate frequency constants. The Temkin-Pyzhev accounts for the influence of composition by partial pressures, whereas the other equations utilize component activities. The Dyson & Simon equation expresses the ratio of forward and backward rate using an equilibrium constant (K_{eq}).

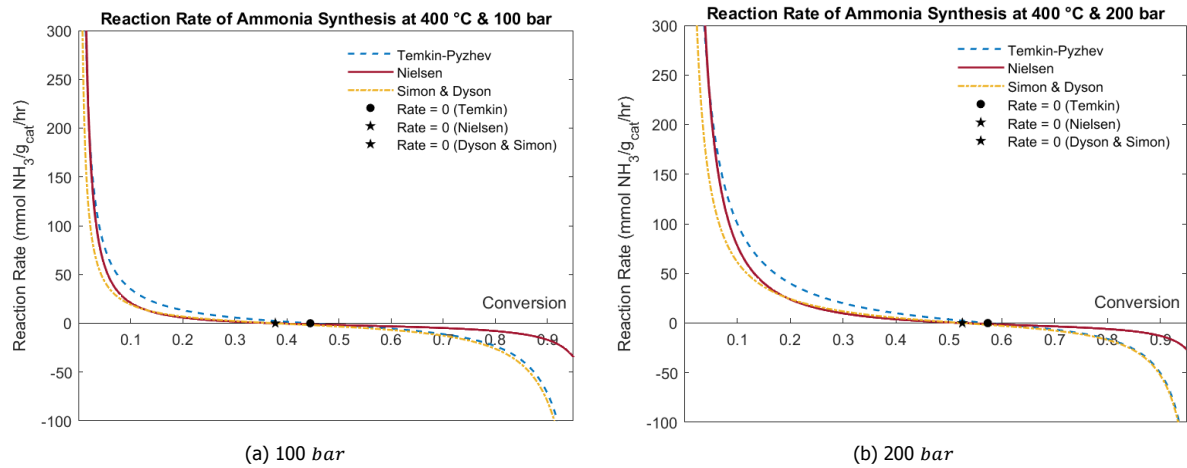


Figure 5.1: Reaction rate of ammonia synthesis plotted versus conversion for various equations

Table 5.1: Selected rate equations and parameters

Name	Equation [$kmol NH_3/m^3 h$]	Parameters	Source
Temkin-Pyzhev	$r_{NH_3} = 2fk_f P_{N_2} \left(\frac{P_{H_2}^3}{P_{NH_3}^2} \right)^\alpha - k_b \left(\frac{P_{NH_3}^2}{P_{H_2}^3} \right)^{1-\alpha}$	$k_f = 1.79 \times 10^4 e^{-87,090/RT}$ $k_b = 2.57 \times 10^{16} e^{-198,464/RT}$ $\alpha = 0.5$ $f = 4.75$ (Catalyst activity factor)	[91]
Dyson & Simon	$r_{NH_3} = k_b \left(K_{eq}^2 a_{N_2} \left(\frac{a_{H_2}^3}{a_{NH_3}^2} \right)^\alpha - \left(\frac{a_{NH_3}^2}{a_{H_2}^3} \right)^{1-\alpha} \right)$	$k_b = 1.7698 \times 10^{15} e^{-170,560/RT}$ K_{eq} (Gillespie & Beattie [31]) $\alpha = 0.5$	[66]
Nielsen	$r_{NH_3} = A_c \left[\frac{AK \left(K_{eq}^2 a_{N_2} - \frac{a_{NH_3}^2}{a_{H_2}^3} \right)}{\left(1 + K_a \frac{a_{NH_3}}{a_{H_2}} \right)^{\frac{2\alpha}{\alpha}}} \right]$	$AK = 3.945 \times 10^{10} e^{-\frac{5622}{T}}$ $K_{ad} = 2.94 \times 10^{-4} e^{\frac{12104}{T}}$ K_{eq} (Gillespie & Beattie [31]) $\alpha = 0.654$ $w = 1.523$ $A_c = 1$ (Catalyst activity factor)	[85]*

*The misprint in equation from source has been corrected here

The equation from Nielsen et al. also incorporates an equilibrium term, as well as a rate term ($AK =$ specific rate constant) and a catalyst activity factor. The additional adsorption term ($K_{ad} =$ adsorption equilibrium constant) in the denominator considers the inhibition of nitrogen adsorption to the catalyst surface due to adsorption of hydrogen and ammonia. This term eliminates division-by-zero issues with the reaction rate when the concentration of ammonia is very low.

The three selected rate equations were plotted at 100 & 200 bar and 400 °C in MATLAB® for comparison in Figure 5.1 for a hydrogen to nitrogen mole fraction ratio of 3.

Observations

- ⇒ For an NH_3 mole fraction of zero, the reaction rate of Temkin-Pyzhev and Dyson & Simon is infinite. This property is expected to be a cause of complications for the Aspen dynamic solver. The reaction rate equation of the Nielsen eliminates this problem by the composition of the denominator. However, for an NH_3 mole fraction of zero, the reaction rate is around 25,000 $mmol NH_3/g_{cat}/hr$ at 200 bar which is suspected to be unrealistically high.
- ⇒ Nielsen and Dyson & Simon both use the equilibrium correlation of Gillespie & Beattie to determine the equilibrium. As a consequence, both equations have the same equilibrium point marked with a star symbol ★, whereas the Temkin-Pyzhev is marked with a dot •.
Equilibrium conversion at 100 bar: ★ = 0.378, • = 0.445
Equilibrium conversion at 200 bar: ★ = 0.526, • = 0.574

Figure 5.2 displays the three equation rates as a function of the conversion at 200 bar for different values of the catalyst activity factor f of the Temkin-Pyzhev equation.

(a) $f = 3$ (b) $f = 3.5$

Figure 5.2: Reaction rate of ammonia synthesis plotted versus conversion for various equations at 200 bar

Observations

- ⇒ For an activity factor of $f = 3$, the forward reaction rate of Temkin-Pyzhev is almost equal to the Dyson & Simon's forward reaction rate (shown in Figure 5.2a).
- ⇒ Further, for an activity factor $f = 3.5$, all three forward reaction rate lie close to each other and have comparable shapes in the range depicted, as shown in Figure 5.2b.

Conclusion The shape of the forward reaction rate-curves is similar for the three considered kinetic models at conversion values not close to zero. The Nielsen equation is best suited for the Aspen PLUG FLOW reactor, as it allows for an NH_3 inlet concentration of zero without alterations. Both Nielsen and Dyson & Simon describe the equilibrium more accurately than Temkin-Pyzhev, as they have the equilibrium conditions integrated into the rate equation. However, equilibrium is determined by a correlation that depends on the temperature in the reactor, which is constantly changing. Determination of the correlation into an Aspen Plus simulation requires employing computationally demanding User Kinetics Routines in Excel or Fortran, which may cause complications in dynamic studies of the of the system.

5.1.2. Modified Temkin LHHW equation

For kinetics, Temkin-Pyzhev equation is the most well-known equation and has been widely used ever since its introduction in 1940. For this reason, it was selected as kinetics model for the present study. However, the Temkin-Pyzhev equation has two important disadvantages for the application in this study.

1. Firstly, the reaction rate approaches infinity when the mole fraction of NH_3 in the feed reaches zero. This is not realistic.
2. Secondly, the Temkin-Pyzhev equation consists of a forward and backward reaction term, each with their own reaction rate constant, K_1 and K_2 . At the equilibrium conditions, these terms should cancel each other out and result into a net reaction rate of zero. The reaction rate constants are experimentally established at fixed temperature and pressure. This leads to an inaccurate description of the equilibrium conditions, especially for a wider temperature and pressure range.

To overcome these limitations, a transformation of the equation was carried out, removing the two disadvantages. The transformation is discussed in the following sections.

Solution 1st Drawback The first drawback could be solved by application of a multiplication factor X [92]:

$$X = \frac{K_3 P_{\text{NH}_3}}{(1 + K_3 P_{\text{NH}_3})} \quad (5.1)$$

where $K_3 = 2 \text{ atm}^{-1}$ [92].

This alteration casts the equation into the so-called LHHW format, which is formulated as follows:

$$r = \frac{(\text{Kinetic factor})(\text{Driving force expression})}{(\text{Adsorption expression})} \quad (5.2)$$

For a reversible reaction (say $A + B \leftrightarrow C + D$), the LHHW expression can be re-written as:

$$r = \frac{k_f [A][B] - k_b [C][D]}{\text{Adsorption expression}} \quad (5.3)$$

Temkin-Pyzhev is multiplied by multiplication factor X 5.1:

$$X \times \frac{2f}{\rho_{cat}} \left(\frac{k_f P_{\text{N}_2} P_{\text{H}_2}^{1.5}}{P_{\text{NH}_3}} - \frac{k_b P_{\text{NH}_3}}{P_{\text{H}_2}^{1.5}} \right) \quad (5.4)$$

Resulting in the following rate equation, the LHHW form of the Temkin-Pyzhev:

$$r = \frac{2f}{\rho_{cat}} K_3 \frac{k_f P_{N_2} P_{H_2}^{1.5} - \frac{k_b P_{NH_3}^2}{P_{H_2}^{1.5}}}{1 + K_3 P_{NH_3}} \quad \text{with } k = k_0 \cdot e^{\frac{-E}{RT}} \quad (5.5)$$

Plots of both equations, Temkin-Pyzhev (Powerlaw-like) and Temkin-Pyzhev (LHHW) are depicted in Figure 5.3. It proves that the factor indeed eliminates the unfavorable behavior at very low ammonia concentrations, while the reaction rate remains unaltered for higher concentrations.

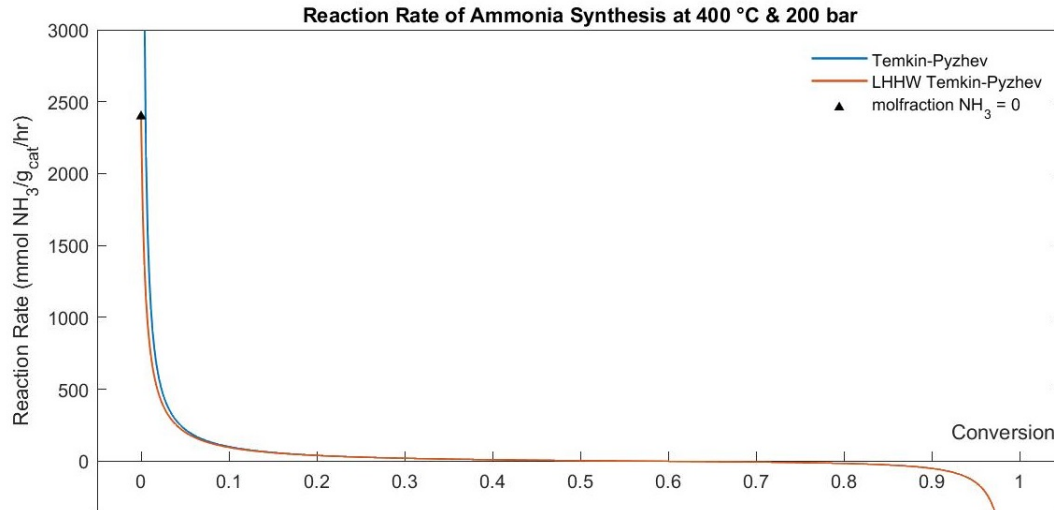


Figure 5.3: Reaction Rate (p,T) vs. Conversion at 400 °C & 200 bar

A validation was performed by comparison of this Langmuir-Hinselwood-Hougen-Watson equation with literature data [93]. Under the same conditions, an adiabatic plug flow reactor was simulated in Aspen Plus using the LHHW kinetic equation. The resulting Conversion vs. Pressure and Conversion vs. Feed temperature plots were compared to data from literature. There was found to be satisfactory fit. Details of the comparison are provided in in Appendix A.1.

Solution 2nd Drawback

The second drawback of Temkin-Pyzhev related to inaccurately representing the equilibrium was solved by adjusting the forward and backward rate constants. To create an equation that better describes the equilibrium conditions, an equilibrium correlation is required. For this, the data correlation from Haber & Le Rossignol (1908) [94] was selected:

$$K_a(T) = 10^{2.10 + \frac{1}{4.571} \left(\frac{9591}{T} - 0.00046T + 0.85 \cdot 10^{-6} T^2 \right) - \frac{4.98}{1.985} T} \quad atm^{-1} \quad (5.6)$$

Even though the Gillespie & Beattie correlation for the ammonia equilibrium is widely applied, it has been derived from a wider range of pressure and temperature (10-1000 atm, 325-952 °C). In this work, therefore it has been decided to use the correlation from Haber & Le Rossignol which uses data points from a smaller pressure range (1-200 atm), more specific to the application in this work. The Haber & Le Rossignol was also found to have an excellent fit to the experimental data at 200 atm and between 300 to 600 °C. Further details on the correlation of equilibrium conditions are given in the Appendices A.2 and A.3.

The Haber & Le Rossignol correlation is rewritten into the form of $e^{-E/RT}$. This results in Equation 5.7, which can then be combined with Equation 5.5.

$$K_a(T) = \frac{e^{\frac{53}{RT}}}{9.8 \cdot 10^5} \quad bar^{-1} \quad (5.7)$$

Appendix A.4 elaborates further on this adaptation.

Derivation of the Modified LHHW

Equation 5.8 gives the LHHW form of Temkin-Pyzhev equation (Equation 5.5) with the forward and backward rate terms expanded.

$$r = \frac{2fK_3 \left(k0_f e^{-\frac{E_f}{RT}} P_{N_2} P_{H_2}^{1.5} - \frac{k0_b e^{-\frac{E_b}{RT}} P_{NH_3}^2}{P_{H_2}^{1.5}} \right)}{\rho_{cat} (1 + K_3 P_{NH_3})} \quad (5.8)$$

At equilibrium conditions, the reaction rate is zero ($r = 0$) and the forward and backward reaction rate are equal ($r_f = r_b$), which reduces Equation 5.8 to:

$$\frac{k0_f \exp\left(\frac{-E_f}{RT}\right)}{k0_b \exp\left(\frac{-E_b}{RT}\right)} \cdot \frac{P_{N_2} P_{H_2}^3}{P_{NH_3}^2} = 1 \quad (5.9)$$

On the basis of stoichiometry, the equilibrium for ammonia synthesis reaction is given by Equation 5.10.

$$K_{eq} = \frac{P_{NH_3}}{P_{N_2}^{0.5} \cdot P_{H_2}^{1.5}} \quad (5.10)$$

Substituting Equation 5.10 in Equation 5.9 results in:

$$\frac{k0_f}{k0_b} \cdot e^{-\frac{E_f + E_b}{RT}} = K_{eq}^2 \quad (5.11)$$

The simplified data correlation from Equation 5.7 ($K_{eq} = \frac{\exp(\frac{53}{RT})}{9.8 \cdot 10^5}$), is then substituted to give the following result:

$$\frac{k0_f}{k0_b} \cdot e^{-\frac{E_f + E_b}{RT}} = \left(\frac{e^{\frac{53}{RT}}}{9.8 \cdot 10^5} \right)^2 \quad (5.12)$$

From this relation, the 'adjusted' parameter values (k_f, E_f) can be derived in order to satisfy the equilibrium condition ($R = 0$ and $R_f = R_b$).

$$k0_{b,mod} = 1.72 \cdot 10^{16} \text{ kmol/m}^3 \text{ hr}$$

$$E_{b,mod} = 193,085 \text{ J/mol}$$

By substitution of these values in Equation 5.8, we arrive at what in this work is referred to as the Modified Temkin-Pyzhev LHHW Equation or in short, Modified LHHW. The obtained expression is expected to a suitable kinetics model for dynamic reactor simulations in Aspen.

$$R = \frac{2fK_3 \left(k0_f e^{-\frac{E_f}{RT}} P_{N_2} P_{H_2}^{1.5} - \frac{k0_b e^{-\frac{E_b}{RT}} P_{NH_3}^2}{P_{H_2}^{1.5}} \right)}{\rho_{cat} (1 + K_3 P_{NH_3})} \quad \left[\frac{\text{mmolNH}_3}{\text{g}_{cat} \text{hr}} \right] \quad (5.13)$$

with

$$k0_f = 1.79 \cdot 10^4 \text{ kmol/m}^3 \text{ hr}$$

$$E_f = 87,085 \text{ kgm}^2/\text{s}^2 \text{ mol}$$

$$k0_b = 1.72 \cdot 10^{16} \text{ kmol/m}^3 \text{ hr}$$

$$E_b = 193,085 \text{ J/mol}$$

$$K_3 = 2 \text{ atm}^{-1}$$

$$f = 4.75$$

The activity factor f used here, was determined by Morud & Skogestad (1998) [89] and is based on data from an industrial ammonia plant.

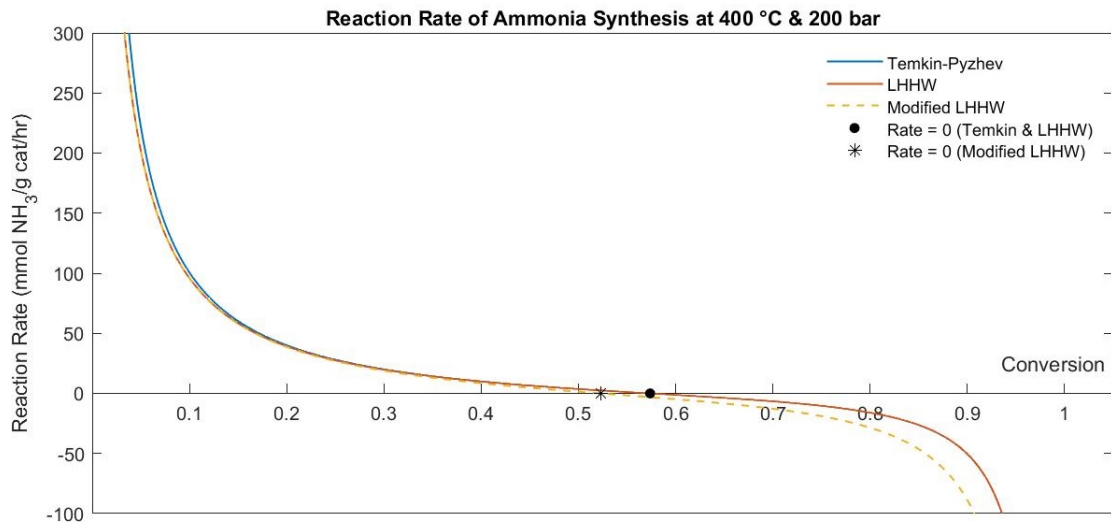


Figure 5.4: Reaction Rate (p,T) vs. Conversion at 400 °C & 200 bar

As a result of the alterations, a new variant of the Temkin-Pyzhev was obtained. This variation is suitable for an NH_3 inlet concentration of (close to) zero and describes the equilibrium with better accuracy. The reaction rate predicted by the Modified LHHW is plotted as a function of conversion in Figure 5.4. The original Temkin-Pyzhev equation is also shown for comparison. It is clear that the Modified LHHW equation does not deviate much from the original Temkin-Pyzhev equation in the forward reaction rate, yet both obstructions for application to dynamic process simulations have been resolved. In addition, the Modified LHHW provides ease of implementation in the simulations since the LHHW format is supported in Aspen Plus without the need for any additional programming.

Validation of equilibrium

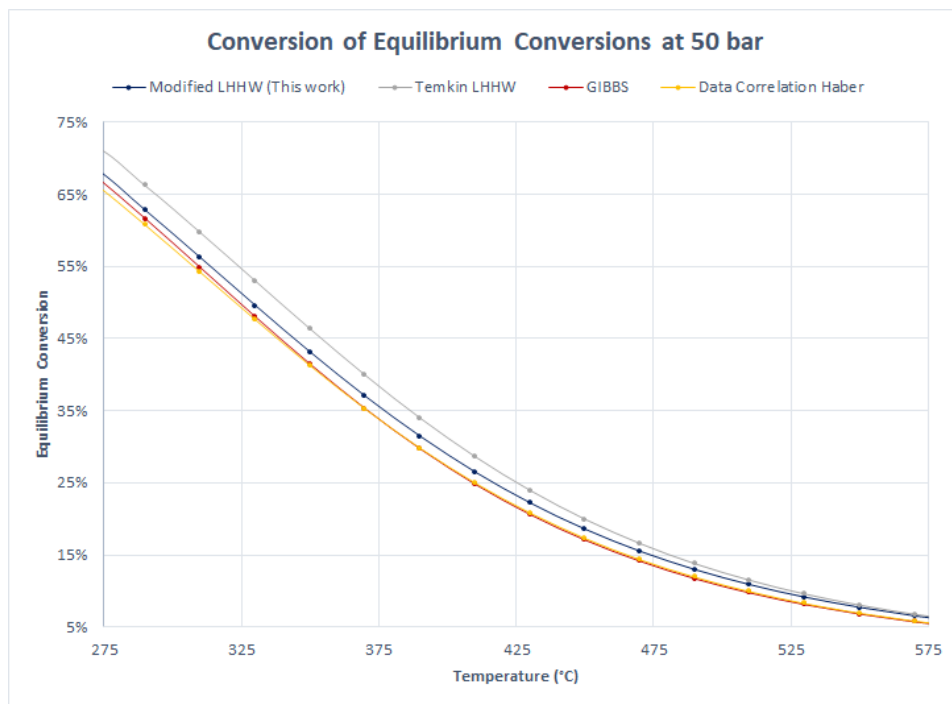
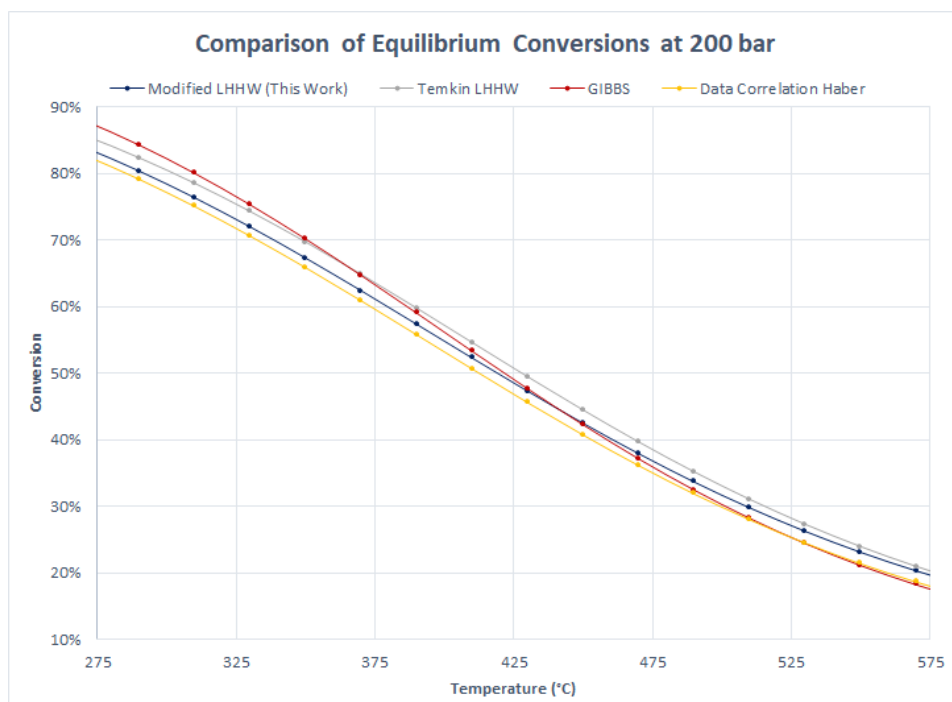
Before proceeding with this equation, a validation was performed to analyze whether the kinetic model indeed adequately predicts the equilibrium composition over a range of conditions. This was done by plotting the Equilibrium conversion vs. Temperature for reactors in Aspen Plus based on:

- Minimization of Gibbs Free Energy - RGIBBS
- Temkin-Pyzhev (LHHW form) - Infinite RPLUG
- Modified Temkin-Pyzhev (LHHW form) - Infinite RPLUG

As a reference the data correlation from Haber & Le Rossignol [94] was also included. For the PLUG FLOW reactor simulations, the reactors were given an infinite length. This excluded the simulation to be kinetic limited and resulted in giving the maximum equilibrium conversion under the operating conditions.

The Temkin-Pyzhev (LHHW form) was expected to have the lesser accuracy in representation of the equilibrium because it depends on two constants (forward and backward rate constants) that were experimentally established only at certain process conditions. The GIBBS reactor was predicted to have a better result since this correlation determines the conversion by minimizing the Gibbs free energy for each temperature and pressure. Compared to the latter two, the Modified LHHW from this work is expected to present an equilibrium conversion closer to the reference correlation from Haber, due to the incorporation of equilibrium correlation (based on experimental data) in the rate equation.

The equilibrium conversion as function of the reactor temperature (isothermal) for the three cases and reference correlation have been plotted at 50 and 200 bar (Figure 5.5 and Figure 5.6 respectively). These figures illustrate that indeed the Temkin LHHW equation demonstrates the most deviation from the reference correlation. Compared to this, the GIBBS free energy correlation gives a better result. It was also concluded that the Modified Temkin LHHW equation predicts the equilibrium with acceptable accuracy.

Figure 5.5: Validation Modified LHHW at 50 *bar*Figure 5.6: Validation Modified LHHW at 200 *bar*

⇒ **Takeaway:** The Temkin-Pyzhev rate equation was successfully modified to establish an equation that satisfactorily describes the equilibrium, has no issues with low NH_3 mole fractions, and provides ease of implementation in Aspen Plus due to its LHHW format.

5.2. Reactor configuration

The conversion of ammonia synthesis is not only dictated by catalyst activity but also by the operating conditions in the loop, as discussed in Chapter 4. The conversion is furthermore affected by the feed ratio of $H_2:N_2$, the flow velocity and the reactor type.

In industrial practice, catalyst activity is commonly characterized by a parameter referred to as SV, which is defined by:

$$\text{Space Velocity} = \frac{\text{Volumetric Flow Rate of Reactants at STP}}{\text{Volume of Catalyst}} \quad (5.14)$$

The production rate of ammonia in the reactor is directly linked to the space velocity. The typical relationship between reactor conversion and space velocity is depicted in Figure 5.7 for various catalysts. The flow rate of the reactants, which is governed by the recycle flow, and the volume of the catalyst both determine the space velocity. In industrial applications, the space velocity is commonly increased to improve the production capacity of the reactor and reducing the required reactor volume and amount of catalyst. However, there exists a balance since increasing the recycle flow will suppress the synthesis efficiency and result in a higher pressure drop. This eventually leads to cooling of the recycle gas and a higher power utilization in the recycle compressor and ammonia separation.

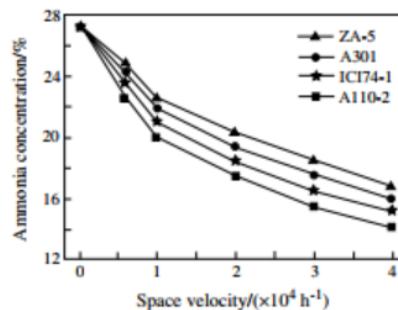


Figure 5.7: Activity vs. Space Velocity of ZA-5, A301, ICI74-I and A110-2 Catalyst ($P = 150 \text{ bar}$, $T = 425 \text{ }^\circ\text{C}$)

Source: [25]

Table 5.2 summarizes some key parameters of industrial ammonia production processes of industrial plants. The space velocities of these industrial plants served as a reference to determine the reactor size for the current study. The next sections provide additional information on the influence of space velocity and several other design aspects of the reactor on the conversion.

Table 5.2: Plant Data from Various Industrial Haber-Bosch Plants

Processes	Small and medium	Kellogg	Industrial scale	Braun	ICI-AMV
	scale ammonia plants		Topsøe		
Pressure (MPa)	31.38	14.7	26.5	15	10.3
Space Velocity (hr^{-1})	20,000	10,000	12,000	7,600	4,000
Inlet content inert gas at reactor (%)	18	13.6	2	1-2	8.8
Inlet ammonia concentration (%)	2	2.17	3.63	4	4.18
Outlet ammonia concentration (%)	10-12	12.03	16.0	21	17.18
Conversion (%)	15-18	18	22	29	23

Ammonia synthesis catalysts: innovation and practice [25]

5.2.1. Isothermal vs. Adiabatic Reactor Behaviour

The first design choice is whether to select an isothermal reactor that is maintained at a constant temperature or an insulated adiabatic reactor without heat losses to the environment. Accordingly, ammonia mole fraction versus length coordinate of the reactor bed¹ for single pass adiabatic and isothermal reactors was analyzed under influence of different space velocity and inlet temperature values. The simulation was done for a single-pass, where the volumetric flow rate of the reactants

¹In this work, the graphic showing the ammonia mole fraction versus various positions along the reactor bed will be referred to as the *reactor profile*.

remained almost constant. The space velocity was varied by changing the reactor volume without changing the feed flow rate. Figures 5.8a and 5.8b illustrates the adiabatic and isothermal reactor profiles (ammonia mole fraction versus position along the reactor bed) for a space velocity of $\sim 25,000 \text{ hr}^{-1}$ at $300 \text{ }^\circ\text{C}$ and $400 \text{ }^\circ\text{C}$. Figure 5.9a and 5.9b shows the same at a space velocity of $\sim 50,000 \text{ hr}^{-1}$.

The space velocities might seem quite high compared to industrial values. This is because the analysis was done for a single stage reactor, whereas industrial plants commonly make use of the multi-stage reactor with intercooling or cold shot. Meaning the total volume of these multiple stages will be greater. In such plants, two or three (adiabatic) reactors are placed sequentially, each reactor increases slightly in volume. After each stage, when the reaction has reached its equilibrium, the stream is cooled down to break this equilibrium before it enters the next stage.

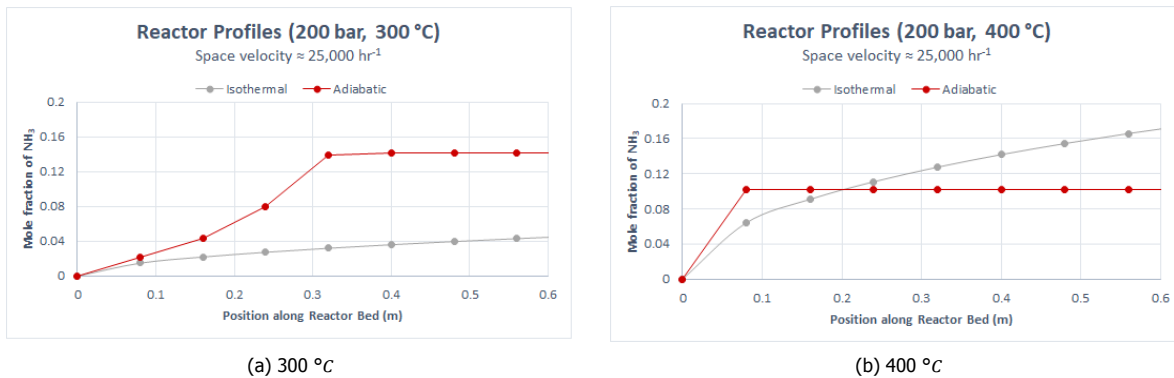


Figure 5.8: Space Velocity of $25,000 \text{ hr}^{-1}$

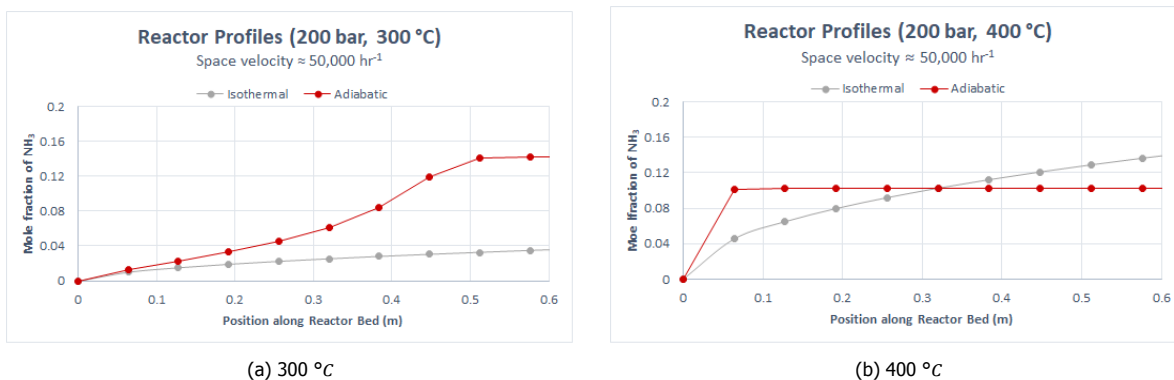


Figure 5.9: Space Velocity of $50,000 \text{ hr}^{-1}$

The following conclusions can be drawn from the reactor profiles with respect to the influence of space velocity and temperature on the conversion:

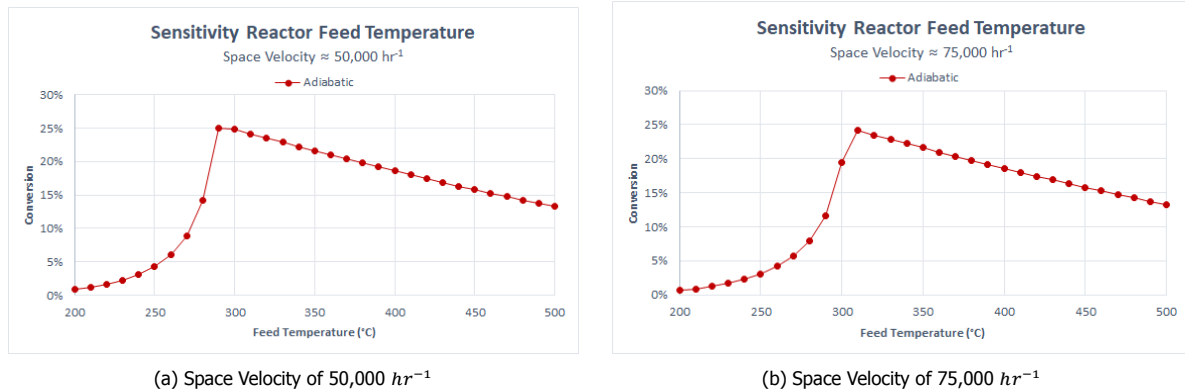
- ⇒ **Takeaway:** Adiabatic reactor reaches a maximum conversion much faster than an isothermal reactor. An adiabatic reactor has a lower maximum conversion than an isothermal reactor. This is due to the effect on the equilibrium of the heat that is formed during the reaction.
- ⇒ **Takeaway:** An isothermal reactor operates better under a higher reactor temperature because of the influence of temperature on kinetics, whereas an adiabatic reactor performs better for a lower inlet temperature.
- ⇒ **Takeaway:** Depending on the diameter, there is a minimum required reactor length to reach equilibrium. It is important to not make the reactor longer than necessary, especially for an adiabatic reactor as it has a much lower equilibrium value.
- ⇒ **Takeaway:** At the same operating conditions, an isothermal reactor requires a bigger catalyst volume to reach the maximum possible conversion.

In this work, an adiabatic reactor was selected because the mechanical design of this reactor is considerably simpler, especially at high pressures, and because scale-up is easier.

Furthermore, a radial flow configuration was selected, and length vs. diameter ratio was fixed at a value of 8. For the sake of simplicity, it was decided that no "cold shot" intercooling will be modeled.

5.2.2. Reactor inlet temperature (Adiabatic reactor)

The effect of feed inlet temperature on the reactor conversion was also investigated. Figure 5.10a and Figure 5.10b show the conversion as function of different feed temperatures at space velocities of $\sim 50,000$ and $\sim 75,000 \text{ hr}^{-1}$ respectively. A sharp maximum conversion is noticed in both curves at a feed temperature of approx. $300 \text{ }^\circ\text{C}$. Before reaching this maximum, the conversion is governed by reaction kinetics, whereas after this point the thermodynamic equilibrium is the dominant factor.



(a) Space Velocity of $50,000 \text{ hr}^{-1}$

(b) Space Velocity of $75,000 \text{ hr}^{-1}$

Figure 5.10: Influence of Reactor Inlet Temperature on the Conversion, $p = 200 \text{ bar}$

Figure 5.11 shows the reactor profile with two feed inlet temperatures for an adiabatic reactor with a space velocity of $50,000 \text{ hr}^{-1}$. In conjunction with Figure 5.10a, this figure proves that:

- Temperature lower (even 15%) than the optimum reactor inlet temperature, inhibits the acceleration of the reaction, resulting in a low conversion.
- At a higher than optimal reactor inlet temperature, the speed of the reaction is high but the conversion is limited by the thermodynamic equilibrium.

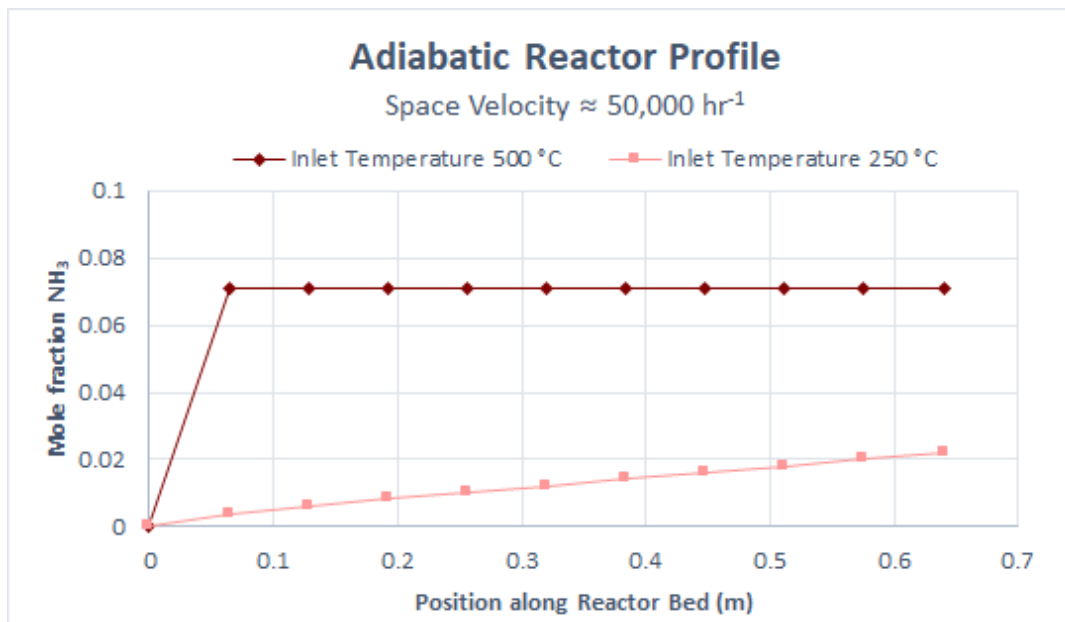


Figure 5.11: Adiabatic reactor profiles at inlet temperature of $250 \text{ }^\circ\text{C}$ vs. $500 \text{ }^\circ\text{C}$

From the discussion, the following can be concluded:

- ⇒ **Takeaway:** The inlet feed temperature is critical for the design of the system as the conversion is strongly influenced by the reactor inlet temperature.

⇒ **Takeaway:** For given reactor dimensions and operating conditions, an optimum feed temperature value exists for reaching the highest possible conversion.

5.2.3. Reactor Dimensions

Catalyst Another important factor for reactor design is the catalyst and its properties. It was decided to focus the study on conventional iron-based catalyst at operation conditions within the industrial range. Several industrial iron catalysts with typical performance properties, such as the activation temperature² and heat-resistant temperature,³ are shown in Table 5.3. Operation at temperatures outside this catalyst activity range impairs the catalyst performance. For this application, the ZA-5 iron catalyst was selected due to its low activation temperature of 300 °C. The heat-resistant temperature for all catalyst is the same, 500 °C. These temperature limitations pose restrictions on the system and must be taken into consideration while designing the reactor.

Table 5.3: Operating Temperatures of Various Iron Ammonia Catalysts

Type	Activation Temperature (°C)	Heat-resistant Temperature (°C)
A110	370	500
A201	360	500
A301	325	500
ZA-5	300	500

[25]

For the selected catalyst (wüstite-based, ZA-5), a bulk density of 2200 kg/m³ was taken, along with a bed voidage⁴ of 0.33 based on literature ([95] [89]).

It has been shown earlier that the optimal feed temperature depends on the dimensions of the reactor. For an adiabatic reactor, a lower feed temperature results into formation of higher amount of ammonia. However, this holds only as long as that the low temperature does not make the synthesis reaction too slow. Due to the requirements of activation, the minimum inlet temperature is limited by the catalyst activation temperature of 300 °C. In addition, due to the exothermic nature of the reaction, the allowed conversion is limited by the maximum allowed temperature of 500 °C. The latter requirement may be satisfied by selection of the operating pressure.

The goal of the reactor design is to maximise the conversion under the discussed constraints. Summarizing, the following decisions have been made on the design parameters:

- A single-stage adiabatic radial reactor is selected with a length-over-diameter ratio of 8.
- The feed is supplied with the stoichiometric ratio of H₂:N₂ = 3:1
- Minimal feed temperature of 300 °C is required for catalyst activation.
- The maximum temperature in the reactor of 500 °C should not be exceeded due to the heat resistance of catalyst.
- Bed voidage = 0.33 & Catalyst bulk density = 2200 kg/m³.

Dimensioning of the reactor involves implementation of these properties in the simulation model and identification of an appropriate pressure.

²Minimum required temperature to ensure optimal catalyst performance.

³Maximum allowed temperature for the catalyst to prevent deactivation and accelerated catalyst aging.

⁴The fraction of bed volume that is occupied by the voids in the reactor.

5.3. Absorption

The following sections will elaborate on the modelling of absorption as part of simulation *MODEL 2* (Section 5.3.1 *Simulation*) and the conceptual design for an absorber for real-life implementation (Section 5.3.2 *Design*). The assumptions that were made for the absorption process in this work are as follows:

Assumptions

- The absorption efficiency is 100%, no NH_3 exists in recycle stream.
- The breakthrough curve is steep, thus the absorption/desorption process is very fast.
- The kinetics of the absorption reaction are ignored.
- H_2 & N_2 are inert towards the salt.

5.3.1. Modelling of absorption

The main objective for modelling the absorber was determining the cooling requirements of the system. The information on the kinetics of the absorption reaction was limited. To keep the focus on the reactor and minimize the complexity, kinetics of the absorption reaction were not considered. As mentioned earlier, it is assumed that the breakthrough curve is steep, caused by low mass transfer resistance.

The best way to simulate this absorber in steady-state is by means of a stoichiometry reactor. The absorption reaction (Equation 2.9) was implemented and a conversion of 100% was specified. Both, $\text{Sr}(\text{NH}_3)\text{Cl}_2$ and $\text{Sr}(\text{NH}_3)_8\text{Cl}_2$ are available in the component database of Aspen Plus as solids. In actual operations, the Strontium Chloride salt will remain in the bed during absorption and regeneration cycles. Here, however, the Strontium Chloride salt is simulated so as to enter the bed as $\text{Sr}(\text{NH}_3)\text{Cl}_2$, and leave the bed as $\text{Sr}(\text{NH}_3)_8\text{Cl}_2$ after taking up 7 NH_3 . After this operation unit, an additional separation unit has been implemented to separate $\text{Sr}(\text{NH}_3)_8\text{Cl}_2$ from the recycle stream (H_2 , N_2).

For the absorption of ammonia in strontium chloride, the heat of formation is significant. If not cooled, this can lead to reduced absorption capacity or even NH_3 desorption. Hence, the reactor is modelled as an isothermal stoichiometry reactor.

The hot outlet stream of the heat exchanger still has a significantly higher temperature than the desirable absorption temperature. Therefore, cooler C-01 was added to reduce the temperature of the heat exchanger's outlet. The process simulation of the absorption section is displayed in Figure 5.12.

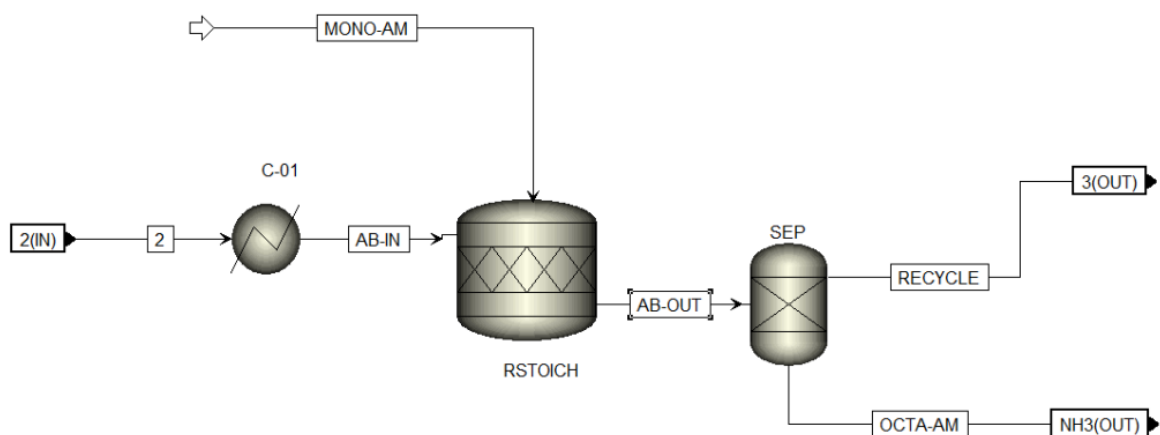


Figure 5.12: Steady-state simulation of Absorber section (Absorber Hierarchy)

5.3.2. Absorber Design

Requirements

To get a feeling on the dimensions of the absorber unit, the absorption bed was assumed to be switched every hour for regeneration. This implies that 146.8 $kmol$ of NH_3 has to be absorbed every hour at the design capacity of 60 $tons/day$. Knowing that 7 NH_3 molecules can be taken up by 1 salt molecule, the $SrCl_2 \cdot NH_3$ requirement is 3.7 $tons/hr$. As mentioned earlier, a continuous cooled absorber is required in order to maintain the desired operating temperature.

Volume

Using the bulk and true densities of the mono-ammine and octa-ammine, the volume increase of the Strontium Chloride salt after taking up 7 molecules of NH_3 was determined to be 45%. It was assumed that the salt would reach its maximum volume after complete absorption. The initial volume of the required salt was calculated to be 5.75 m^3 and on saturation, the salt would occupy 8.33 m^3 . Hence, the required bed volume can be calculated as per Equation 5.15.

$$\text{Volume of absorption bed} = \frac{\text{Volume of salt}}{1 - \text{Bed voidage}} = 11.9 \text{ m}^3 \quad (5.15)$$

This value was computed under the assumptions that the salt particles are spherical and the bed voidage is 0.3 when the salt gets saturated.

Shell & Tube absorber

For the absorber, a Shell & Tube configuration is proposed. In this design, the tubes are filled with absorbent particles and the shell side has the cooling fluid. The absorbent material particles were assumed to be spherical and have a diameter of 2 mm (comparable to the size of catalyst particles). After absorption, the salt volume would increase to 145% of the initial volume ($d = 2.9 \text{ mm}$). Table 5.4 gives some of the design parameters of the absorber.

Table 5.4: Absorber Specifications (Shell & Tube type)

Parameter	Value	Unit
Switch Time	1	hour
Bed Voidage	0.3	
Required Mass of Salt ($SrCl_2 \cdot NH_3$)	3687	kg
Volume of Saturated Salt ($SrCl_2 \cdot 8 NH_3$)	8.33	m^3
Particle Diameter Salt (Saturated)	2.9	mm
Volume of Absorber Bed	11.9	m^3

If the tube diameter and length are assumed to be 0.2 m and 2 m , then the required numbers of tubes amounts to 190 in order to fulfill the volume requirements.

5.4. Pressure drops

Ergun's equation is suitable for computing the pressure drop across a packed-bed reactor [96] and is given by Equation 5.16. This equation was selected to determine the pressure drop over the Plug Flow reactor.

$$\frac{\Delta P}{L_b} = 150 \frac{(1 - \epsilon)^2}{\epsilon^2} \frac{\mu U}{D_p^2} + 1.75 \frac{1 - \epsilon}{\epsilon^3} \frac{\rho_f U^2}{D_p} \quad (5.16)$$

ΔP = Pressure Drop [N/m^2]

L_b = Length of Solid Bed [m]

ϵ = Void Fraction

μ = Fluid Viscosity [Ns/m^2]

U = Superficial Velocity [m/s]

D_p = Particle Diameter

ρ_f = Fluid Density [m^3/kg]

For the other components, fixed pressure drops have been implemented which are not dependent on any empirical correlations. For the heat-exchanger a pressure drop of 1 bar and for the absorber vessel

(stoichiometry reactor) a pressure drop of 2 *bar* was assumed.

A summary of these details and other specifications of the unit operations can be found in Appendix B.1.

5.5. Reactor heat exchanger

The heat-exchanger is a key operation in the simulation to realistically represent practical application. A heat exchanger is a common choice in the ammonia synthesis process as it integrates the high temperature of the reactor outlet stream with the cooler reactor inlet stream. The temperature of the cold outlet of the heat exchanger was specified as 300 °C. A counter-current stream configuration was selected because of its efficiency. Figure 5.13 represents the Aspen Plus model of the reactor hierarchy with an integrated heat exchanger. The heater (H-01) serves as a dummy operation unit. This is to ensure that, in the first iteration of the solver, the inlet temperature of the reactor is 300 °C and thus sufficient to start the reaction. Without this heater the simulation does not run successfully. However, in the steady state, the heat duty of the heater is 0 and does not affect the simulation outcome.

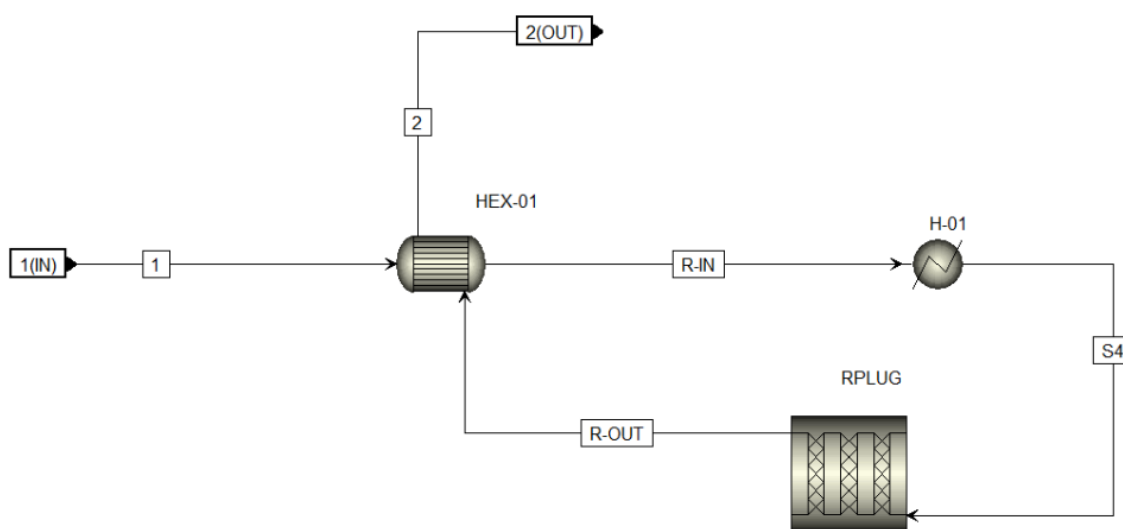


Figure 5.13: Steady State Simulation of Reactor Section (Reactor Hierarchy)

5.6. Results

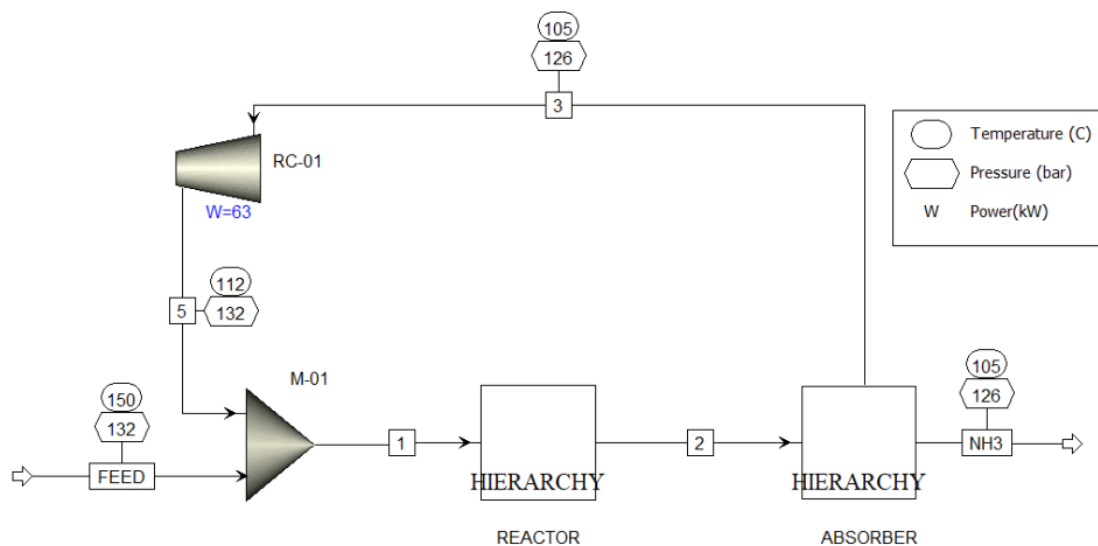


Figure 5.14: MODEL 2: Detailed Steady State Simulation

Figure 5.14 shows the complete Aspen flow sheet of MODEL 2. This consists of two separate hierarchies made for the synthesis reaction and for absorption. The details of the two hierarchies are shown separately in Figure 5.15a and 5.15b. These flow sheets with corresponding stream tables can be found in Appendix B.2.

To satisfy the upper temperature limit of 500 °C within the reactor, the NH₃ formation had to be limited. The conversion can be controlled by restraining the equilibrium in the reactor, this is accomplished by reducing the system pressure. At a pressure of 130 bar and an inlet temperature of 300 °C, the outlet temperature was found to be just below 500 °C. A conversion of 22.1% is the maximum achievable conversion under the conditions and constraints imposed by the system.

A system relying on condensation for ammonia separation cannot achieve such high conversion levels. The improvement is due to the use of absorption as a separation process. Absorption allows for a significantly better separation of the ammonia from the recycle stream, giving close to zero NH₃ in the inlet stream of reactor. This eventually results in more NH₃ production before the reaction is inhibited by the equilibrium. Consequently, the equipment and operating costs at a reduced pressure will be significantly decreased.

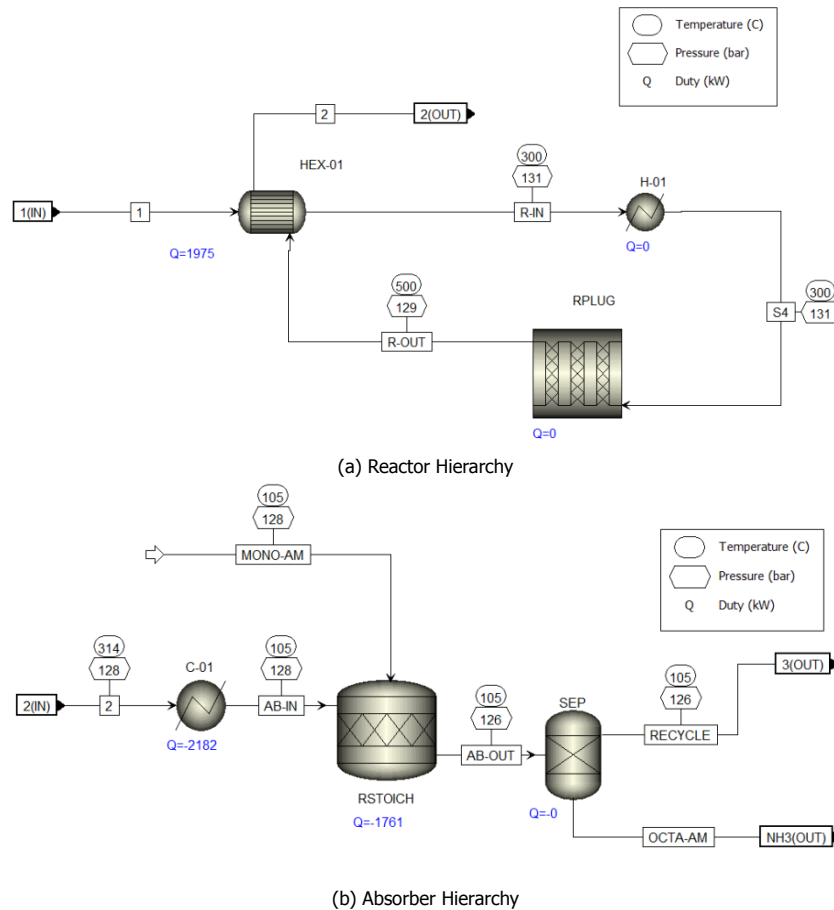


Figure 5.15: Hierarchies MODEL 2

5.6.1. Reactor hierarchy

The reactor dimensions were determined in accordance with the parameters discussed in Section 5.2, with the objective to reach the maximum attainable conversion at the applied operating conditions. The system pressure was set to 130 *bar* to avoid overheating of the catalyst. The corresponding reactor dimensions to achieve conversion of 22.1% while maintaining a L/d ratio of 8 details are summarized in Table 5.5. This table also summarizes the heat exchanger results around the reactor, assuming a heat transfer coefficient of $850^5 \text{ W/m}^2/\text{K}$. The resulting reactor profile is depicted in Figure 5.16.

Table 5.5: Results Reactor Hierarchy

Reactor Dimensions		
Bed Length	6.4	<i>m</i>
Diameter	0.8	<i>m</i>
Heat Exchanger		
Heat Duty	1975	<i>kW</i>
Heat Transfer Coefficient	850	$\text{W/m}^2/\text{K}$
Heat Exchange Area	12.4	m^2

⁵ Default value Aspen Plus

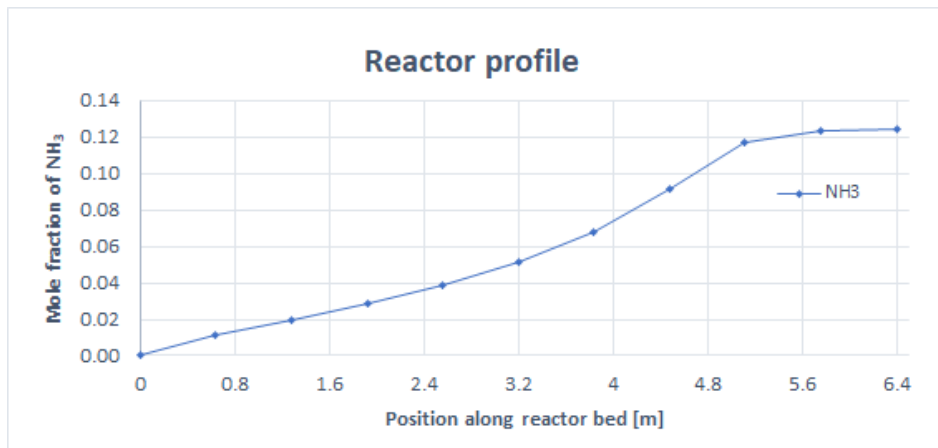


Figure 5.16: The adiabatic plug flow reactor profile in model 2

5.6.2. Absorber hierarchy

According to the explanation in Section 2.6.2, it was found that at a system pressure of 130 bar (partial pressure of NH₃ of 16.3 bar), the corresponding equilibrium absorption temperature is ~ 103 °C. Therefore, the absorption temperature at the system conditions is set at 105 °C. In specifications of the stoichiometry reactor, the temperature has been fixed at 105 °C, making the operation isothermal. Running the simulation model at these conditions, where 146.8 kmol/hr of NH₃ is absorbed in Strontium Chloride Metal Ammines, the required cooling duty of the isothermal reactor was found to be -1762 kW. This corresponds to a temperature increase of the outgoing stream to 304 °C if the stoichiometry reactor is modelled as adiabatic. The pre-cooler C-01 that reduces the stream temperature to the desired absorption temperature requires a duty of -2182 kW.

Table 5.6: Results Absorption Hierarchy

Parameter	Value	Unit
Temperature	105	°C
Heat Duty Pre-cooler (C-01)	-2182	kW
Heat Duty Absorber	-1762	kW

Absorber design validation

The absorber heat transfer coefficient was assumed to have an average value of 165 W/m²/K [97]. By changing the absorber vessel type to adiabatic and simulating an additional heat exchanger to satisfy the cooling requirements, the minimal required exchanger surface area was determined (see Figure 5.17). As the objective for this work was a decentralized mini ammonia process that might have no access to cooling water at the specific location, ambient air of 40 °C at atmospheric pressure was chosen as the cooling fluid. The total heat duty required for the absorption process was 1761 kW, which is satisfied by supplying an air flow rate of 40 kg/s. Applying the assumed heat transfer coefficient, the required area was found to be 83.9 m². The exchanger specifications and results have been summarized in Table 5.7.

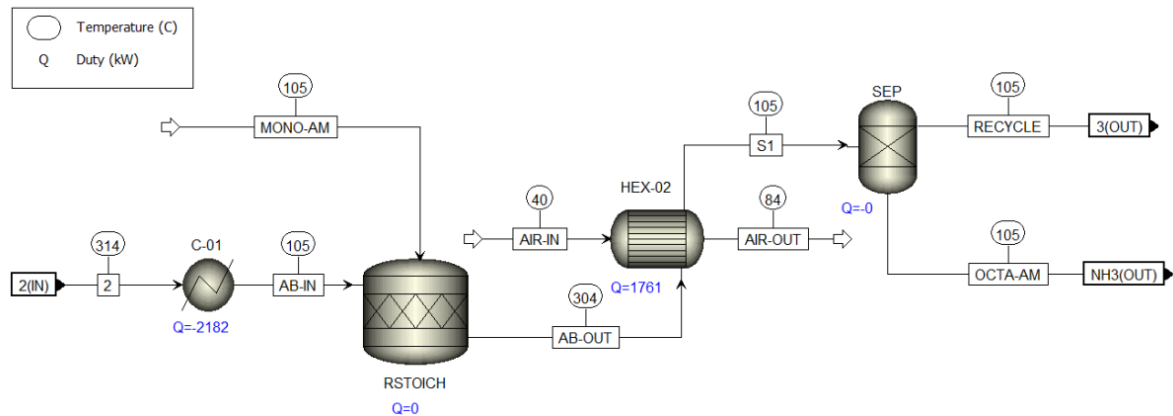


Figure 5.17: Decomposed Absorption Reaction and Cooling with Heat Exchanger in Absorption Hierarchy

The conceptual proposal from Section 5.3.2 for the Shell & Tube design has 190 tubes. Each of the tube had a length of 2 m and a diameter of 0.2 m. This resulted in a total exchange area of 238.8 m² available for cooling. This area exceeds the required heat exchanger area, such that this design is considered to be feasible.

Table 5.7: Absorber HEX Simulation Details

Parameter	Value	Unit
Type	Counter-current	
Minimum Temperature Approach	30	°C
Cooling Fluid	Ambient Air	
Pressure	1	atm
Mass Flow Rate Air	40	kg/s
Inlet Temperature	40	°C
Outlet Temperature	84	°C
Absorbent		
Average Heat Transfer Coefficient SrCl ₂ · NH ₃	165 [97]	W/m ² /K
Inlet Temperature	304	°C
Outlet Temperature	105	°C
Results		
Calculated Heat Duty	1761.5	kW
Required Exchanger Area	83.86	m ²

In case there is sufficient supply of clean water, it is recommended to use water as a cooling fluid for the absorption process. Water is great option because it can control the temperature in the tubes of heat exchanger perfectly as it converts into steam. Boiling water will result in a uniform temperature as it flows through the tubes. In addition, the steam can then be used to for process heat. For example, ~ 180 kg/hr of saturated steam at 100 °C can be produced from the reaction heat of absorption.

5.7. Model validation

In *MODEL 2*, the space velocity and conversion in the synthesis loop were found to be ~ 13,200 hr⁻¹ and 22.1%. Using Table 5.2, these results can be compared to industrial plant data. The achieved conversion from *MODEL 2* is comparable to the industrial cases and the space velocity lays within the range of space velocities as presented by Table 5.2. The conversion and space velocity values are especially close to the Topsøe ammonia process. Even though the pressure in this process is significantly higher, which reduces the space velocity. Additionally, the ammonia and inert gas inlet concentrations in the process are 3.6% and 2% respectively, inhibiting the reaction, however, a multi-stage reactor with intercooling increases the attainable conversion. The feed stream in this work is purely H₂ and N₂ but the conversion is limited by the reactor temperature. Nevertheless, the space velocity proves to be similar as it is relative to the conversion, and the effect of the different factors of *MODEL 2* and

the Topsøe plant, balance each other out.

Additionally, the kinetic equation that was implemented in this model had been validated in a Plug Flow Reactor (Section 5.1). Hence, the simulation model is considered validated with the means available.

Note: The noticeable difference in space velocity of *MODEL 2* versus the Reactor Profile graphs (5.8 and 5.9) and the Feed Temperature Sensitivity graphs (5.10) from Section 5.2 is caused by the difference in pressure. The reduced pressure in *MODEL 2* (130 bar versus 200 bar) requires an increased catalyst volume in order to achieve the same conversion, thus reducing the space velocity.

5.8. Heat integration

In this section, the options for heat integration of streams in the synthesis loop are discussed. In *MODEL 2* heat integration was already applied between the out-going and in-coming reactor streams using a heat-exchanger (HEX-01). After the absorption step which occurs at 105 °C, the outlet stream loops back and is heated up before entering the reactor. From Figure 5.14 and Figure 5.15 it can be seen that stream 1, after the recycle loop merges with the make-up gas, is warmed up by HEX-01 to the desired reactor inlet temperature (300 °C). Hence, the reaction heat is sufficient to heat the reactants.

The results of *MODEL 2* indicate that for cooling down to the absorption temperature (105 °C) and continuously cooling during absorption of ammonia, heat duties of -2182 kW and -1761 kW are required respectively. These heat duties provide a great opportunity to use this process heat in the regeneration of the Sr(NH₃)₈Cl₂ bed. When two metal halide beds are operated at the same time, one for ammonia take-up and the other for regeneration, the heat from the first bed can be utilized for regeneration of the second bed.

Assuming that the desorption enthalpy is equal to the absorption enthalpy. The total duty of the two cooling steps, taking into account heat losses and integration efficiency, should suffice to regenerate the absorption bed.

6

Dynamic Simulation (*MODEL 3*)

Figure 6.1 visualises the required steps to transition from steady-state model to a dynamic model. The steps colored in blue will be discussed in this section and the results are analysed in Chapter 7. The steady state model from Section 5 was employed as starting point. Some alterations were required for the dynamic simulation environment, including implementation of controllers and control strategy.



Figure 6.1: Step approach to a Dynamic simulation

6.1. Scenario & assumptions

As discussed in Chapter 3, in this part of the work, it is assumed that the diurnal variability in VRES imposes a maximum reduction in the hydrogen feed (10%, 25% or 50%) over a period of 30 minutes. The system is ramped-up again at the end of every period.

Furthermore, the following additional assumptions were made for the dynamic simulation model.

Assumptions

- Since the focus of this work are deficiencies in the hydrogen feed, it is assumed that no limitation exist on the nitrogen availability for this simulations (a sufficiently large N_2 buffer is assumed to be present).
- Only the hydrogen feed flow rate is affected by variations in renewable electricity supply, no other unit operation/equipment is affected.
- The dynamic behaviour of the absorption and regeneration beds is not simulated.
- Only essential controllers were implemented in the control structure of the model, hence:
 - No heating/cooling medium controllers (the heaters and coolers respond instantaneously).
 - No purge control with Argon concentration measurements is included.
 - No $H_2:N_2$ ratio controller in the loop was added that overrules the feed control command.

6.2. Prepare the Dynamic Simulation

The first step in the preparation of a dynamic simulation is to select a simulation type, a (simpler) Flow-Driven or (more rigorous) Pressure-Driven simulation. Before exporting the simulation into Aspen Plus Dynamics, the dynamic simulation mode must be selected. In appendix the difference between the two simulation modes and the selection of the pressure-drive type is explained.

6.2.1. Additional steps for pressure-driven simulations

There are additional steps that are required to prepare a steady-state simulation for pressure-driven simulations:

- Removal of unsupported blocks: SEP, EXTRACT, DUPL, DISTL
- Additional blocks to create pressure/ flow relationships (valves, pumps, holding tanks)
- Proper definition of inlet and outlet pressures

Pressure-driven simulations generally require more blocks to model the pressure/ flow relationship throughout the model. The simulation model must consist of a balanced pressure network where the inlet pressures are greater than the outlet, and the individual components must have specified pressure loss relations to ensure the correct flow rates. To create pressure differentials between components, valves were implemented. Before exporting the steady-state simulation to Aspen Dynamics, the built-in pressure checker presents a useful tool to verify the pressure distribution in the network. Additionally, not all components available in Aspen Plus are supported in the Pressure-driven simulation of Aspen Dynamics. One such block is the SEP block. The SEP block utilised in the steady-state ammonia absorption unit was replaced by another operation type (FLASH2) which is discussed in detail below.

6.3. Specification of Dynamic data

In Aspen Plus, once the steady state model has converged, the dynamic mode is selected. When this dynamic mode is turned on, the dynamic properties for each of the operation units become accessible for specification. These dynamic data include vessel geometry, process/ equipment heat transfer and initial vessel conditions. If the dynamic behavior of a block can be considered fast-responding, the dynamics can be ignored. In such case, the unit is specified as *Instantaneous* in the Dynamic section. Other adjustments comprise the addition of valves to create the correct pressure distribution and incorporation of an alternative ammonia recovery unit. Below, a list of alterations that were made to the steady-state model are given, with a brief discussion of additional specifications required for export to the Aspen Dynamics.

Feed The make-up gas stream from *MODEL 2* was split up to control the hydrogen and nitrogen feed streams separately. The pressure of both streams was set to 200 bar. This prevented any effect on the flows (post feed valves) due to the pressure drop over the valves and the pressure fluctuations in the synthesis loop.

Mixer (M-01 & M-02) The mixers were assumed to be instantaneously responsive; the mixers are tee's with effectively no volume or residence time. No pressure drop over the mixers is allowed in Aspen Dynamics pressure-driven simulation. A fixed condition for this equipment is thus that in-going and out-going pressures are equal.

Plug Flow Reactor (RPLUG) No additional specifications have been made to the plug flow reactor and it was decided not to include any heat exchange with the environment.

Heat-Exchanger (HEX-01) In *MODEL 2*, the heat exchanger has been simulated with a constant output temperature of 300 °C for the reactor feed stream. This method yields the required heat exchanger area as output. The evaluated value for the surface area in steady state was used as unit specification for the dynamic simulation. The heat exchanger area was the input for this option. The pressure drop in the heat exchanger was expressed by:

$$\Delta P = K * \rho * F_v^2 \quad (6.1)$$

where F_v represents the volumetric flow rate, ρ is the density, and K is a characteristic constant for the exchanger.

Heater (H-01) In the simulation, the heater H-01 represents both an electrical heater and a by-pass on the heat exchanger (HEX-01). The combination regulates the reactor feed temperature at a fixed temperature of 300 °C. This optimal temperature was determined in section 5.2 on the reactor configuration. In the specifications for this heater, the instantaneous type was selected and a constant outlet temperature was specified. The pressure drop in Aspen Dynamics was also given by to Equation 6.1.

Knock-out Drum (ABS Hierarchy) As discussed in *Preparing the Dynamic Simulation*, the species separation unit (SEP) is not supported in Aspen Dynamics. The separation block is an operation unit that functions by simply splitting the different components over the two discharge streams as specified. This virtual operation is inconsistent with Pressure-driven dynamic simulation, which requires specification of real physical properties, such as separator equipment volume. Therefore, a different method was applied to represent the absorber in the model. A FLASH2 unit operation was implemented which, under low temperature and constant pressure, functions as a condenser drum by removing the liquid ammonia.

The volume of this vessel affects the response time of the system. Hence, it was crucial that the residence time of the gases in this vessel matches the expected absorber residence time as closely as possible. In Section 5.3.2, the absorber volume had been established assuming a 1-hour switch time. Combining absorber volume with the volume flow rate of the inlet stream, the expected vapor residence time can be determined by:

$$\text{Vapor Residence time(s)} = \frac{\text{Bed voidage} \times \text{Absorber bed volume}}{\text{Volume flow rate going into the Absorber}} = 27s \quad (6.2)$$

The residence time of 27 s for the vapor phase can be used to calculate the dimensions for the FLASH2 vessel. The liquid volume fraction is required as initial condition. A vertical vessel geometry with an elliptical head type was selected. A reasonable length-to-diameter ratio was assumed to be 4. The length and diameter were derived to be 2.42 m and 0.61 m. To achieve a 27 s residence time for the vapor under these parameters, the initial specification for the liquid volume fraction was determined to be 0.38. In the dynamic simulation the liquid level must be maintained and therefore, a level controller was implemented. This level controller opens or closes the liquid ammonia outlet valve to achieve this.

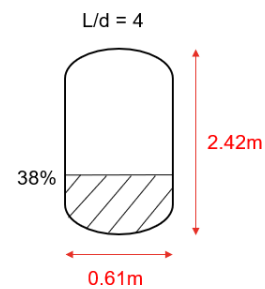


Figure 6.2: FLASH2 Vessel Dimensions (Absorber)

A rather low operating temperature was chosen for the condenser vessel FLASH2, in order to achieve a highly effective recovery of ammonia from the recycle stream, as is expected for the actual absorber unit. The properties of the FLASH2 unit operating temperature was chosen such that the condensing temperature is $-180\text{ }^{\circ}\text{C}$. Following the FLASH2 vessel, a heater (H-02) is included to raise the temperature back up the actual absorption temperature. These two blocks together form the absorption hierarchy, which is intended to represent the absorber step in the dynamic simulation.

Recycle Compressor (RC-01) An isentropic compressor was selected. In the steady-state Aspen Plus simulation, the compressor outlet pressure must be specified. However, when converting the model to a dynamic pressure-driven simulation, Aspen determines the corresponding power input and shaft speed under the simulation conditions. These values remain fixed in the dynamic simulation. For the sake of simplicity, the instantaneous mode was selected in the *Dynamic* tab as the dynamic behaviour of the compressor is not in the scope of this work. That means no performance efficiency curves were used. As per the Aspen Dynamics documentation, default curves were fitted around the operating point calculated in Aspen to offer realistic behaviour. These typical curves are Head vs. suction volumetric flow rate and Isentropic efficiency vs. suction volumetric flow rate of a centrifugal compressor.

Aspen gives the following equation for the power of isentropic compression:

$$\text{Power} = \frac{\dot{m} \times \text{Head}}{\eta_{\text{isen}}} \quad (6.3)$$

$$\text{Head} = \frac{ZRT}{MW} \frac{k}{k-1} \left[\frac{p_2^{\frac{k-1}{k}}}{p_1} - 1 \right]$$

Where

$$k = \frac{c_p}{c_v}$$

For a di-atomic fluid k equals $\frac{7}{5}$.

6.4. Run the Simulation

After preparation, the Aspen Plus model was exported to Aspen Dynamics. Figure 6.3 shows the dynamic simulation model.

Details on input specifications and information on the blocks can be found in Appendix C.3.

Each block functions as a node, with a specific pressure-dependency. For the valves, the compressor, and the heat exchanger flow rate and pressure drop are related directly. For the absorber (FLASH2) and RPLUG, the vessel pressure is set from the volume and vapor amount. The mixers M-01 and M-02 have no pressure drop in the model. More information on the nodes in a dynamic simulation can be found in Appendix C.1.

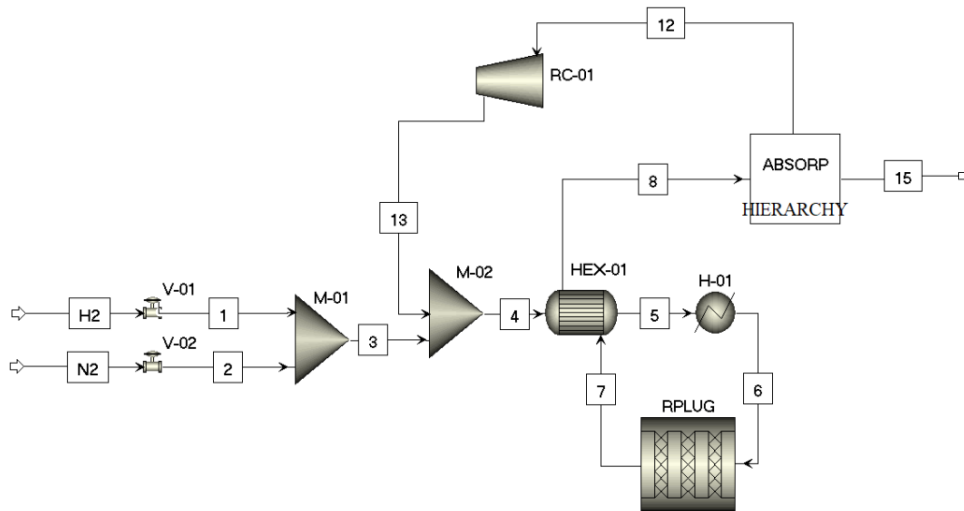


Figure 6.3: *MODEL 3*: Dynamic simulation

6.5. Add a Control strategy

The control scheme is designed to cope with temporary shortage in the hydrogen supply in anticipation fluctuations in the available power for water electrolysis. A reduced feed flow rate will cause the system pressure to drop. Large pressure fluctuations are undesired because such changes may cause metal fatigue phenomena for the equipment construction materials. Therefore, the main objective is to control the synthesis loop in such a way that the pressure fluctuations remain acceptable.

Three different methods have been pre-selected for assessment of the effectiveness in sustaining the system pressure. The first method is the reduction of the reactor's temperature in order to reduce the ammonia reaction rate. The second method is a decrease of the flow rate of the recycle stream in order to slow down the reaction and extend the residence time. Thirdly, the supply of N_2 may be increased, thereby departing from the ideal molar ratio and effectively introducing nitrogen partly as an inert.

From Section 5.2, it was seen that the relationship between the temperature and reaction rate was very sharp and thus difficult to control. For this reason, the reactor temperature control option was rejected.

Hence, two possible control strategies are considered for dynamic modeling to test the effectiveness in retaining the system pressure in case of hydrogen shortage. These are:

1. Compensation of hydrogen deficiency by increasing the nitrogen flow rate instead (Loop $H_2:N_2$ ratio $\neq 3$)
2. Control of recycle flow rate to slow down the reaction (Loop $H_2:N_2$ ratio = 3)

6.5.1. Base control structure

A default control scheme can always be created by Aspen Dynamics in the form of auto-generated controllers. For example, upon selection each valve receives a flow controller and for the FLASH2 vessel, both a pressure and level controller can be automatically included. However, the auto-generated controllers are not sufficient to achieve control of the plant. Hence, it is extended to achieve a more stable regulatory structure.

To prove that an additional control structure is required, a base control scheme was tested with a 10 % ramp-down and ramp-up of the hydrogen feed flow rate. Before any control philosophy implementation the models had the following controllers (with specifications) (Figure 6.4):

- A flow controller on the H₂ feed stream that controls the valve opening (FC-01)¹. Reverse acting feedback control with a proportional gain and integral time of 1 %/% and 1 min, respectively.
- A level controller on the absorber (FLASH2) unit operation (LC-01). Direct acting feedback control with a proportional gain and integral time of 10 %/% and 1 min, respectively.

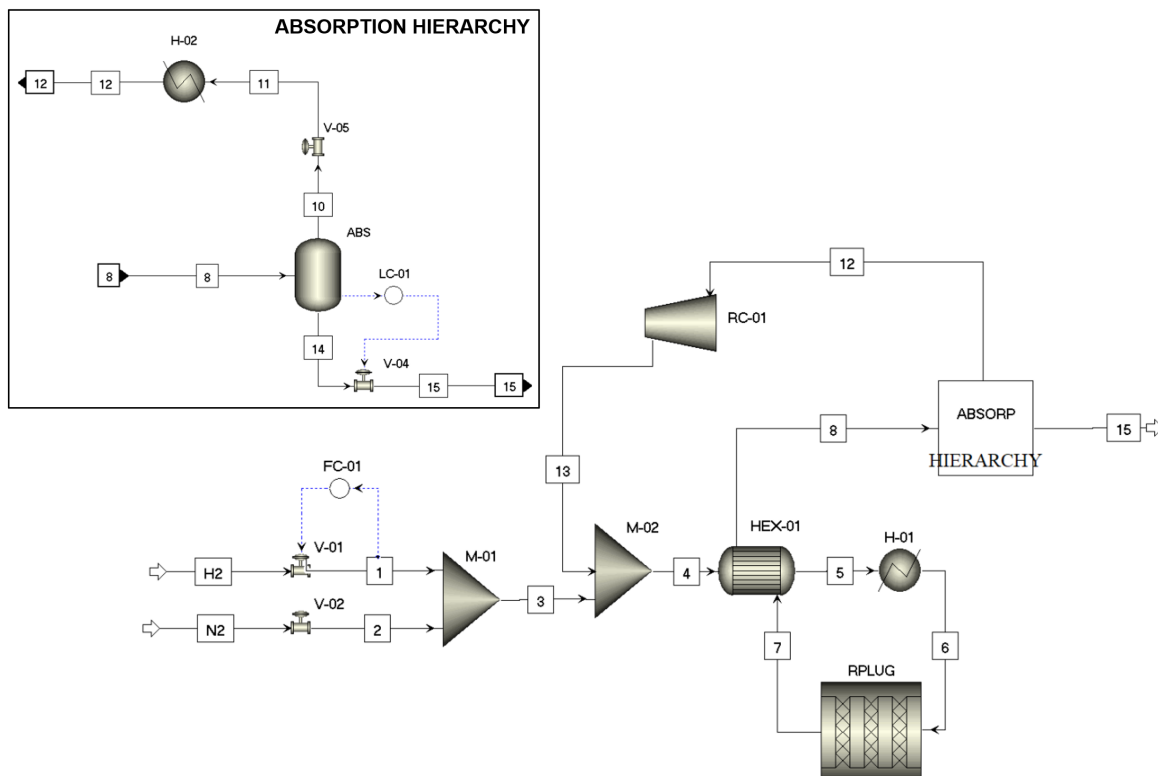


Figure 6.4: Dynamic model with a base control structure

¹The controller parameters have been established by trial and error using the recommendations from Aspen as starting point (Appendix C.2).

Results

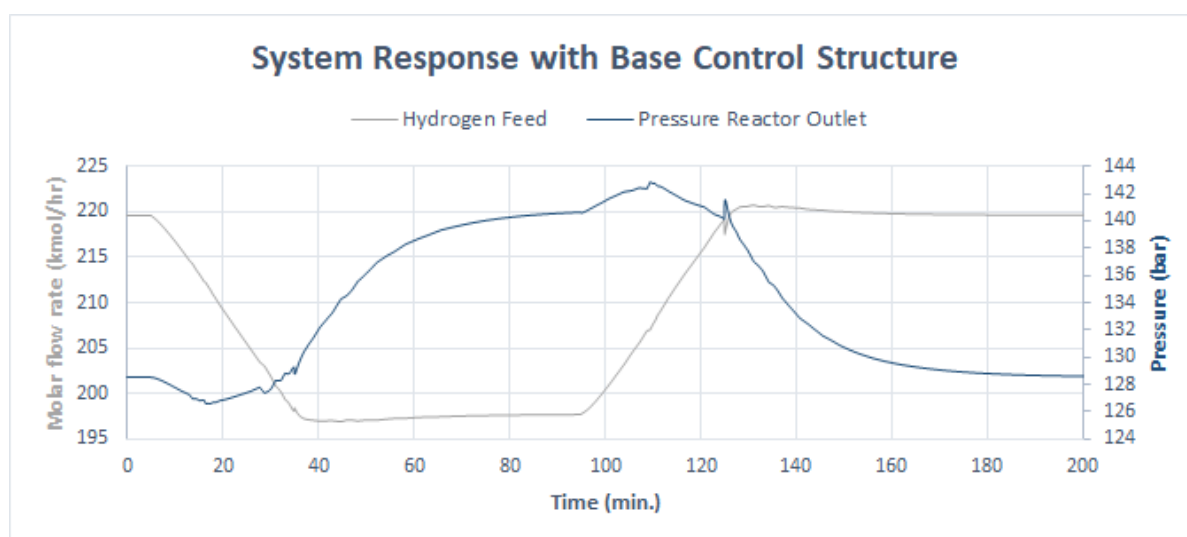


Figure 6.5: System response to a 10% ramp-down in hydrogen feed with base control structure

A 10% ramp-down was expected to be a high frequency event over the lifetime of the plant. Figure 6.5 depicts the hydrogen feed flow rate which is subjected to a linear ramp-down (over 30 min) to 90% of its initial value starting at the 5 *minute* mark. The hydrogen feed is ramped-up to the initial value starting at the 95 *minute* mark. The *blue* line represents the pressure at the outlet of the reactor as consequence of the hydrogen feed variation (*grey* line). It is observed that pressure is not controlled and remains at an elevated position in the reduced (-10% H₂) state. The pressure also fluctuates by 16 *bar*. Such large pressure variation for a relatively small hydrogen feed flow rate disturbance was assumed to confirm the need for additional controllers to specifically reduce the pressure variation.

6.5.2. Additional information

For this study, the focus was put on only key elements of the control scheme that influence the dynamic response of the system. In reality, other controllers could be included in the synthesis loop. The following control loops were deemed not essential to the objective and were excluded:

- Heating/Cooling fluid flow rate and/or medium temperature controls to manage the required heat duties. The heaters and coolers were assumed to operate instantaneously and not display any dynamic behaviour.
- Loop ratio control (H₂ to N₂) = 3:1 that would periodically measure the ratio and overrules the command of the feed ratio control in case the ratio in the loop needs to be corrected.
- Periodic measurements of the gas composition in the loop, coupled with occasional purging when this exceeds a certain threshold (Inerts like Argon are not present in the model at all).

The proposed control philosophies are to maintain the system pressure when hydrogen gets ramped-down, therefore, the pressure controller on the absorber unit is excluded to avoid interference. In the next section the control structures of philosophy 1 and 2 are discussed.

6.5.3. Control Philosophy 1

In addition to the hydrogen feed flow rate controller and the absorber level control, this control structure requires one more controller to maintain the pressure in the loop. The concept of this control method relies on the replacement of hydrogen deficiency with surplus nitrogen to retain the system pressure. The controller measures the reactor's pressure to actuate the nitrogen feed valve when the reactor pressure deviates from its set-point. The principle is illustrated in Figure 6.6. The reverse-acting controller FC-01 operates with a proportional gain of 10 %/% and has a time constant of 1 *min*. The brake power of the compressor was kept constant in this simulation. The details and parameters of the controllers have been summarized in Table 6.1.

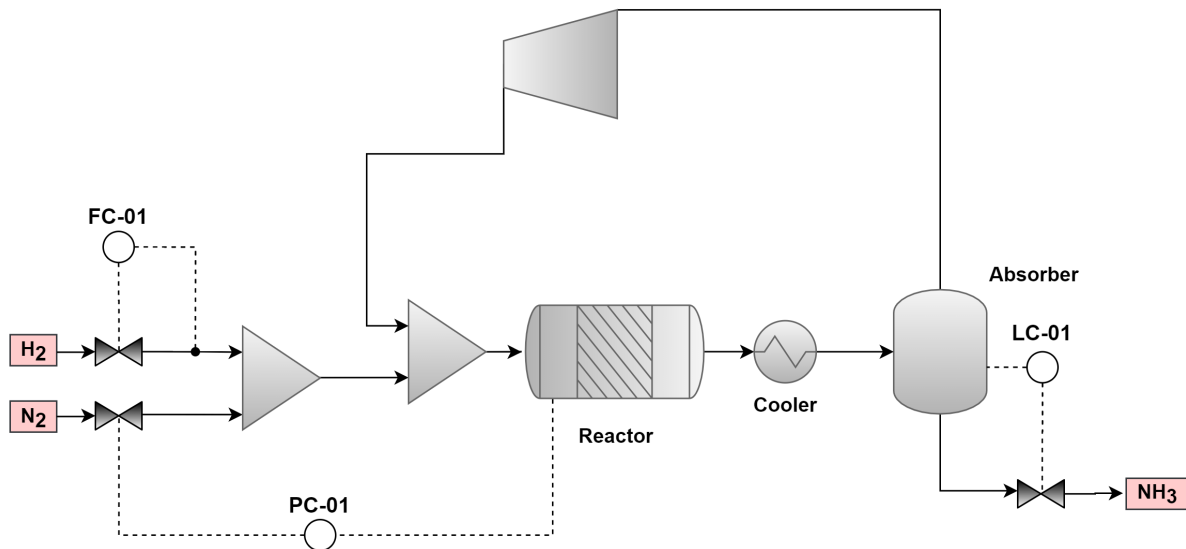


Figure 6.6: Concept Visualization of Control Philosophy 1

Table 6.1: Controller Parameters for Control Structure 1

	Proportional Gain (%/%)	Integral Time (min.)	Controller Action	Controlled Variable	Manipulated Variable
FC-01	1	1	Reverse	Hydrogen feed flow rate	Valve V-01 opening
LC-01	10	1	Direct	Liquid level flash	Ammonia outlet flow rate (Valve V-04 opening)
PC-01	10	1	Reverse	Outlet pressure RPLUG	Nitrogen feed flow rate

6.5.4. Control Philosophy 2

The operating principle of the second control structure is to vary the recycle flow rate to control the ammonia production in the reactor. The idea is to balance the mass of ammonia produced to the mass of the reactants fed to the system. This method does not alter the $H_2:N_2$ feed ratio. Controlling the recycle flow rate is realised by adjusting the brake power of the recycle compressor. The second control philosophy requires two additional controls:

- A flow controller in combination with ratio measurements that makes sure the $H_2:N_2$ feed ratio is maintained at the stoichiometric ratio of the reaction. The ratio block measures the ratio of the molar flow rates of hydrogen and nitrogen. When the ratio deviates from the setpoint, the ratio block sends a signal to valve in the nitrogen feed line to manipulate the nitrogen feed flow.
- A pressure controller that varies brake power in response of pressure variation, measured after the recycle compressor.

Figure 6.7 illustrates the second control philosophy to maintain the pressure by adjusting the compressor brake power. The details and parameters of the controllers have been summarized in Table 6.2.

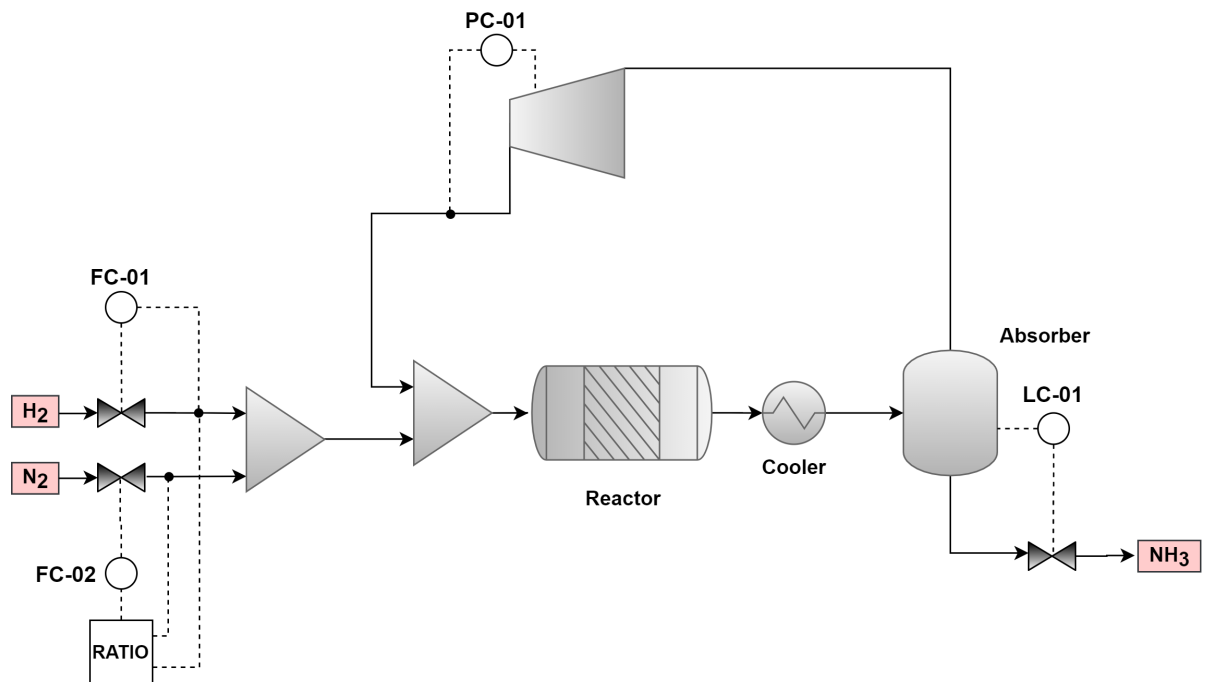


Figure 6.7: Concept Visualization of Control Philosophy 2

Table 6.2: Controller Parameters for Control Structure 2

	Proportional Gain (%/%)	Integral Time (min.)	Controller Action	Controlled Variable	Manipulated Variable
FC-01	1	1	Reverse	Hydrogen feed flow rate	Valve V-01 opening
LC-01	10	1	Direct	Liquid level flash	Ammonia outlet flow rate (Valve V-04 opening)
FC-02	1	1	Direct	Feed ratio H ₂ :N ₂	Nitrogen feed flow rate
PC-01	1	1	Direct	Pressure in loop (after compressor)	Compressor Brake Power

7

Results & discussion of dynamic simulation

In this chapter the results of the simulations are presented and discussed. In the previous chapter two control structures were designed which will be tested and validated here. Sustained system pressure was achieved by either nitrogen feed flow control or by recycle feed flow rate control, which were labeled *Control Philosophy 1* and *Control Philosophy 2*.

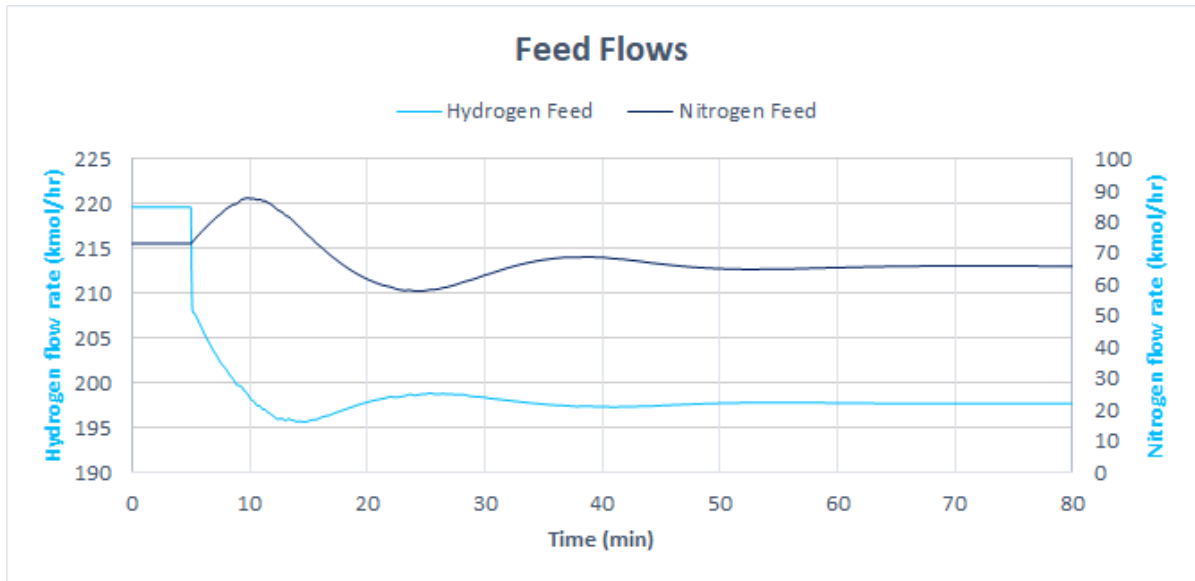
Two types of variability in hydrogen availability have been considered in the performed simulations. Section 7.1 considers a scenario with an abrupt decrease in the hydrogen feed flow rate. Section 7.2 is focused on the scenario for which a hydrogen storage buffer is installed, which entails into a more gradual change of the hydrogen feed flow rate.

Section 7.2.3 provides a summary and discussion of the dynamic simulation results.

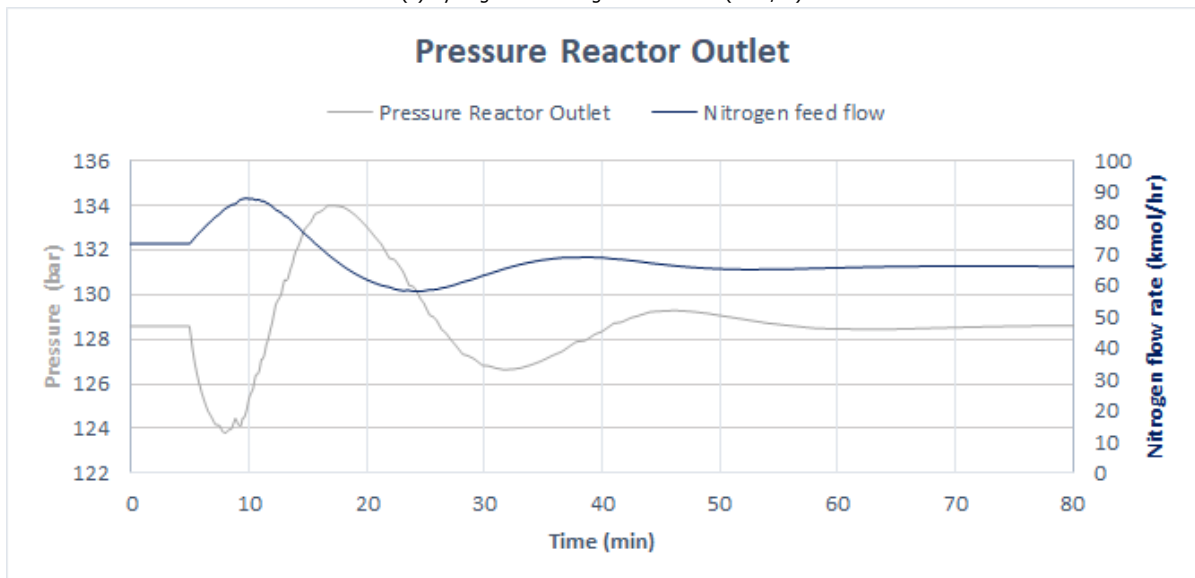
7.1. Abrupt change in hydrogen feed

In this scenario it was assumed that there is no hydrogen storage buffer for the plant. To understand the effect of this, a sudden reduction in electrolyser's hydrogen generation capacity to 90% was assumed. This was modelled as a 10% step-down function.

The impact of this 10% step decrease in the H₂ feed on the system pressure is shown in Figure 7.1 (*Control Philosophy 1*) and Figure 7.2 (*Control Philosophy 2*).

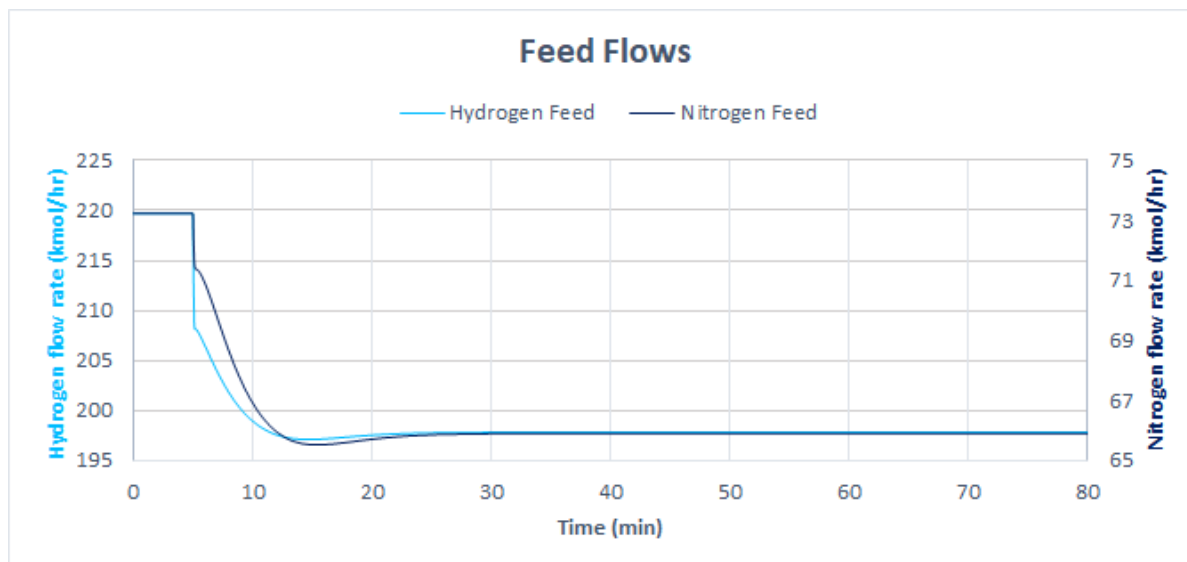


(a) Hydrogen and Nitrogen Feed Flows (kmol/hr)

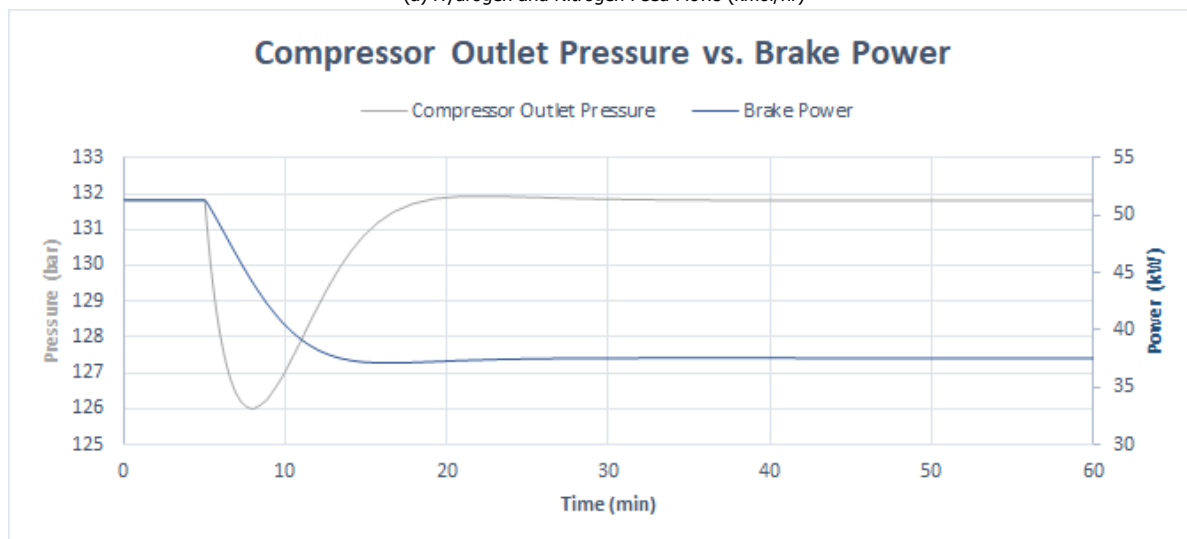


(b) Pressure at Reactor Outlet (bar) and Nitrogen Feed Flow (kmol/hr)

Figure 7.1: 10 % Step-down scenario Control Philosophy 1



(a) Hydrogen and Nitrogen Feed Flows (kmol/hr)



(b) Pressure at Reactor Outlet (bar) and Brake Power of the Compressor (kW)

Figure 7.2: 10 % Step-down scenario Control Philosophy 2

Discussion

- ⇒ With *control structure 1*, the largest pressure fluctuation measured at the reactor outlet is 10 bar.
- ⇒ With *control structure 2*, the largest pressure fluctuation measured at the reactor outlet is 6 bar.
- ⇒ In both cases, the initial step decrease of hydrogen is only 5% after which it tapers down to the imposed 90% of the initial molar flow. This effect is a result of the fact that the desired flow rate decrease is imposed by valve FC-01 in Fig 6.8, as opposed to a step-wise boundary condition change for the feed flow rate itself. The new setpoint for the flow controller cannot be instantly met by a single change of the valve stem position. The varying pressure conditions downstream of the valve cause a more gradual approach to the flow rate setpoint, as the valve position is readjusted several times.

Key takeaway

Both the nitrogen compensation and recycle flow control structures may require hydrogen storage to dampen the deficiency in hydrogen to avoid significant pressure swings; just a 10% drop results in pressure fluctuations of 6 bar (= 4.5%) and 10 bar (= 7.5%) respectively. The next section investigates

the effect of a more gradual feed flow rate change, as would be achieved with a system that includes a hydrogen storage buffer.

7.2. Gradual change in hydrogen feed (with H₂ buffer)

This section addresses a plant with hydrogen buffer included in the system configuration. This hydrogen buffer compensates a lack of hydrogen availability. However, this compensation can only happen over a limited time period, determined by the storage size and the duration of the upset. Three ramp-down values have been considered here which vary by the degree of hydrogen feed flow rate reduction.

The results of a single hydrogen deficiency scenario (25% Ramp-down and Ramp-up) will be discussed in this section. The results have been divided in two parts, the first is *primary action*, where the graphs show the hydrogen feed flow drop and the controller response to maintain the pressure. Then, the *consequences* of this control action on other parameters in the system are displayed. The results of the other scenarios (deficiency of 10% and 50%) are comparable and can be found in Appendix F.

The transient operation scenario discussed in detail in this section involves ramp-down of 25% in hydrogen feed, after some time followed by ramp-up to recover the original state. The ramp-down is a linear 25% reduction of hydrogen over 30 minutes. After the system stabilizes and finds a new steady state, another 30 minute period is imposed with linear increase back to the original hydrogen feed flow rate. This simulation ends after attaining the final steady state. The specific steps of the simulation with corresponding time stamps can be found in Table 7.1.

Table 7.1: Timeline simulation

Time (min)	Occurrence
0	Start simulation
5	Hydrogen feed is linearly ramped down to 75%
35	End ramp-down
approx. 80	New steady state is reached
95	Hydrogen feed is linearly ramped back up to the initial value (100%)
125	End ramp-up
180	End simulation

The graphs have been divided in the following regions for ease of reading and discussion.

Region:

- A** H₂ Ramp-down
- B** New steady state
- C** H₂ Ramp-up
- D** Steady state at initial value

7.2.1. Control Philosophy 1

With this control structure the operating pressure is maintained by manipulating the nitrogen feed flow rate. Figure 7.3 presents the Aspen Dynamics model with this control structure.

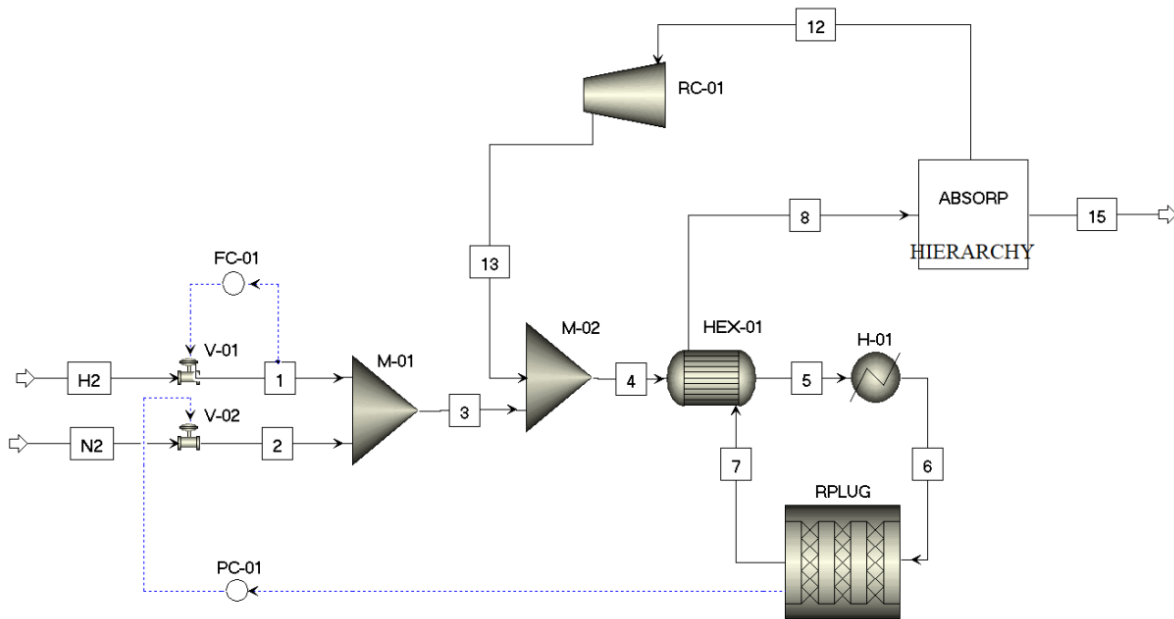
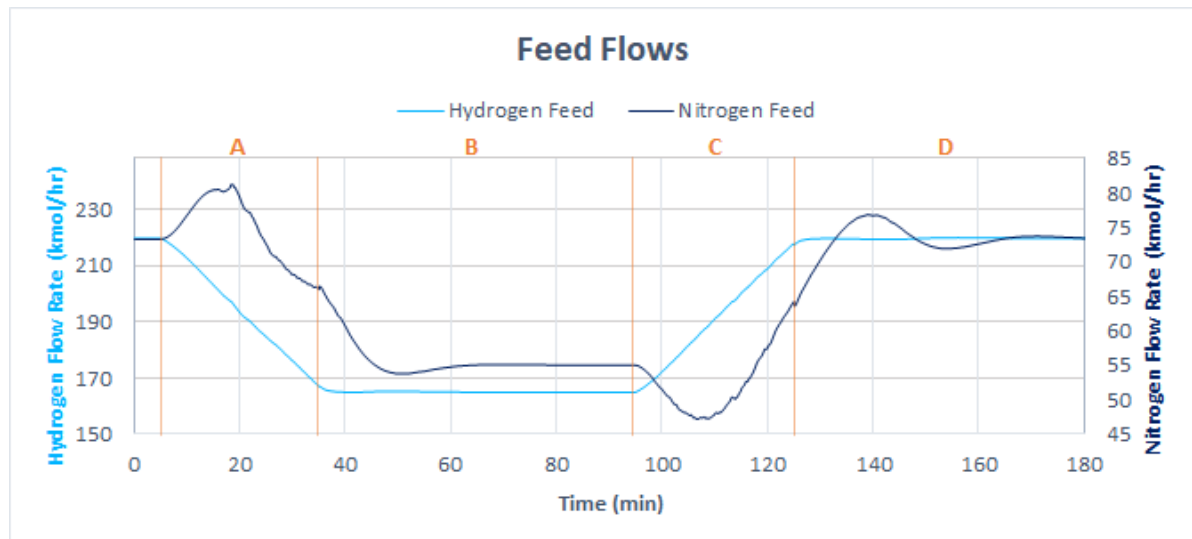


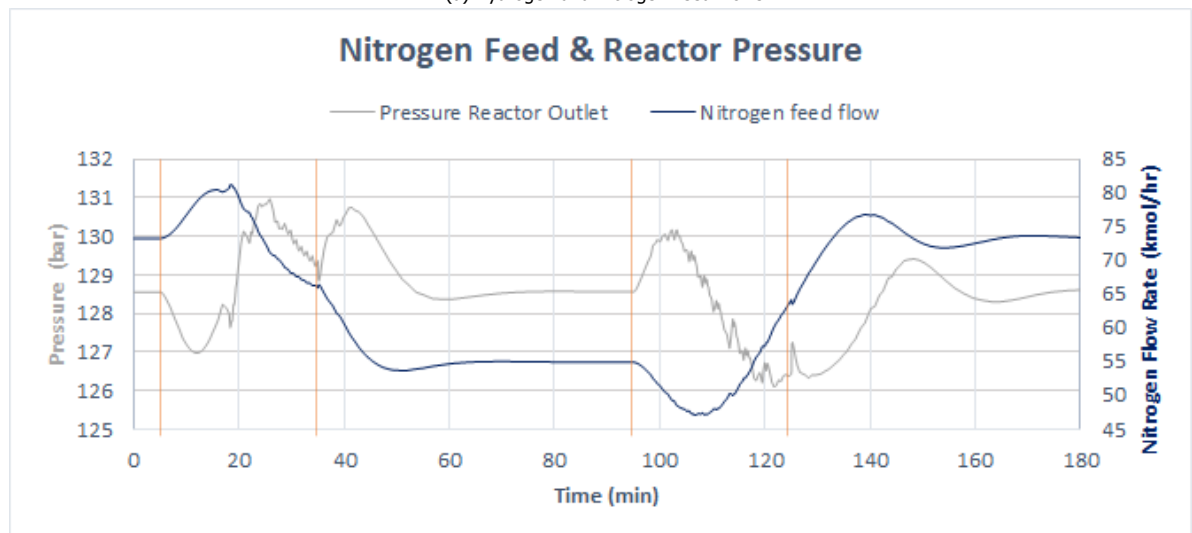
Figure 7.3: Aspen Dynamics flowsheet with Control Philosophy 1

Primary action

The molar flow rate of hydrogen into the loop was ramped down to 75% and back up over a time frame of 180 minutes. The pressure at the reactor outlet is controlled by the nitrogen feed flow rate. Figure 7.4a depicts the feed flow rates and Figure 7.4b shows the resulting reactor outlet pressure along with the nitrogen feed flow rate.



(a) Hydrogen and Nitrogen Feed Flows



(b) Pressure at Reactor Outlet (bar) and Nitrogen Feed Flows

Figure 7.4: Time series for 25% Ramp-down/up scenario - *Control Structure 1*

Discussion

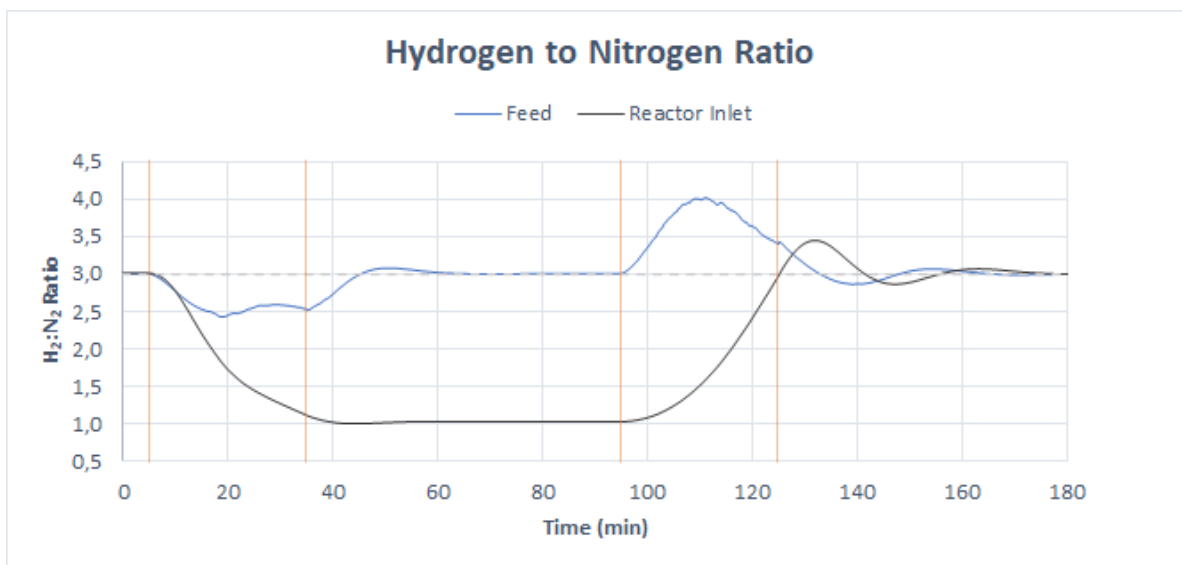
- ⇒ **Region A:** The response to the disturbance of the hydrogen feed is not immediate for the selected values of the control parameters (PI). An initial pressure drop is observed before the nitrogen compensation kicks in. When it does, the nitrogen flow rate increases and peaks. At this peak, the pressure has already reached the set point and the valve starts to close. The pressure first overshoots the set-point a little before valve action reduces the nitrogen feed flow rate. After the nitrogen feed peak, the nitrogen feed flow rate decreases with a gradient similar to the hydrogen ramp-down.
- ⇒ **Region B:** When the hydrogen ramp down ends, the pressure starts to rise again because excess nitrogen is still being added to the system. As the deviation between setpoint and process variable grows, the gradient of the nitrogen flow rate also increases. Finally, the nitrogen feed rate settles at 75% of its initial value, as dictated by the mass balance.

- ⇒ **Region C:** Similar behavior to region A is observed when the hydrogen flow rate is increased to its initial value from the ramped down value. The pressure reaches a maximum value just before the minimum in the nitrogen flow occurs, after which the increasing hydrogen content starts to remove the excess nitrogen in the system to form ammonia.
- ⇒ **Region D:** The nitrogen feed flow continues to increase even after the hydrogen feed flow rate plateaus. The sinusoidal wave in this region (for nitrogen and reactor pressure) is the second order response. This is typical behaviour seen in controllers (discussed in Section 2.7) where the response first overshoots its setpoint before settling at the steady-state value. When settled (at ~ 170 minutes), the hydrogen to nitrogen ratio returns to the value 3.

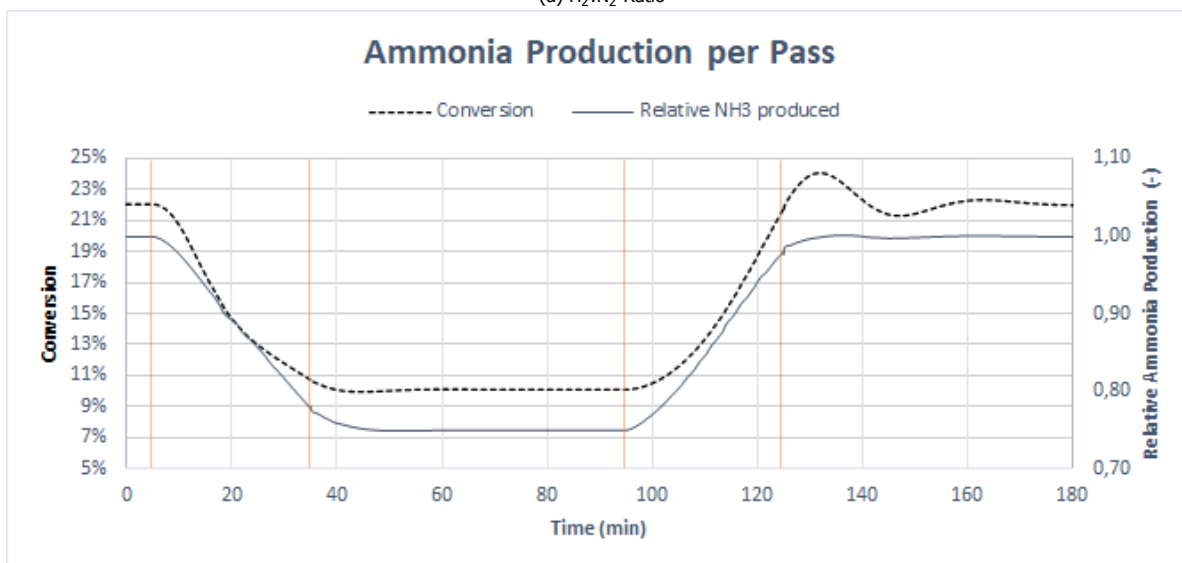
Secondary effects of the control actions

The control action affects various process parameters. There are consequences for the H₂ to N₂ ratio, the conversion, reactor temperature and heating requirements.

Figure 7.5a presents the hydrogen versus nitrogen ratio in both the feed and at the inlet of the reactor. While Figure 7.5b depicts the conversion and the ammonia production rate relative to the initial capacity, as result of changes in the H₂:N₂ ratios.



(a) H₂:N₂ Ratio



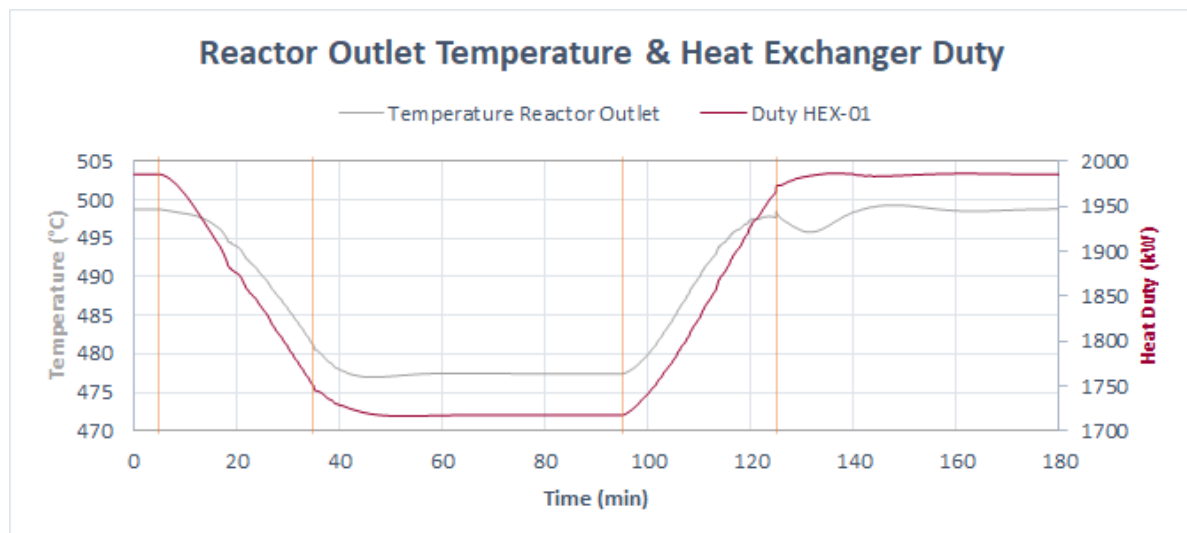
(b) Conversion vs. relative ammonia production

Figure 7.5: Time series for 25% Ramp-down/up scenario - Control Structure 1

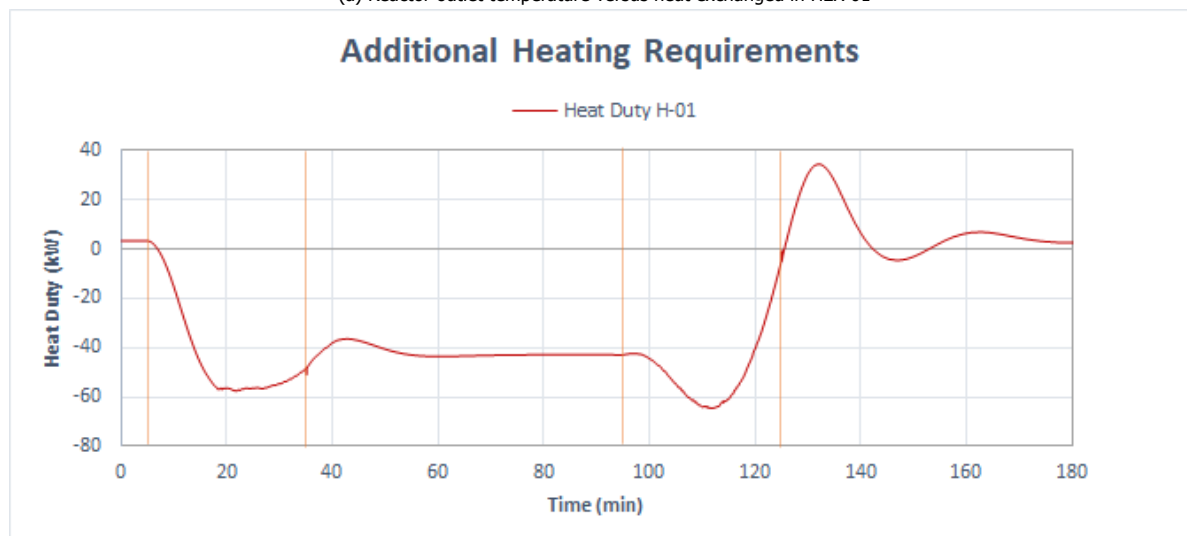
Discussion

- ⇒ The feed ratio of hydrogen to nitrogen returns to 3 when the system has stabilized (**Region B and D**).
- ⇒ However, in the loop for **Region B**, the $H_2:N_2$ ratio remains persistently reduced because the excess nitrogen substitutes hydrogen until the hydrogen feed is ramped back up.
- ⇒ Conversion depends on the $H_2:N_2$ ratio at the inlet of the reactor (Equation 4.2). Therefore, the conversion and $H_2:N_2$ ratio lines are similar in shape. Since there is excess nitrogen present in the loop, the conversion drops to 10 % (**Region B**).
- ⇒ The line representing ammonia production has the same shape as the hydrogen feed. Hydrogen becomes stoichiometrically the limiting reactant for ammonia production. That's why, in **Region B**, the ammonia production settles at 75% of the initial value.
- ⇒ In **Region D** (post completion of hydrogen feed flow ramp-up), the lines clearly show second order response as the parameters are directly related to nitrogen feed flow rate.

Figure 7.6 depicts the effects of the control action on reactor outlet temperature and, the heat duties of heat exchanger HEX-01 and heater H-01.



(a) Reactor outlet temperature versus heat exchanged in HEX-01



(b) Additional heat requirement provided by heater H-01

Figure 7.6: Time series for 25% Ramp-down/up scenario - Control Structure 1

Discussion

- ⇒ It is clear that the reduction in ammonia production (**Region B**) results in lower heat released by the reaction. The drop in exothermic heat lowers the heat that can be exchanged in HEX-01, its heat duty therefore drops proportionally to the amount of ammonia formed. At the same time, the mass flow rate notably rises in this control philosophy which causes the reactor outlet temperature to drop, as given in Table 7.2.
- ⇒ Even though Figure 7.6a depicts that the reactor outlet temperature and HEX-01 duty both decrease in **Region B**, the cold stream leaving the heat exchanger becomes warmer. This can be explained by the fact that the total molar flow rate has reduced and therefore the heat exchanger area becomes too big. This effect is amplified by the increased concentration of nitrogen in the system that alters the specific heat capacity. Consequently, in order to maintain the desired reactor inlet temperature (300 °C), the heat duty of heater H-01 becomes negative to cool down this feed stream. Here, the heater functions as a by-pass around the heat exchanger (HEX-01) to achieve this. This negative heat duty remains until the hydrogen feed is ramped up again.

Details on the heat exchanger inlet and outlet temperatures, and the specific heat capacity can be found in Appendix E.1.3.

- ⇒ In **Region D** the heater H-01 has to briefly warm the reactor feed. This is because of the spike in the specific heat capacity of the reactor feed stream, this is evident from the increase in H₂:N₂ ratio at the reactor inlet. The influence of the hydrogen content causes cold outlet stream of the heat exchanger to be lower, therefore, additional heating to 300 °C is required.

More details on the results can be found in Appendix E.

Limitations & problem solving

Both a 10% and 25% ramp-down and ramp-up were performed successfully with this control structure. However, the simulation gave an integration error when the drop in hydrogen was more than 27%, regardless of the time period. The simulation failed around the point when H₂ feed flow rate reached 159 kmol/hr.

It is thought that the issue is caused by the fact that the density of nitrogen is significantly higher than hydrogen (more than 13 times at these conditions). When the drop in hydrogen feed flow is compensated by increasing the nitrogen feed rate, the mass flow rate in the loop increases substantially. This could have repercussions for each component in the loop and how it functions.

Initially, it was thought that the compressor would succumb under the notable increase in the mass flow rate (the brake power and shaft speed both remain constant). From Figure 7.7 it can be derived that compressor theory supports this reasoning. The figure presents a typical centrifugal compressor map¹. Following the constant shaft speed (rpm) lines in direction of an increased nominal flow², it will eventually end up on the choke line. Compressor choke is an unstable operating condition which takes place when the compressor works at a high flow rate and low discharge pressure. This causes elevated gas velocity which can eventually lead to a point where no more flow passes through the compressor [98].

¹Refer to Section 6.3 for the compressor equations used in the simulation

²Nominal flow signifies mass flow rate

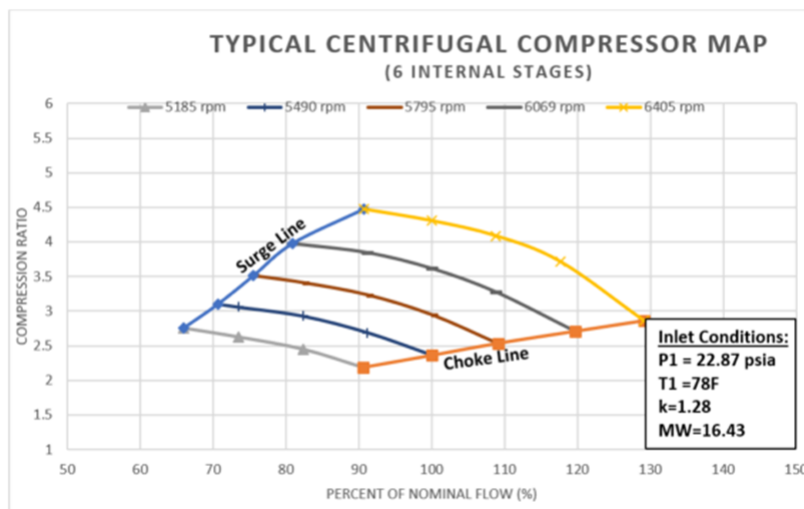


Figure 7.7: Compressor map of a typical centrifugal compressor (source: [Turbomachinery International](#))

Several steps were undertaken in order to establish whether the rise in mass flow rate of the gases was the underlying cause of the problem. And, if so, which component(s) posed the issue. The following test simulations were performed, details on each of them can be found in Appendix D:

1. Inverse compensation: Drop in nitrogen feed flow is compensated with increase in hydrogen feed flow.
2. Isolation of the compressor (in a loop).
3. Removal of the heat exchanger from the simulation.
4. Isolation of the reactor.
5. Isolation of the reactor + absorber.
6. Reduction of the absorber volume.
7. Change/removal of the valve above the absorber.

The first two simulations showed that the increased mass flow rate of the compressor is not the cause for the observed issue, as choking is simply not included in the compressor relations in Aspen Plus Dynamics. The remainder of the simulations were performed to try and find the cause of the failure in the simulation by isolation of certain equipment blocks. Thus, the issue was narrowed down to the absorber section (FLASH2 vessel + valves). The available time frame for the current work has prevented further analysis into more specific causes and resolution options.

7.2.2. Control Philosophy 2

With this control structure the pressure is maintained by reducing the brake power of the compressor when a pressure change is detected due to a hydrogen fluctuation. The Aspen Dynamics flowsheet with this control structure is presented in Figure 7.8.

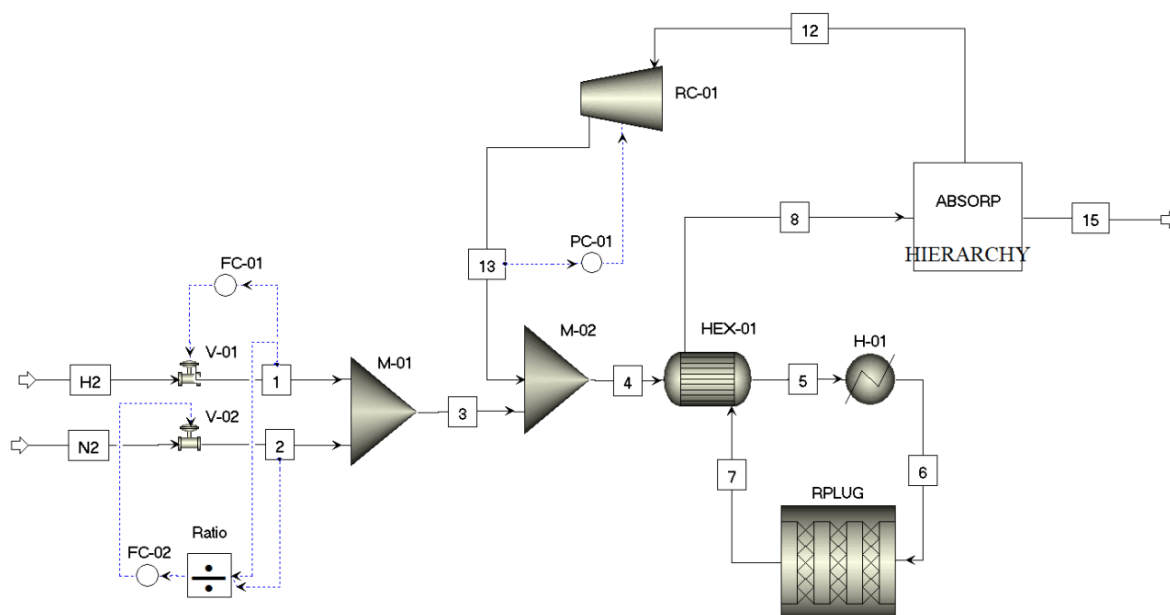
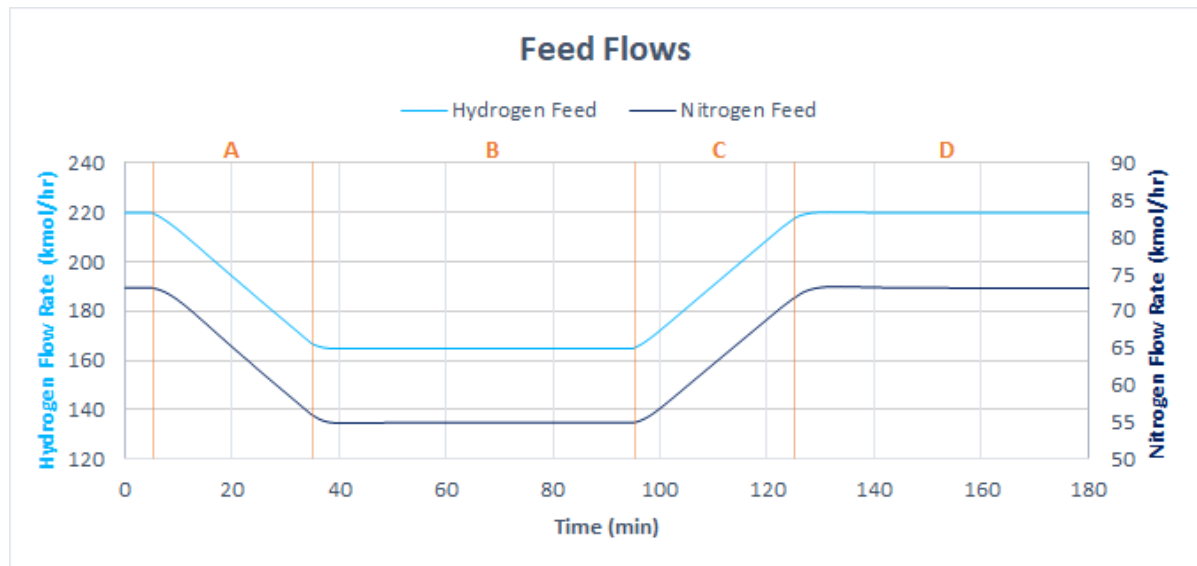


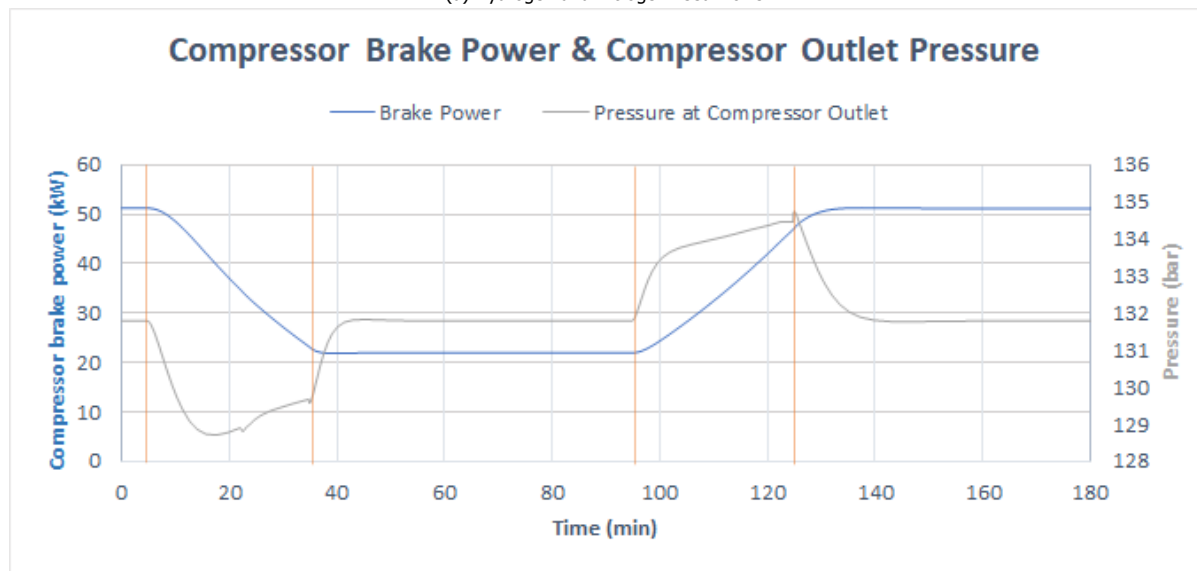
Figure 7.8: Dynamic Model with Control Philosophy 2

Primary action

The primary action is visualized in two graphs. Figure 7.9a depicts the feed flow rates as function of time. Figure 7.9b displays the pressure and compressor brake power in the loop. As in Section 7.2.1, the molar flow rate of hydrogen into the loop was ramped down to 75% and back up over a time frame of 180 minutes. For the present scenario, the feed ratio of hydrogen to nitrogen was controlled and thus maintained constant. The pressure was regulated by the brake power of the compressor. This action affects the recycling flow rate and thus the ammonia reaction rate. If the conversion yield is close to equilibrium yield, the conversion is expected to show little dependence on the residence time. Figure 5.16 with the reactor profile shows that the equilibrium is reached due to the proper dimensioning of the reactor. Therefore, the operating pressure of the original feed flow rates can be maintained with lower flow rates.



(a) Hydrogen and Nitrogen Feed Flows



(b) Recycle compressor brake power vs. Pressure at the compressor outlet

Figure 7.9: Time series for 25% Ramp-down/up scenario - Control Structure 2

Discussion

- ⇒ **Region A:** As a result of the initial pressure reduction caused by the reduced fresh feed flow rate, the controller reduces the brake power of the recycle compressor. The system pressure subsequently recovers from the initial decrease.
- ⇒ **Region B:** Steady state is reached at the original pressure level, with lower compressor power.
- ⇒ **Region C:** As the hydrogen and nitrogen feed flows ramp up again, so does the pressure in the system. The brake power is increased again, enhancing the ammonia production rate.
- ⇒ **Region D:** The pressure gradually decreases to the original value before the experiment.

Consequences

Discussion

⇒ The reactor inlet flow directly follows the brake power of the recycle compressor, as expected.

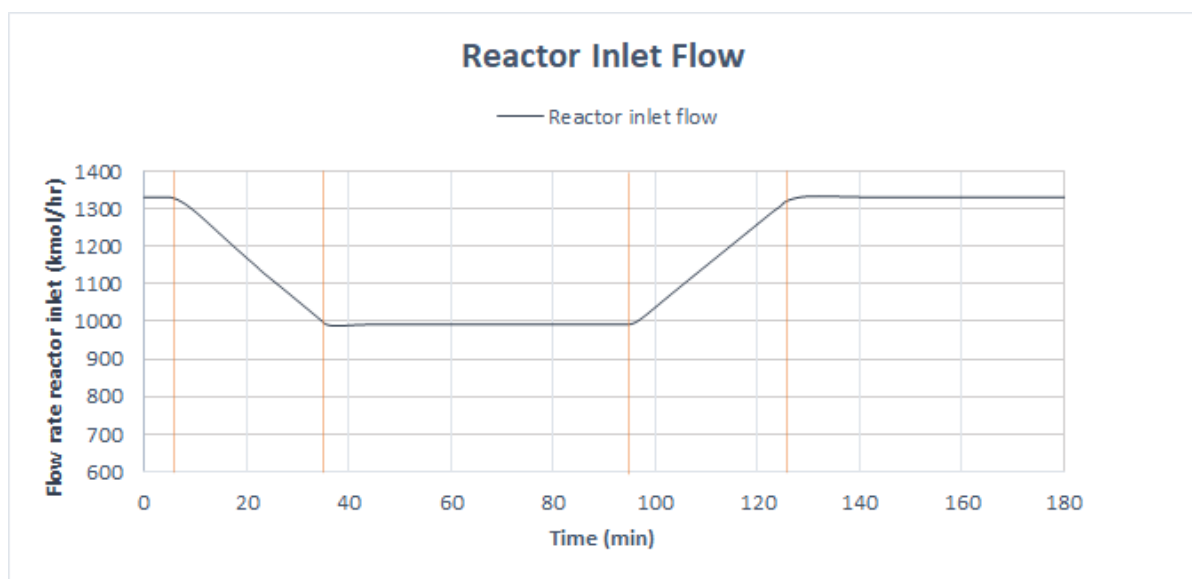
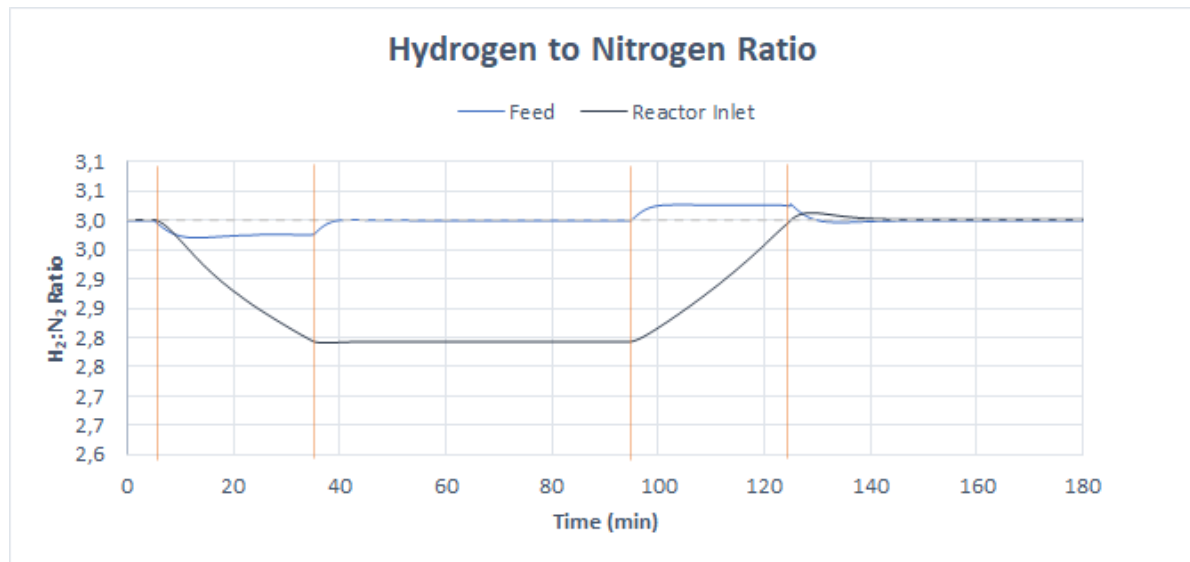
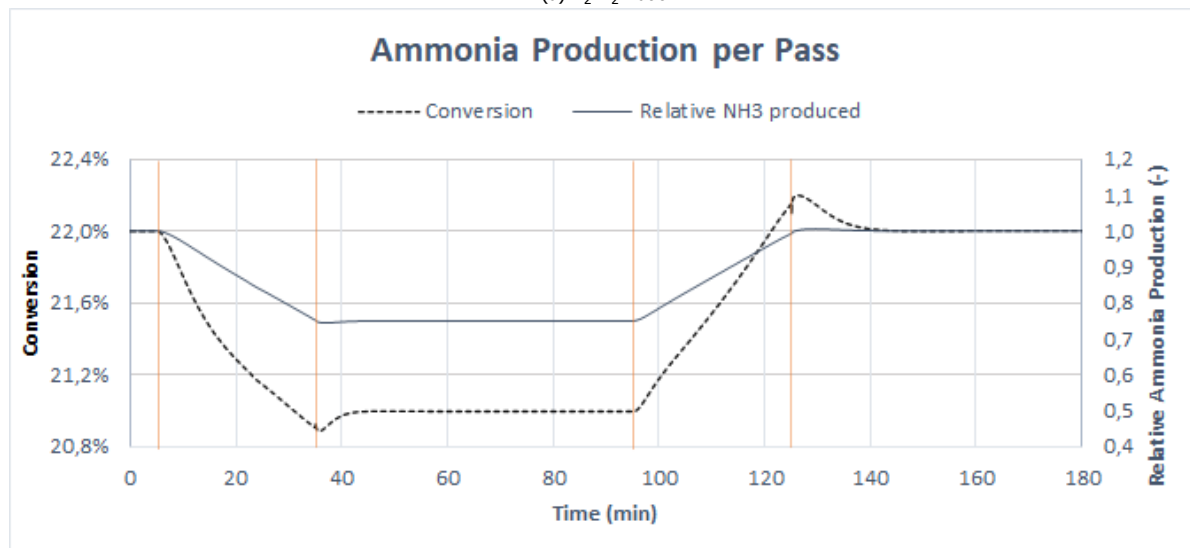


Figure 7.10: Residence time vs. inlet flow rate reactor (25% Ramp-down/up scenario - *Control Structure 2*)

(a) $H_2:N_2$ Ratio

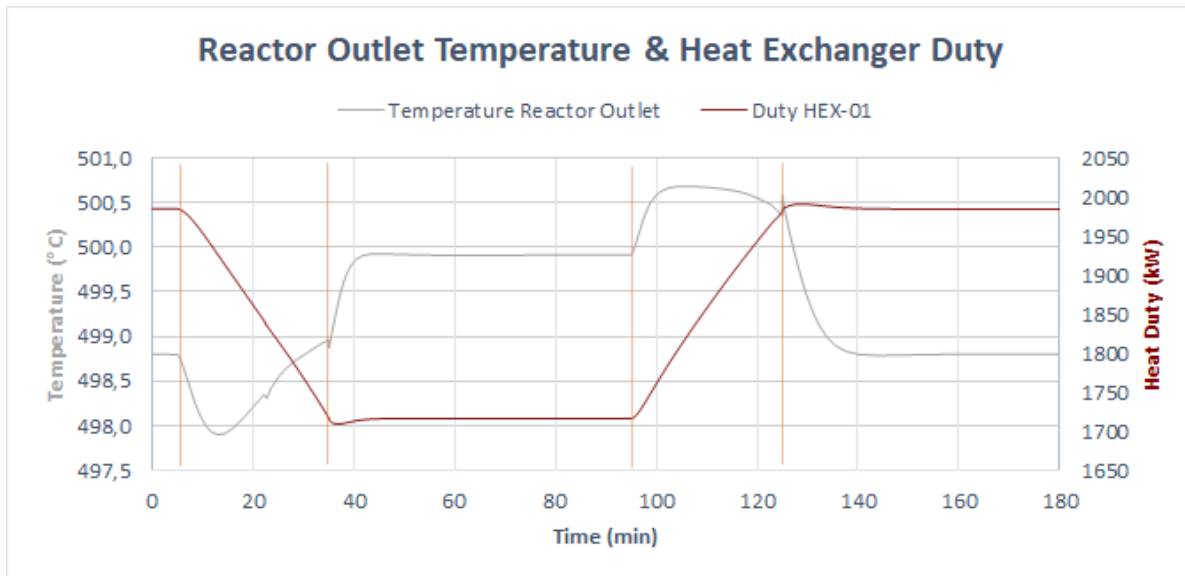
(b) Conversion vs. relative ammonia production

Figure 7.11: Time series for 25% Ramp-down/up scenario - *Control Structure 2*

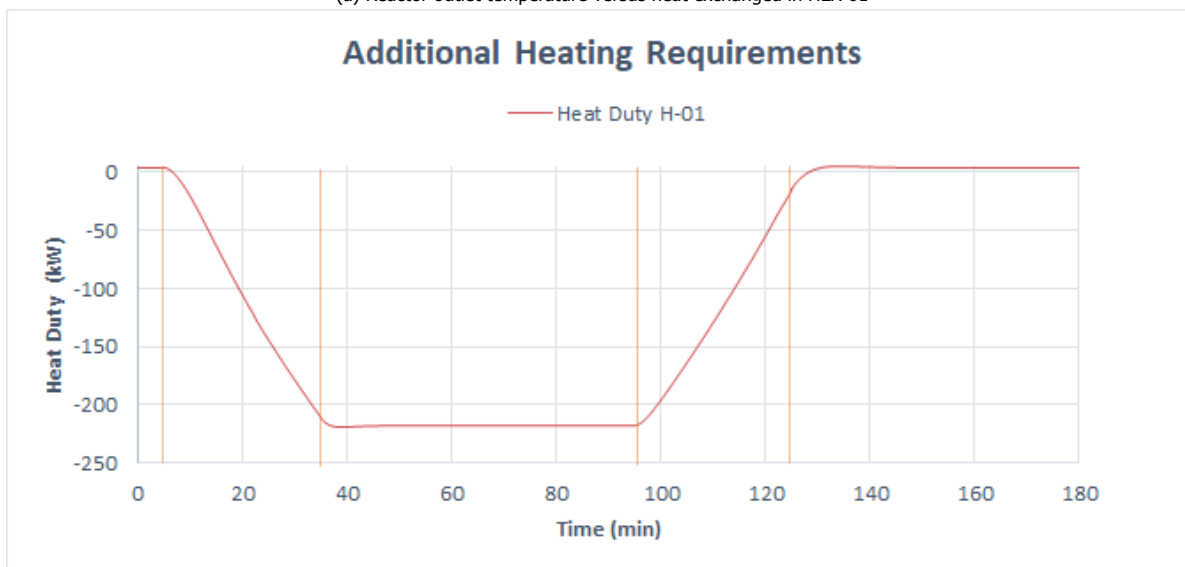
Discussion

- ⇒ The feed $H_2:N_2$ ratio is controlled at a setpoint of 3. It briefly deviates from the setpoint during the ramp-up and ramp-down periods because the ratio control cannot keep up with these disturbances ([Region A and C](#)). The feed ratio returns to 3 in [Region B and D](#) after the system has had enough time to correct.
- ⇒ In [Region B](#), it is interesting to note that the ratio in the loop for *control structure 2* does not completely return to 3. This is because process variable (hydrogen feed flow/nitrogen feed flow) of the controller that regulates the reactant flows is measured for the make-up gas, and not in the loop. As result of the delay in response time this causes a deviation in $H_2:N_2$ ratio in the loop itself. It seems that the disturbance in N_2 feed in [Region C](#) exactly cancels the disturbance that originates in [Region A](#).
- ⇒ Like *Control Structure 1*, the conversion is directly linked to the hydrogen-to-nitrogen ratio. Here, the conversion only drops by a few percent since the aim here was to keep the feed at a stoichiometric ratio. The reason the conversion is a bit lower, is because at the inlet of the reactor the ratio reduces to 2.8 ([Region B](#)), as described above.

⇒ The bumps in the conversion graph during the transfer from [Region A to B](#) and [Region C to D](#) are result of the influence of the pressure on the conversion.



(a) Reactor outlet temperature versus heat exchanged in HEX-01



(b) Additional heat requirement provided by heater H-01

Figure 7.12: Time series for 25% Ramp-down/up scenario - *Control Structure 2*

Discussion

- ⇒ The reactor outlet temperature line looks the same as the pressure line in [Figure 7.9b](#). Because the H₂:N₂ ratio and reactor inlet temperature stay (almost) constant in this simulation, the reaction conversion remains only dependent on the pressure in the reactor. The reactor outlet temperature only slightly changes due to this.
- ⇒ The duty of the heat exchanger is not shown to be dependent on the reactor outlet temperature; no influence is seen from the reactor temperature graph. It is dependent on the H₂:N₂ ratio and the flow rate into the reactor (this flow governs the ammonia production rate). The graphs showing the hydrogen to nitrogen ratio in the reactor feed has the same shape as the HEX-01 duty graph, including the slight deviations in the transition periods after the ramp-down and ramp-up.
- ⇒ In [Region B](#), it is seen that heat-exchanger (HEX-01) duty settles at a decreased value while the reactor outlet temperature increases. This is because, even though the ammonia production

lowers, the reactor outlet temperature only slightly changes. In the HEX-01 however, the reduced flow rate in the system combined with the same heat exchanger area results in much higher outlet temperatures. The heater H-01 must now compensate for this elevated temperature, and reduces this to the desired 300 °C (by-pass function), resulting in a negative heat duty.

More details on the results can be found in Appendix E.

Limitations

As opposed to the results of section 7.2.1, no limitations have been observed in ramping-down the hydrogen feed to 50% of its initial value with pressure control on the basis of recycle flow rate.

In reality, however, the compressor brake power is not as flexible as assumed in the Aspen Dynamics equations for the recycle compressor and would not work with low brake power.

7.2.3. Summary & comparison

In Table 7.2 and Table 7.3 the most important parameters of all scenarios (10%, 25% and 50%) for both *Control Structure 1* & 2 are summarized in support of the following.

Table 7.2: Summary table comparing the two control philosophies

Process parameter	Unit	Control structure 1			Control Structure 2			
		Reference	10%	25%	Reference	10%	25%	50%
Time	min	Initial	New steady-state		Initial	New steady-state		
Hydrogen feed	kmol/hr	219.7	197.7	164.7	219.7	197.7	164.8	109.9
Nitrogen feed	kmol/hr	73.2	66.0	55.0	73.2	65.9	54.9	36.6
Feed ratio	-	3.0	3.0	3.0	3.0	3.0	3.0	3.0
Reactor inlet ratio	-	3.0	1.8	1.0	3.0	2.9	2.8	2.7
NH3 production rate	kmol/hr	146.4	131.8	109.8	146.5	131.8	109.9	73.2
Conversion	%	22	15.4	10.1	22	21.6	21.0	20.4
Exchanged heat (HEX-01)	kW	1985	1883	1718	1985	1888	1717	1347
Heat Duty Required (H-01)	kW	3.13	-57.7	-43.2	3.6	-96.6	-217.8	-341
Brake Power	kW	51.2	51.2	51.2	51.3	37.5	22.0	6.7
Residence time	s	6.7	7.2	8.0	6.7	7.4	8.8	13.1
Molar flow rate reactor inlet	kmol/hr	1331	1216	1103	1332	1194	993	661
Recycle mass flow rate	kg/hr	8843	11350	14552	8846	8112	6932	4745
Recycle volume flow rate	m ³ /h	275.8	253.4	235.2	276.0	245.5	202.3	133.1
Temperature reactor outlet	°C	498.8	494.8	477.4	498.8	499.6	499.9	500.2

Table 7.3: Range of Pressure fluctuations at the reactor outlet for each ramp-down/up scenario

	Control structure 1		Control structure 2		
	10%	25%	10%	25%	50%
Initial pressure	128.6	128.6	128.5	128.5	128.5
Minimum pressure	127.5	126.1	127.4	125.9	123.3
Maximum pressure	129.6	131.0	130.0	131.6	134.0
Maximum pressure difference	2.04	4.91	2.55	5.73	10.72

For both control strategies, the ammonia production rate is directly proportional to the hydrogen feed flow rate supplied to the system. The NH₃ production will thus settle at 90%, 75% and 50% in the 'new' steady state after hydrogen reduction has been imposed. From this also derives the fact that the heat exchanged in HEX-01 is similar in both control structures. Another observation is that the cold stream outlet temperature increases in both cases because the heat exchanger area has become too big for the reduced flow rates.

The main differences that can be observed between the two control scenarios are as follows:

- **Reactor inlet H₂:N₂ ratio** Due to the nature of the control philosophies, *control structure 1* has a significantly lower ratio in the recycle loop (1.8 and 1.0) while *control structure 2* has a ratio around ~ 3. The first control structure replaces the lack of hydrogen with nitrogen and the latter aims to keep the ratio constant.
- **Conversion** The conversion is expressed in terms of nitrogen (Equation 4.2) and since the first control scheme has a much higher nitrogen content, the conversion computes to be lower.

In the first control structure the H₂:N₂ ratio moves away from the stoichiometric ratio, so the conversion does not represent a viable parameter to measure the process efficiency. Therefore, if the conversion is calculated for *control structure 1* it significantly drops during the simulation compared to the second control structure, even though the same amount of ammonia is produced. If instead the conversions were calculated in terms of hydrogen consumed, they would be the same for both controls.

- **Mass flow rate of recycle stream** In both cases the molar flow rate into the reactor reduces and since the H₂:N₂ ratio remains close to constant for *control scheme 2*, the mass flow rate decreases too. For *control structure 1*, however, the mass flow rate increases significantly due to the rise in nitrogen vs. hydrogen ratio (see 7.2).
- **Reactor outlet temperature** Both scenarios produce the same amount of ammonia (so the amount of exothermic heat released is equal). For *control philosophy 2*, the mass flow rate through the reactor is decreased by the same ratio, resulting in a similar outlet temperature compared to the initial state. Whereas, in *control philosophy 1* the recycle mass flow rate the system does not decrease significantly, resulting in a distinctly lower reactor outlet temperature.
- **Cold stream temperature increase HEX-01** The heat duty of the heat exchanger (HEX-01) is the same in both control philosophies, which is lower compared to their initial state due to the reduction in produced NH₃. Conversely, the $\Delta T_{cold} = T_{5-4}$ over the heat exchanger has increased after the ramp-down, 5.4 °C in *control structure 1* and 28.7 °C in *control structure 2*, as is seen in 7.13.

The energy in this stream can be described as:

$$Q_{HEX-01} = \dot{m} * C_p * \Delta T_{5-4}$$

Where,

\dot{Q} = Energy flow [W]

\dot{m} = Mass flow [kg/s]

C_p = Specific heat capacity [J/(kg°C)]

ΔT_{cold} = Temperature difference between outlet and inlet [°C]

Using the equation above, the contradicting result can be explained:

- *Control structure 1*: the mass flow rate has increased but this is compensated by the higher specific heat capacity (C_p) of the mixture with the higher concentration nitrogen stream. Resulting in a ΔT_{cold} increase of 5.4 °C.
- *Control structure 2*: the mass flow rate in the system has reduced, while keeping the same heat exchange area and specific heat capacity. Resulting in a ΔT_{cold} increase of 28.7 °C.

The additional heater H-01, effectively representing a by-pass for the hot stream over the heat exchanger HEX-01, has to cool this reactor feed stream for both control structures.

- **Heat duty for H-01** For both control structures, the negative heat duty from H-01 increases because it has to cool the outlet stream of the heat exchanger to the desired reactor inlet temperature. For *control structure 2* this cooling requirement is even bigger since the increase in ΔT_{cold} is greater than in *control structure 1*.

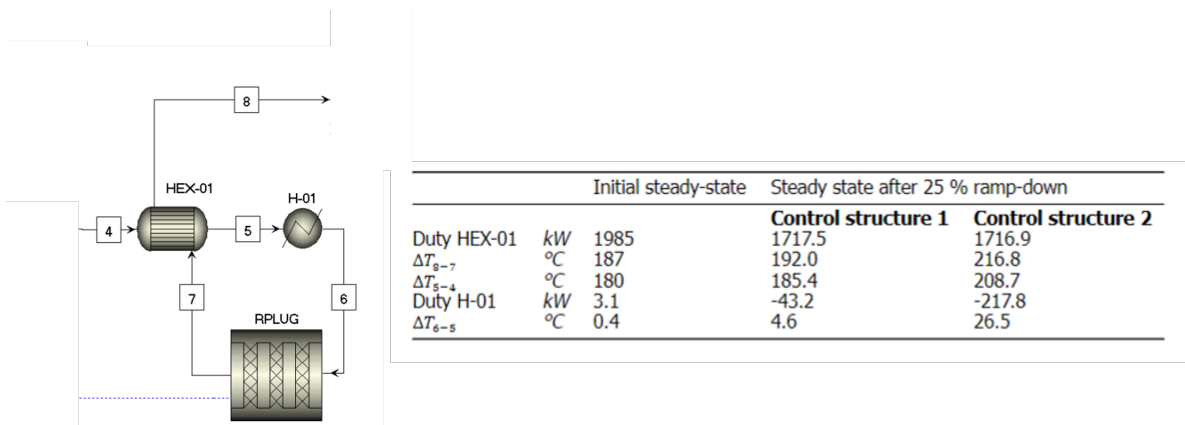


Figure 7.13: Heat duties and temperature differences in the reactor loop

More details on the temperatures and pressures in the system before and after the hydrogen ramp-down can be found in [Appendix E](#).

8

Conclusions & recommendations

The objective for this research was the analysis of the dynamics of a 60 *tons/year* ammonia synthesis plant which utilizes an iron-based catalyst and employs ammonia recovery by chemisorption. This chapter presents the conclusions and recommendations of this work. First, a short summary is given with results and take-aways leading up to the dynamic simulation.

8.1. Summary of Steady-state simulations

8.1.1. Kinetics

An initial steady-state model was created to investigate the thermodynamic limitations and maximum attainable conversion for the synthesis process *MODEL 1*. Subsequently, a second steady-state model incorporating reaction kinetics, ammonia absorption model and heat integration was made *MODEL 2*. This was used to determine the reactor size, heating/ cooling requirements and operating pressure of the system.

For reaction kinetics, the three most common equations, Temkin-Pyzhev, Nielsen and Simon & Dyson, were selected from literature. The latter two were found to be incompatible with Aspen Plus due to their equilibrium expression. Hence, the widely applied Temkin-Pyzhev (1940) rate equation was selected. However, this expression posed a few drawbacks for the application in the simulation model:

1. The reaction approaches infinity when the ammonia concentration is zero.
Solution: This was solved by using a multiplication factor and casting the equation into Langmuir-Hinselwood- Hogan- Watson (LHHW) format. This format suited easy implementation into Aspen Plus.
2. An inaccurate description of the equilibrium (especially for a wide range of temperatures)
Solution: This was solved by incorporating an equilibrium correlation based on Haber & Le Rossignol data. This equilibrium correlation was rewritten for the operating conditions range of the process, such that it could be plugged in the LHHW format for Aspen Plus.

The proposed modified rate equation was successfully validated in this work before implementation into the Aspen Plus models, see Equation 5.13.

8.1.2. Simulation results

Reactor

A single-stage adiabatic reactor with a length-over-diameter ratio of 8 (simulated as an RPLUG reactor) was selected. Compared to an isothermal reactor, the mechanical design of an adiabatic is considerably simpler. From the reactor profile, it was concluded that reactor inlet temperature strongly influences the conversion and the reactor size. Consequently, the inlet temperature determines the amount of ammonia that can be formed before the equilibrium is reached. This is due to the exothermic nature of the reaction. Thus, lower inlet temperature corresponds to a higher ammonia production capacity. However, the reactor inlet temperature must not be lower than the activation temperature of the catalyst. The most important results are:

- The ZA-5 iron catalyst was selected for its wide activation range, setting the minimum reactor inlet temperature to 300 °C.

- The pressure was fixed at 130 *bar* to obtain maximum possible conversion without overheating the catalyst.
- The reactor was sized to reach this conversion under the system conditions, which is 22.1%.

Absorber

The absorber, employing Strontium chloride amine ($\text{SrCl}_2 \cdot \text{NH}_3$) as absorbent, was modelled as a stoichiometric reactor to include the absorption reaction and enthalpy. Using its absorption characteristics and the Van 't Hoff equation, the operating temperature was determined to be approximately 105 °C as function of the partial NH_3 pressure. This is a significantly higher temperature than conventional condensation would require. Under these conditions, the heat duty of the absorber was found to be -2182 *kW*. To avoid desorption in the bed due to the exothermic heat released in the reaction, a shell & tube configuration was suggested to cool the metal halides during the absorption process.

If the absorption beds switch every hour for regeneration, the absorption of 146.8 *kmol* of NH_3 (60 *tons/year*) requires about 3.7 *tons* of $\text{SrCl}_2 \cdot \text{NH}_3$. The mass of the absorption and regeneration beds could pose complications for the application of this separation method.

8.2. Conclusions of Dynamic simulations

The steady-state simulation (*MODEL 2*) was transformed into a dynamic simulation in Aspen Plus Dynamics (*MODEL 2*). Control structures were developed and various simulation runs were performed in order to answer the following research questions:

- How can variations in the hydrogen feed flow of a flexible small-scale ammonia synthesis loop be controlled?
- What are the effects of these variations and controls on the system?

Initially, a step reduction of 10% was applied to the hydrogen feed flow rate. This led to significant pressure deviations. For *control philosophy 1* and *control philosophy 2*, the maximum deviation from the initial pressure measured at the reactor outlet were 10 *bar* and 6 *bar* respectively. Therefore, it was concluded that a hydrogen buffer will be required to allow for a more gradual reduction of the hydrogen feed.

Next, different scenarios with a hydrogen buffer were tested for each control philosophy. The presence of a H_2 buffer was translated into a linear ramp-down and ramp-up in the hydrogen feed flow. The hydrogen feed was ramped down over 30 *minutes* with a 10%, 25% and 50% reduction compared to the initial hydrogen feed flow rate. Afterwards, the system is given enough time to settle at a new steady-state. At the 95th *minute* the hydrogen feed flow was ramped back up over the same time period. The ammonia production is directly related to the hydrogen fed into the system, resulting in a 10%, 25% and 50% reduction in ammonia leaving the system for both control structures.

How can variations in the hydrogen feed flow of a flexible small-scale ammonia synthesis loop be controlled?

The development and evaluation of *Control philosophy 1 and 2* for the synthesis loop have proven that hydrogen feed flow variations can be controlled for the scenarios tested in this work. The aim of the control structures was to maintain the system pressure when the system was subjected to these hydrogen fluctuations. This was required in order to avoid metal fatigue in the equipment. *Control philosophy 1* relies on the compensation of hydrogen deficiency with surplus of nitrogen to retain the system pressure. For *Control philosophy 2* the recycle flow rate was varied to control the ammonia production and increase the residence time.

The following conclusions were drawn with respect to the control philosophies:

- It was realized that by merely applying a default control structure, the operating pressure increased by 16 *bar* for a 10 % linear reduction of the hydrogen feed flow rate (See Subsection 6.5.1). With either of the control *philosophies 1 or 2*, the pressure could be maintained (at the same value) and the variations during transition were significantly lower.
- Both control philosophies were successfully applied to control the system pressure for the 10% and 25% H_2 ramp-down/up scenarios. The greatest pressure range measured in the 25% ramp

down scenario for *control philosophy 1* and 2 were 4.91 bar and 5.73 bar, respectively. This corresponds to a pressure range of 3.8% and 4.5% with respect to the initial pressure ¹.

- Unlike *control philosophy 2*, *control philosophy 1* was limited to a maximum reduction of 25% in the hydrogen feed. The 50% ramp down case ran into simulation errors. This was further studied but the exact cause of this error was undetermined. It is highly likely that the significant increase in mass flow rate (due to nitrogen compensation) plays a role.

What are the effects of these variations and controls on the system?

From the results & discussions (See Chapter 7) of the simulated scenarios the following conclusions with respect to impact on the synthesis loop were drawn:

- Both control structures show better response even to a 25% H₂ gradual ramp-down pattern than compared to the 10% step down scenario. Therefore, it is desirable to have a hydrogen buffer (in addition to a nitrogen buffer) to ensure a more gradual ramp-down.
- In all investigated scenarios for both control structures there is an increased cooling requirement to maintain the desired inlet temperature of the reactor at 300 °C. The heat exchange area (HEX-01) in the new steady-states becomes too big for the reduced flow rates. One of the ways to counter-balance this effect can be to create a by-pass for the hot stream around the exchanger.
- In *control philosophy 1*, the hydrogen deficiency is compensated by supplying additional nitrogen. Since the density of nitrogen is higher than hydrogen, the mass flow rate in the loop significantly increases as the nitrogen concentration goes up. In practical applications, the increased mass flow rate poses a fair concern for the components in the system, especially for the compressor.

¹This is lower than the operation of the relief valve setting as per the ASME Boiler and Pressure Vessel Code (BPVC) Section VIII (2013) [99] and higher than depressurisation limit where compressor seal failure and other possible equipment failure can occur instantaneously [100]

8.3. Recommendations

This section discusses recommendations for future research. Several improvements are proposed for the dynamic model to represent more realistic operation or to model the process more accurately:

- Control structure:
 - Further optimization of the tuning parameters of the controller to obtain a faster/ more fluent response.
 - Incorporating a time delay in the feedback control loops instead of immediate control measurement signal.
 - For *control philosophy 2* a feedback control loop could be implemented for the H₂:N₂ ratio in the loop. This control should overrule the feed ratio controller. This could solve any discrepancy in the H₂:N₂ ratio between feed stream and recycle loop due to delays in response of the system. Another solution is the application of a purge stream.
- Absorber dynamics:
 - Modelling of switching between two absorber/ desorber beds that are batch-wise operated
 - Including absorption and regeneration kinetics
- Unit operations:
 - Incorporating flow-dependent pressure drops for the system components other than the reactor.
 - Taking into account the heat losses in the unit operations.
 - Implementing performance curves for the compressor for more accurate simulation.

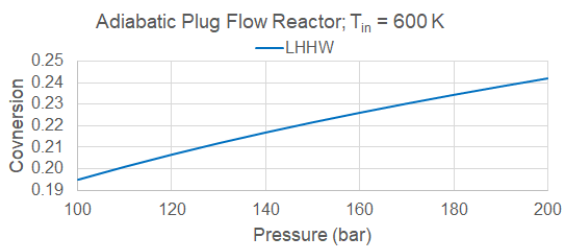
The following topics are proposed for further research:

- This primary study should be expanded with more elaborate scenarios, such as a start-up and shut-down and various buffer scenarios.
- Investigation of the permissible flow rate variation range for different compressor types.
- The potential pressure drop across the absorption bed with the proposed shell-and-tube cooling design.
- The evaluation of economics was beyond the scope of this study. Therefore, a study of cost analysis for a flexible ammonia plant utilising absorption could be carried out.
- Consultation of material and equipment specialists to determine acceptable range of pressure fluctuations in the synthesis loop. A design considering material fatigue is suggested.

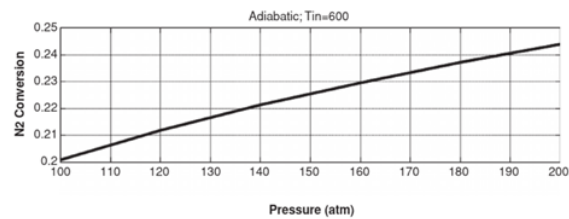


Reaction kinetics

A.1. Validation LHHW rate equation

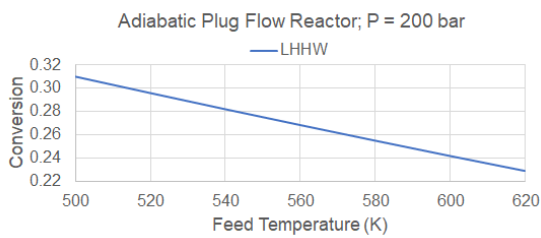


(a) Data Aspen Plus Model

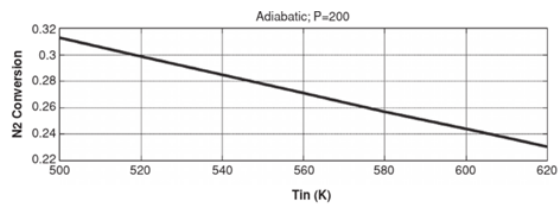


(b) Plant wide control book [93]

Figure A.1: Conversion vs. Pressure ($T_{feed} = 600\text{ K}$) Adiabatic Plug Flow Reactor with LHHW Temkin Kinetics



(a) Data Aspen Plus Model



(b) Plantwide control book [93]

Figure A.2: Conversion vs. Feed Temperature ($p = 200\text{ bar}$) Adiabatic Plug Flow Reactor with LHHW Temkin Kinetics

Table A.1: Simulation information for LHHW validation

Adiabatic Reactor		
Rate Equation	Temkin-Pyzhev in LHHW format	
Catalyst Activity Factor	$f = 4.75$	
Feed		
Hydrogen	300	kmol/hr
Nitrogen	100	kmol/hr
Ammonia	1	kmol/hr

A.2. Experimental Data Fit to Haber & Le Rossignol Correlation

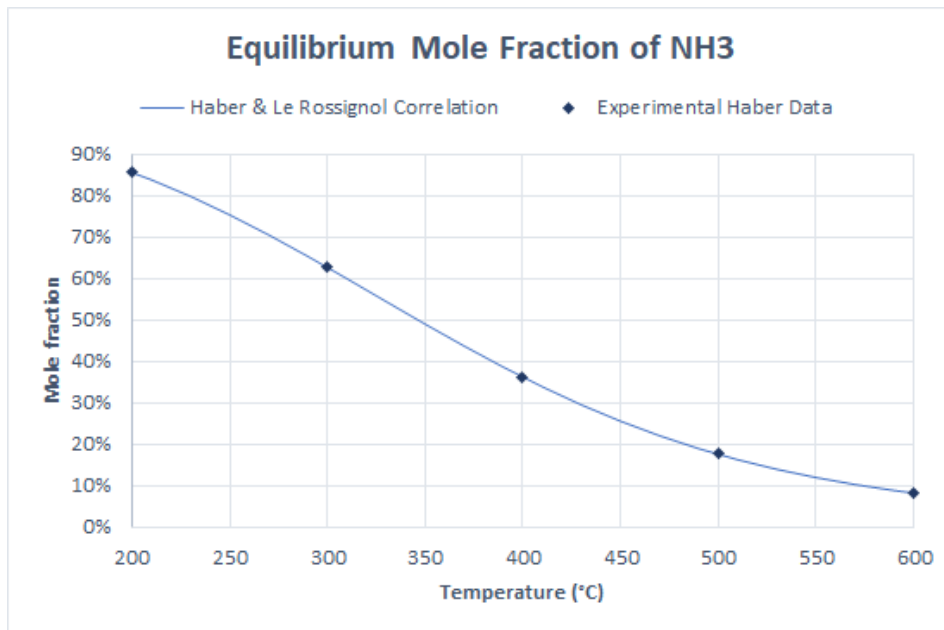


Figure A.3: Experimental Data Points According to Haber Compared to the Haber & Le Rossignol Equilibrium Correlation

A.3. Haber & Le Rossignol vs. Gillespie & Beattie equilibrium correlations

Haber & Le Rossignol (1908) [94]:

$$K_{eq}(T) = 10^{2.10 + \frac{1}{4.571} \left(\frac{9591}{T} - 0.00046T + 0.85 \times 10^{-6} T^2 \right) - \frac{4.98}{1.985} T} \quad (\text{A.1})$$

Gillespie & Beattie (1930) [31]:

$$K_{eq}(T) = 10^{-2.691122 \log_{10} T - 5.519265 \times 10^{-5} T + 1.848863 \times 10^{-7} T^2 + \frac{2001.6}{T} + 2.6899} \quad (\text{A.2})$$

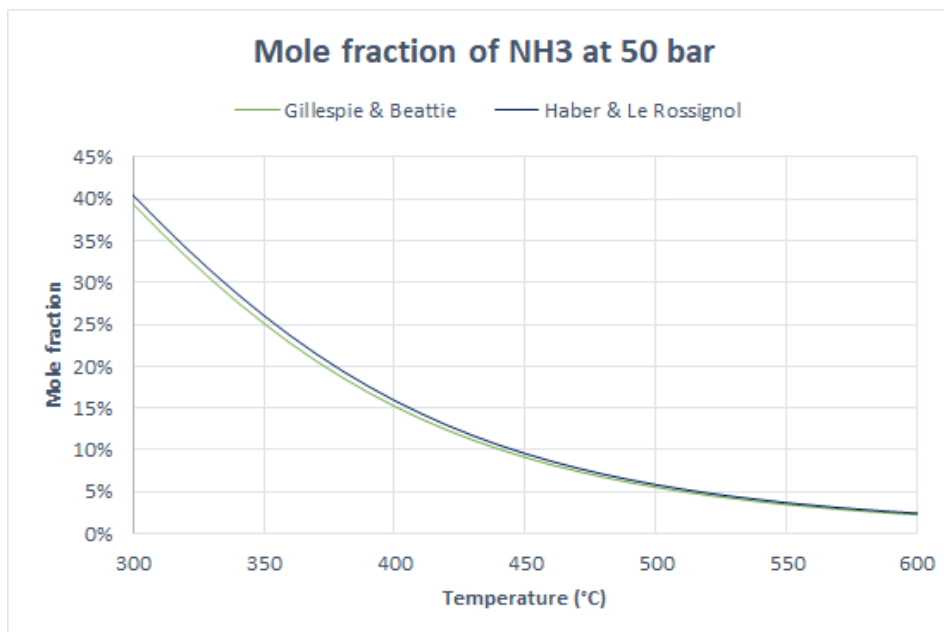


Figure A.4: Haber & Le Rossignol vs. Gillespie & Beattie equilibrium correlation at 50 bar

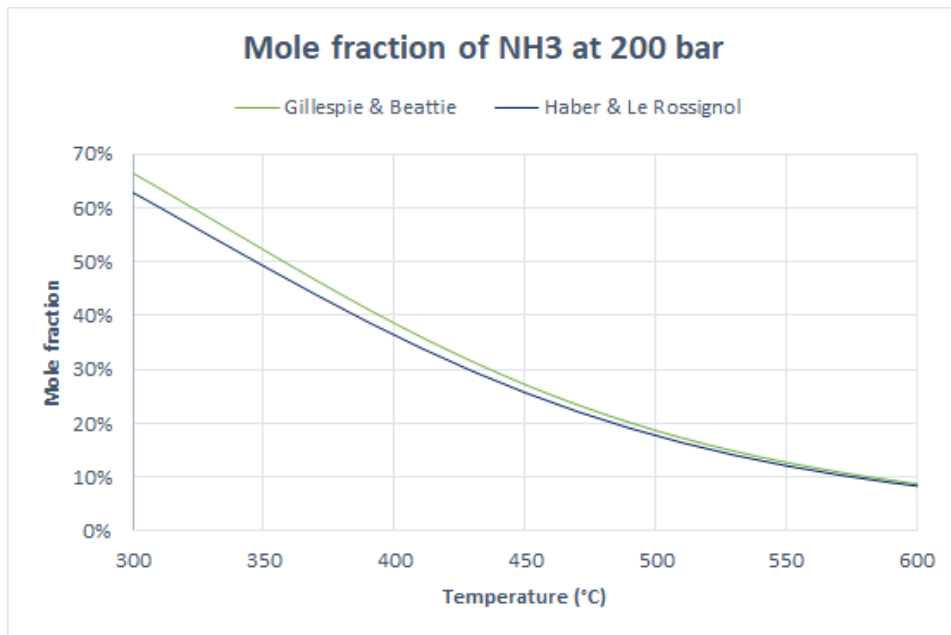


Figure A.5: Haber & Le Rossignol vs. Gillespie & Beattie equilibrium correlation at 200 bar

A.4. Derivation of simplified equilibrium correlation from Haber & Le Rossignol

The equilibrium constant ($K_a(T)$) according to Haber & Le Rossignol's correlation (Equation A.3) was plotted over a logarithmic temperature range of 300 to 600 °C.

$$K_a(T) = 10^{2.10 + \frac{1}{4.571} \cdot \left(\frac{9591}{T} - 0.00046 \cdot T + 0.85 \cdot 10^{-6} \cdot (T)^2 \right) - \frac{4.98}{1.985} \cdot \log(T)} \quad (\text{A.3})$$

Now, the equation of a line was to be found in the form of: $e^{-E/RT}$ that corresponds to the same graph as Haber & Le Rossignol's correlation. This was found by varying the parameters in the equation until the lines were on top of each other, resulting in:

$$K_x(T) = \frac{\exp\left(\frac{53}{R \cdot T}\right)}{9.8 \cdot 10^5} \quad (\text{A.4})$$

A.5. MATLAB® codes

A.5.1. Comparison of kinetic rate equations

```

1 %% Comparing Temkin-Pyzhev & Nielsen & Dyson and Simon
2 clear
3 clc
4 close all
5
6 %% Parameters
7 T = 400 + 273.15; %K
8 p1 = 100*0.986923267; %atm
9 p2 = 200*0.986923267; %atm
10 R = 8.314; % J/(mol*K)
11 rho_cat = 2200; % kg/m^3
12
13 y = linspace(0, 0.95, 1000);
14 yN2 = (1-y)*0.25;
15 yH2 = (1-y)*0.75;
16 conv = 2*y./(1+y);
17
18 keq = 10^(-2.691122*log10(T) - (5.519265*10^(-5))*T + ...
19 (1.848863*10^(-7))*T^2+2001.6/T+2.6899);
20
21 %% Equation Temkin-Pyzhev, alpha = 0.5
22 f = 4.75; % Catalyst activity
23 k1 = (1.79*10^4)*exp(-87090/(R*T)); % E = [J/mol]
24 k_1 = (2.57*10^16)*exp(-198500/(R*T)); % E = [J/mol]
25
26 %Reaction Rate Equation
27 Rtem100 = ((2*f)/rho_cat)*(k1*((yN2.*p1).*(yH2.*p1).^(1.5))./(y.*p1)...
28 -k_1*(y.*p1)./(yH2.*p1).^(1.5)); %kmol/kg cat/hr
29 Rtem200 = ((2*f)/rho_cat)*(k1*((yN2.*p2).*(yH2.*p2).^(1.5))./(y.*p2)...
30 -k_1*(y.*p2)./(yH2.*p2).^(1.5)); %kmol/kg cat/hr
31
32 %% Equation Dyson & Simon
33 % Fugacity Coefficients
34 fcn2 = 0.93431737 + 0.3101804*10^(-3)*T + 0.295895*10^(-3).*p2 - ...
35 0.270729*10^(-6)*T^2 + 0.4775207*10^(-6).*p2).^2;
36 fch2 = exp(exp(-3.8402*T^(0.125))*p2 - exp(-0.1263*T^(0.5)-15.980)*(p2).^2 ...
37 + 300*(exp(-0.011901*T - 5.941))*(exp(-p2./300-1)));
38 fcy = 0.1438996 + 0.2028538*10^(-2)*T - 0.4487672*10^(-3)*p2 ...
39 -0.1142945*10^(-5)*T^2 + 0.2761216*10^(-6)*T^2;
40
41 % Activities
42 ay = y.*fcy.*p2;
43 aN2 = yN2.*fcn2.*p2;
44 aH2 = yH2.*fch2.*p2;
45
46 R3 = 1.987;
47 V3 = (1.7698*10^15)*exp(-40765/(R3*T))*((keq^2).*aN2.*((aH2.^(3/2))./(ay))...
48 - ((ay)./(aH2.^(3/2))));
49
50 V3Dys = V3*1000/2200;
51
52 %% Equation Nielsen et al.
53 Ac = 1; %Catalyst activity
54 alpha = 0.654;
55 w = 1.523;
56 AK = (3.945*10^10)*exp(-5622/T); % Ammonia synthesis rate constant
57 Ka = (2.94*10^(-4))*exp(12104/T); % [kJ*mol/s*atm] Absorption constant
58
59 Rniel100 = Ac*(AK*((yN2.*fcn2.*p1).*(keq^2))...
```

```

60     -((y.*fcy.*p1).^2)./((yH2.*fch2.*p1).^3)))./(1 +...
61     Ka*((y.*fcy.*p1)./(yH2.*fch2.*p1).^w)).^(2*alpha)); % kgmole/m^3/hr
62 Rniel200 = Ac*((AK*((aN2).*(keq^2)-((ay).^2)./(aH2).^3)))./(1 +...
63     Ka*((ay)./(aH2).^w)).^(2*alpha)); % kgmole/m^3/hr
64
65 %% Plot graphs
66 Rtem200bar = Rtem200*10^3;
67 Rniel200bar = (Rniel200/rho_cat)*1000;
68
69 figure
70 p5 = plot(conv, Rtem200bar, '--', 'Color',[0, 0.4470, 0.7410], 'LineWidth', 1.25);
71 hold on
72 p6 = plot(conv, Rniel200bar, 'Color',[0.6350 0.0780 0.1840], 'LineWidth', 1.25);
73 hold on
74 p7 = plot(conv, V3Dys, '-.', 'Color', [0.9290 0.6940 0.1250], 'LineWidth', 1.25);
75 hold on
76 plot(conv(424), Rtem200bar(424), 'ko', 'MarkerFaceColor','k','MarkerSize', 5);
77 hold on
78 plot(conv(376), Rniel200bar(376), 'kp', 'MarkerFaceColor','k','MarkerSize', 6);
79 hold on
80 plot(conv(376),V3Dys(376), 'kp', 'MarkerFaceColor','k','MarkerSize', 6);
81 hold off
82 xlabel('Conversion')
83 ylabel('Reaction Rate (mmol NH_3/g_{cat}/hr)')
84 title('Reaction Rate of Ammonia Synthesis at 400 °C & 200 bar')
85 legend('Temkin-Pyzhev','Nielsen','Simon & Dyson','Rate = 0 (Temkin)',...
86     'Rate = 0 (Nielsen)','Rate = 0 (Dyson & Simon)')
87 ylim([-100 300]);
88 xlim([0 0.95]);
89 ax = gca;
90 ax.XAxisLocation = 'origin';
91 ax.YAxisLocation = 'origin';

```

A.5.2. Validation of Modified LHHW

```

1 clear
2 clc
3 close all
4
5 opengl hardware
6
7 %% Parameters
8 T = 400 + 273.15; %K
9 p = 200*0.986923267; %atm
10
11 y = linspace(0, 0.95, 1000);
12 yN2 = (1-y)*0.25;
13 yH2 = (1-y)*0.75;
14
15 conv = 2*y./(1+y);
16
17 f = 4.75;
18 Rg = 8.314; % J/(mol*K)
19 rho_cat = 2200; % kg/m^3
20
21 k1 = (1.79*10^4)*exp(-87090/(Rg*T)); % E = [J/mol], k01 = [kgmol/m3 hr atm1.5]
22 k_1 = (2.57*10^16)*exp(-198500/(Rg*T)); % E = [J/mol], k02 = [kgmol atm0.5/m3 hr]
23
24 %% Equation Temkin-Pyzhev, alpha = 0.5
25 r = ((2*f)/rho_cat)*(k1*((yN2.*p).*(yH2.*p).^(1.5))./(y*p)...
26 -k_1*(y*p)./(yH2*p).^(1.5)); %kmol/kg cat/hr
27
28 %Different units
29 R = r*10^3;
30
31 figure
32 plot(conv, R, 'LineWidth',1 , 'DisplayName','200 bar');
33 legend('show')
34 xlabel('Conversion')
35 ylabel('Reaction Rate (mmol NH_3/g cat/hr)')
36 title('Reaction Rate of Ammonia Synthesis According to Temkin-Pyzhev at 400 °C')
37 ylim([-350 1000]);
38 xlim([0 1.05]);
39 ax = gca;
40 ax.XAxisLocation = 'origin';
41
42
43 %% LHHW Temkin
44 k3 = 2; %atm-1
45
46 rlhhw = ((2*f*k3)./(rho_cat.*(1+k3*y.*p))).*(k1*((yN2.*p).*(yH2.*p).^(1.5))...
47 -k_1*((y.*p).^2)./(yH2*p).^(1.5)); %kmol/kg cat/hr
48
49 figure
50 plot(conv, R,'LineWidth',1.2 , 'DisplayName','Temkin-Pyzhev');
51 hold on
52 plot(conv, rlhhw*10^3,'LineWidth',1.2 , 'DisplayName','LHHW Temkin-Pyzhev');
53 hold on
54 plot(conv(1), rlhhw(1)*10^3,'k^', 'MarkerFaceColor','k','MarkerSize', 4, ...
55 'DisplayName','molfraction NH_3 = 0');
56 hold off
57 xlabel('Conversion');
58 ylabel('Reaction Rate (mmol NH_3/g_{cat}/hr)');
59 title('Reaction Rate of Ammonia Synthesis at 400 °C & 200 bar');
60 legend('show')
61 ylim([-350 3000]);

```

```
62 xlim([-0.05 1.05]);
63 ax = gca;
64 ax.XAxisLocation = 'origin';
65
66
67 %% Modified LHHW Temkin
68 k1m = (1.79*10^4)*exp(-87090/(Rg*T)); % E = [J/mol], k01 = [kmol/m3 hr atm1.5]
69 k_lm = (1.71912*10^16)*exp(-193085/(Rg*T)); % E = [J/mol], k02 = [kmol atm0.5/m3 hr]
70 rmodlhhw = ((2*f*k3)./(rho_cat.*(1+k3*y.*p))).*(k1m*((yN2.*p).*(yH2.*p).^1.5))...
71 -k_lm*((y.*p).^2)./(yH2*p).^1.5);
72
73 figure
74 plot(conv, R, 'LineWidth',1 , 'DisplayName','Temkin-Pyzhev');
75 hold on
76 plot(conv, rlhhw*10^3, 'LineWidth',1 , 'DisplayName','LHHW');
77 hold on
78 plot(conv, rmodlhhw*10^3, '--', 'LineWidth',1 , 'DisplayName','Modified LHHW');
79 hold on
80 plot(conv(424), rlhhw(424), 'ko', 'MarkerFaceColor','k', 'MarkerSize', 5, ...
81 'DisplayName', 'Rate = 0 (Temkin & LHHW)');
82 hold on
83 plot(conv(373), rmodlhhw(373), 'k*', 'MarkerFaceColor','k', 'MarkerSize', 7, ...
84 'DisplayName', 'Rate = 0 (Modified LHHW)');
85 hold off
86 xlabel('Conversion');
87 ylabel('Reaction Rate (mmol NH_3/g cat/hr)');
88 title('Reaction Rate of Ammonia Synthesis at 400 °C & 200 bar');
89 legend('show')
90 ylim([-100 300]);
91 xlim([0 1.05]);
92 ax = gca;
93 ax.XAxisLocation = 'origin';
```


B

Model 2: Input specifications & additional results

B.1. Summary table input specifications

Table B.1: Equipment specifications for model 2

Name Flowsheet	Type	Phases	Pressure drop	Specifications
M-01	Mixer	Vapor-only	0	Shortcut + Countercurrent
HEX-01	Heat Exchanger	Vapor-only	1 (each side)	Calculation mode: Design with Cold stream outlet temperature specification No heat losses Adiabatic
RPLUG	Plug Flow Reactor	Vapor-only	Ergun	L = 6.4, d = 0.8m. Kinetics: Modified LHHW
C-01	Cooler	Vapor-only	0.5	Isothermal
STOICH	Stoichiometry reactor	Vapor-Liquid	2	Conversion: 100%
SEP	Separator	Vapor-Liquid	0	Heat duty = 0
RC-01	Recycle Compressor	Vapor-only	-2	Isentropic

B.2. Flow sheet and stream tables

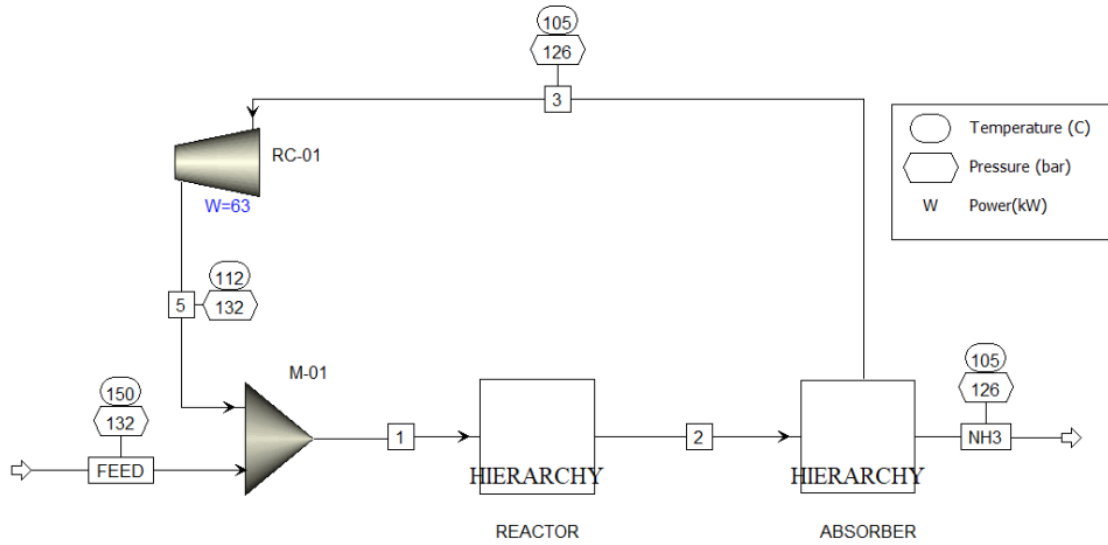


Figure B.1: MODEL 2

Table B.2: Summary Table for MODEL 2

	Units	1	2	3	5	NH3
Phase		Vapor	Vapor	Vapor	Vapor	Solid
Temperature		120	314	105	112	105
Pressure		132	128	126	132	126
Molar Vapor Fraction		1	1	1	1	0
Molar Liquid Fraction		0	0	0	0	0
Molar Solid Fraction		0	0	0	0	1
Mass Vapor Fraction		1	1	1	1	0
Mass Liquid Fraction		0	0	0	0	0
Mass Solid Fraction		0	0	0	0	1
Molar Enthalpy	<i>kJ/kmol</i>	2914	3276	2444	2663	-1531405
Mass Enthalpy	<i>kJ/kg</i>	342.2	342.2	287.0	312.8	-5198.1
Molar Entropy	<i>kJ/kmol - K</i>	-28.0	-24.8	-28.8	-28.6	-5137.8
Mass Entropy	<i>kJ/kg - K</i>	-3.3	-2.6	-3.4	-3.4	-17.4
Molar Density	<i>kmol/cum</i>	4	3	4	4	37
Mass Density	<i>kg/cum</i>	32	23.98	31.84	32.66	10905.33
Enthalpy Flow	<i>kW</i>	1075.2	1075.2	702.3	765.4	-8933.2
Average MW		8.52	9.57	8.52	8.52	294.61
Mole Flows	<i>kmol/sec</i>	0.37	0.33	0.29	0.29	0.01
Mass Flows	<i>kg/sec</i>	3.14	3.14	2.45	2.45	1.72
Volume Flow	<i>cum/sec</i>	0.10	0.13	0.08	0.07	0.00
Mole Fractions						
N ₂		0.25	0.22	0.25	0.25	0
H ₂		0.75	0.66	0.75	0.75	0
NH ₃		0	0.12	0	0	0
Ar		0	0	0	0	0
Air		0	0	0	0	0
MONO-AMMINE		0	0	0	0	0.0014
OCTA-AMMINE		0	0	0	0	0.9986

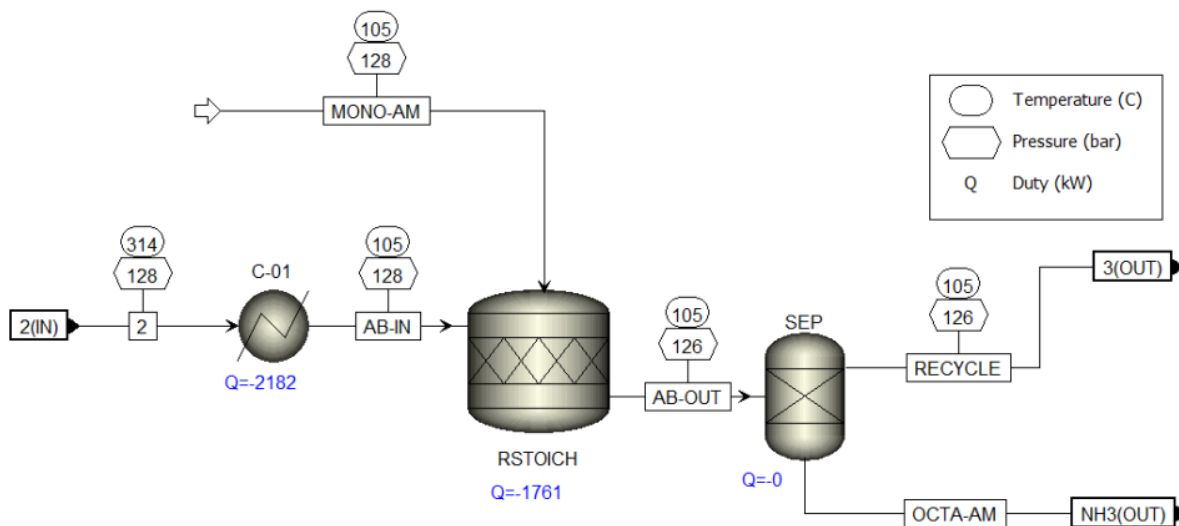


Figure B.2: MODEL 2: Absorber Hierarchy

Table B.3: Summary Table for Absorber Hierarchy

	Units	2	AB-IN	AB-OUT	MONO-AM	OCTA-AM	RECYCLE
Phase		Vapor	Vapor		Solid	Solid	Vapor
Temperature	C	314	105	105	105	105	105
Pressure	bar	128	128	126	128	126	126
Molar Vapor Fraction		1	1	0.98	0	0	1
Molar Liquid Fraction		0	0	0	0	0	0
Molar Solid Fraction		0	0	0	1	1	0
Mass Vapor Fraction		1	1	0.59	0	0	1
Mass Liquid Fraction		0	0	0	0	0	0
Mass Solid Fraction		0	0	0.41	1	1	0
Molar Enthalpy	<i>kJ/kmol</i>	3276	-3372	-28070	-919340	-1531405	2444
Mass Enthalpy	<i>kJ/kg</i>	342.2	-352.2	-1975.8	-5236.7	-5198.1	287.0
Molar Entropy	<i>kJ/kmol - K</i>	-24.8	-38.8	-130.4	-3084.9	-5137.8	-28.8
Mass Entropy	<i>kJ/kg - K</i>	-2.6	-4.1	-9.2	-17.6	-17.4	-3.4
Molar Density	<i>kmol/cum</i>	3	4	4	37	37	4
Mass Density	<i>kg/cum</i>	23.98	36.94	54.09	6498.46	10905.33	31.84
Enthalpy Flow	<i>kW</i>	1075.2	-1106.6		-5362.8	-8933.2	702.3
Average MW		9.57	9.57	14.21	175.56	294.61	8.52
Mole Flows	<i>kmol/sec</i>	0.33	0.33	0.29	0.01	0.01	0.29
Mass Flows	<i>kg/sec</i>	3.14	3.14	4.17	1.02	1.72	2.45
Volume Flow	<i>cum/sec</i>	0.13	0.09	0.08	0.00	0.00	0.08
Mole Fractions							
N ₂		0.22	0.22	0.25	0	0	0.25
H ₂		0.66	0.66	0.74	0	0	0.75
NH ₃		0.12	0.12	0	0	0	0
Ar		0	0	0	0	0	0
Air		0	0	0	0	0	0
MONO-AMMINE		0	0	0.00003	1	0.0014	0
OCTA-AMMINE		0	0	0.020	0	0.999	0

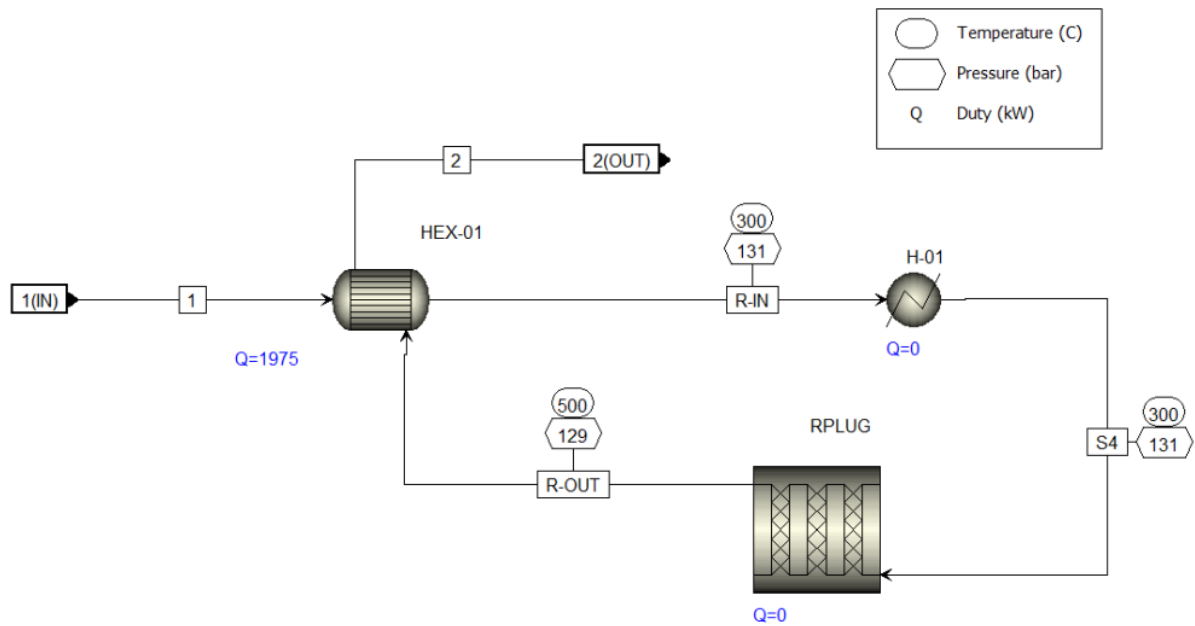
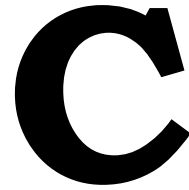


Figure B.3: MODEL 2: Reactor Hierarchy

Table B.4: Summary Table for reactor hierarchy

	Units	1	2	R-IN	R-OUT	S4
Phase		Vapor	Vapor	Vapor	Vapor	Vapor
Temperature	C	120	314	300	500	300
Pressure	bar	132	128	131	129	131
Molar Vapor Fraction		1	1	1	1	1
Molar Liquid Fraction		0	0	0	0	0
Molar Solid Fraction		0	0	0	0	0
Mass Vapor Fraction		1	1	1	1	1
Mass Liquid Fraction		0	0	0	0	0
Mass Solid Fraction		0	0	0	0	0
Molar Enthalpy	<i>kJ/kmol</i>	2914	3276	8268	9295	8268
Mass Enthalpy	<i>kJ/kg</i>	342.2	342.2	970.9	970.9	970.9
Molar Entropy	<i>kJ/kmol - K</i>	-28.0	-24.8	-16.7	-16.0	-16.7
Mass Entropy	<i>kJ/kg - K</i>	-3.3	-2.6	-2.0	-1.7	-2.0
Molar Density	<i>kmol/cum</i>	4	3	3	2	3
Mass Density	<i>kg/cum</i>	32	24	22	19	22
Enthalpy Flow	<i>kW</i>	1075	1075	3050	3050	3050
Average MW		8.51528	9.6	8.51528	9.6	8.51528
Mole Flows	<i>kmol/sec</i>	0.37	0.33	0.37	0.33	0.37
Mole Fractions						
N ₂		0.25	0.22	0.25	0.22	0.25
H ₂		0.75	0.66	0.75	0.66	0.75
NH ₃		0	0.12	0	0.12	0
Ar		0	0	0	0	0
Air		0	0	0	0	0
MONO-AMMINE		0	0	0	0	0
OCTA-AMMINE		0	0	0	0	0
Mass Flows	<i>kg/sec</i>	3.14	3.14	3.14	3.14	3.14
Volume Flow	<i>cum/sec</i>	0.10	0.13	0.14	0.17	0.14



Model 3: Simulation information & input specifications

C.1. Pressure-driven simulation additional information

The two available solver types for Aspen Dynamic simulations are Flow-Driven and Pressure-Driven.

Flow-driven

In an Aspen Plus steady-state simulation, the outlet stream pressures and flow rates of a block are determined from the inlet conditions to the block, and the specifications for the block [101]. Neither the outlet stream pressures or flow rates are affected by the pressure in the downstream blocks. This approach is called flow-driven simulation. Flow Driven dynamic simulations operate similarly to Aspen Plus simulations. For each model, fixed rules are used to determine the properties of the outlet of operation units, given the inlet conditions.

The flow-driven approach is well suited to a wide range of dynamic simulation applications. In effect, this approach makes the assumption of perfect flow control. This is often a good assumption, particularly when modeling liquid only systems. The pressure/flow dynamics for liquids are very fast, and the assumption of perfect flow control is therefore usually accurate.

Pressure-driven

For a realistic system it is considerably better to use a pressure-driven simulation. In a pressure-driven simulation all flow rates are determined by the pressures distribution in the flow sheet, and pressure/flow relationships of each unit operation. The Pressure-driven approach is vital for simulating compressor networks, steam/gas networks, pressure relief systems and several other application types.

In pressure-driven simulations[101]:

- The pressures of all feeds and products are fixed
- Feed flow rates are not fixed
- The flow rates are determined by the pressures and pressure/flow relationships

Table C.1: Pressure-driven vs. flow-driven simulations

Solver Type	
flow-driven	Pressure Driven
<ul style="list-style-type: none">• Outlet flow rates determined by material balance• Assumes perfect flow, independent of pressure• Good approach for liquid systems	<ul style="list-style-type: none">• Outlet flow rates are determined by pressure/flow relationship• System resistance forces a pressure drop• Flows are dependent on the pressure gradients
Liquid processing (pressure has small impact on liquid properties) No importance of pressure Good pressure and flow control pre-exists	Gas phasing required (pressure has large impact on liquid properties) Pressure is important Design of pressure and flow control required

Source: Getting Started with Aspen Dynamics [102]

The main differences between flow-driven and pressure-driven solvers be found in Table C.1. The adoption of relevant simulation mode is determined by the modeling objectives and the type of process. In general, if pressure is of specific importance, then pressure-driven simulation is recommended. Simulations consisting of mostly gas or vapor phase streams will also require pressure-driven mode. Oppositely, simulations that consist of mostly liquid streams will demand flow-driven mode. In the current work, pressure is of high importance and the synthesis loop consists mainly of gaseous streams, therefore the pressure-driven dynamic simulation method was selected.

Nodes in Pressure Driven Simulation

Pressure Nodes	Flow/dp Nodes	Neutral Nodes
Sets the pressure from the volume and vapor amount	Relation between flow and pressure drop	Requires inlet and outlet stream pressures to be equal
Flash2, Flash3, Decanter, Sep2 RadFrac, PetroFrac RCSTR Rplug RGibbs ⚡ Rstois ⚡ Ryield ⚡ Mixer	Valve Compr Mcompr Heater HeatX MHeatX Pipe Pump	FSplit Mixer ⚡ RGibbs ☒ RStois ☒ RYield ☒

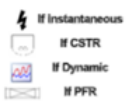


Figure C.1: Additional Information for Pressure Driven Simulations (source: [Getting Started with Aspen Dynamics](#))

C.2. Control parameter recommendations from Aspen

PID Controller – Stability Recommendations

Proportional Integral Derivative control(PID)

Controller	When to Use	When Not to Use
Proportional	Require a quick response	An offset can not be sustained
Proportional Integral	Offsets cannot be tolerated	Oscillations cannot be tolerated
Proportional Integral Derivative	Little or no dead times and large capacities	Noisy controller output that can not be filtered or minimized

Figure C.2: Recommendations for PID controller stability (source: [Getting Started with Aspen Dynamics](#))

Table C.2: Equipment specifications for *MODEL 3*

Name Flowsheet	Type	Phases		Specifications
V-01	Valve	Vapor-only	68.5	Adiabatic flash for specified outlet pressure (pressure changer)
V-02	Valve	Vapor-only	68.5	Adiabatic flash for specified outlet pressure (pressure changer)
M-01	Mixer	Vapor-only	0	Instantaneous
M-02	Mixer	Vapor-only	0	Instantaneous
HEX-01	Heat Exchanger (HeatX)	Vapor-only	1 (per side)	Counter-current Heat exchange area: 11.9814 m ² Calculation mode: Simulation No heat losses
RPLUG	Plug Flow Reactor (Rplug)	Vapor-only	Ergun	Adiabatic L = 6.4m, d = 0.8m
H-01	Heater	Vapor-only	0.5	Instantaneous Constant process temperature
COND	Condenser (flash2)	Vapor-Liquid	0	Vessel type: Vertical Geometry: Elliptical L = 3.75m, d = 0.94m Liquid volume fraction: 0.26
V-03	Valve	Vapor-only	0.1	Adiabatic flash for specified outlet pressure (pressure changer)
V-04	Valve	Liquid-only	97	Adiabatic flash for specified outlet pressure (pressure changer)
H-02	Heater	Vapor-only	0.5	Instantaneous Constant process temperature
RC-01	Compressor	Vapor-only	-5	Isentropic Instantaneous Constant brake power

Controller Tuning - Recommendations

- The values below are recommended starting points for tuning control loops

System	K _c	τ _i (minutes)	τ _d (minutes)
Flow	0.1	0.2	0
Level	2	10	0
Pressure	2	2	0
Temperature	1	20	0

Figure C.3: Recommendations for Controller Tuning (source: [Getting Started with Aspen Dynamics](#))

C.3. Summary table input specifications

D

Model 3: Problem solving Control Structure 1

Scenario where a nitrogen drop is compensated with hydrogen Exact same simulation model is used but instead of regulation the pressure with nitrogen compensation, it is regulated by altering the hydrogen feed stream. The simulation gives an error when the Hydrogen deficiency surpasses 27 %. Therefore, for this test scenario a drop in Nitrogen of 90% is proposed, the reduction in the amount of moles is than equal to 30% drop in hydrogen.

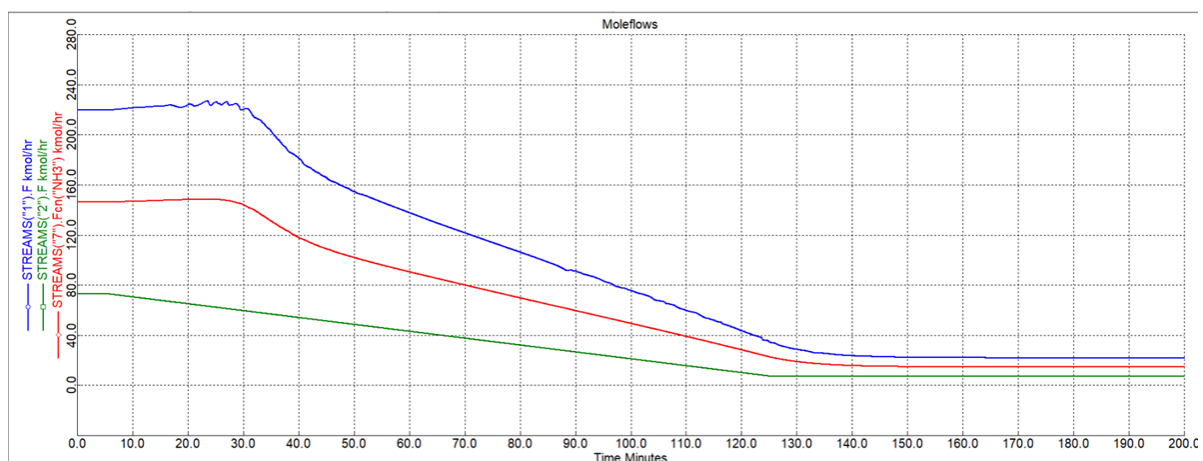


Figure D.1: Result of a 90% drop of the N₂ feed flow

⇒ The Nitrogen can be successfully ramped down to only 10% of its initial value while this is compensated by hydrogen. This proves that increasing the volumetric flow rate is not a problem and this proves that the issue could potentially lay in the density increase of the recycle stream. It cannot be concluded for certain, so more scenarios are implemented to verify this.

Isolation of the compressor In this test, the loop consists of only the recycle compressor, this means the heat-exchanger, heater, reactor and absorber were left out, see Figure D.2. A split operation was placed to ensure a separation to satisfy the mass balance of in going and outgoing moles. The split factor has been set to 12,4 % to create a recycle 5 times bigger than the outlet stream, similar to the control structure 1 model. The aim here is to see whether the compressor experiences any troubles with the increased density of the recycle flow.

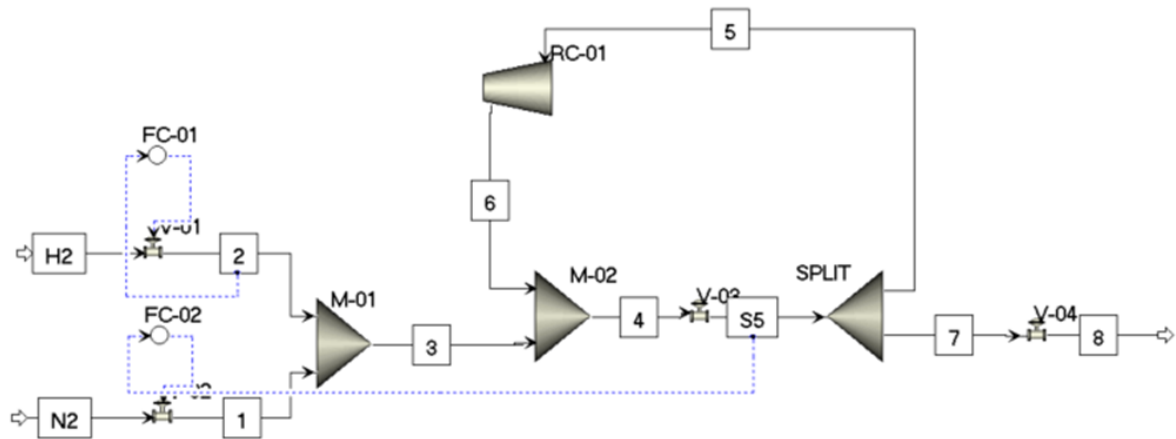


Figure D.2: Isolation of the compressor

- ⇒ The hydrogen feed rate reduced was until it finally reached 0 $kmol/hr$ without any problems or error occurring.
- ⇒ It is important to note that in this model no ammonia is formed, which means that its conversion can not be influenced by the drop in $H_2:N_2$ ratio. This would result in a drop in ammonia leaving the system creating an interesting dynamic in the system. In this test model, the in going and out going mole flows do not change as a result of this.
- ⇒ **Conclusion:** The error could be a combination of factors, but does not solely lie with the compressor. The compressor in Aspen is not programmed to 'choke', however in real life this would pose a limitation.

Removal of the heat exchanger from the simulation. Since the issue does not seem to be the compressor (alone), another approach was applied. Instead a heater and cooler combination was used. An error still occurred with a 30% hydrogen feed reduction, thus the issue does not solely lay on the heat exchanger. (increased system pressure)

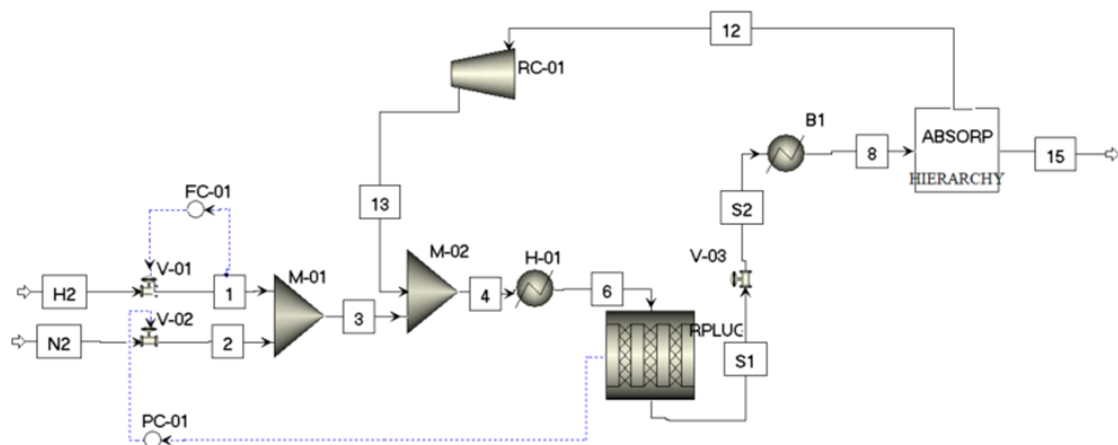


Figure D.3: Removal of the heat-exchanger from the simulation

Isolation the reactor When just the reactor is taken with two feeds of hydrogen and nitrogen and an outlet stream (so no loop), Figure D.4, no issues happened even at a 50% reduction. The nitrogen flow rate here was permanently increased to compensate the hydrogen reduction (in a loop this feed

increase is only temporary). Because the loop lacks, the dynamics cannot properly be tested. The reactor itself does not experience any troubles with the increased nitrogen flow.

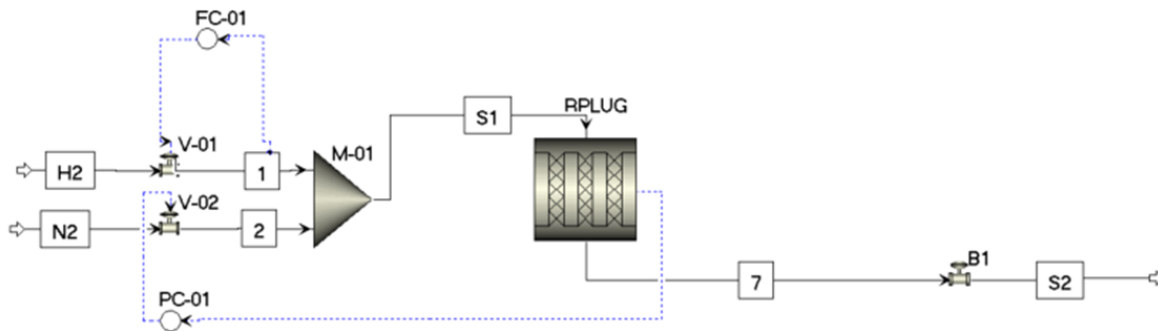


Figure D.4: Isolation of the reactor

Isolation of the reactor + absorber An absorber (flash2) vessel was added to the model in the previous step. The condition of the flash vessel is that the pressure at the inlet, outlet and within the vessel is equal. A ramp-down of hydrogen to 70 % was successfully done. But reducing the flow rate to 50% causes an error. It seems that the condenser level control cannot keep up the disturbance in the system and the pressure and level drop here significantly.

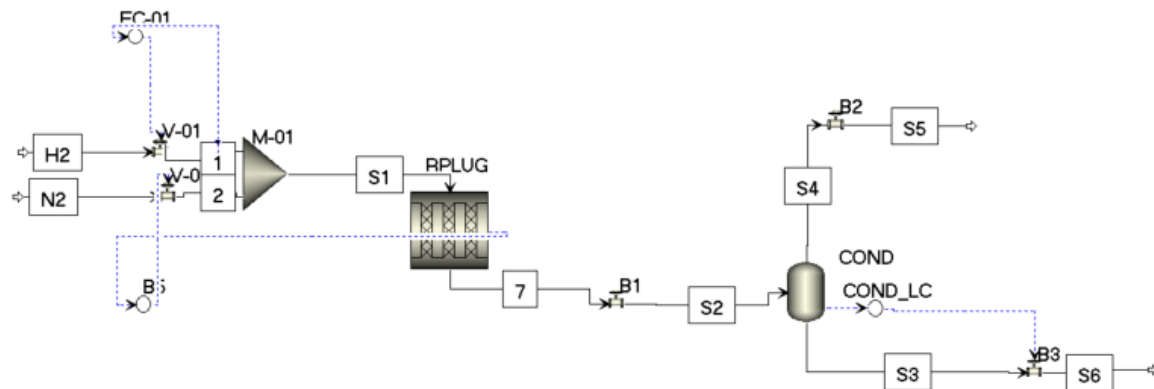


Figure D.5: Isolation of the reactor & absorber

Reduction the absorber volume Lastly, it was tried to change the volume of the absorber vessel in the initial simulation. This would not fix the error but if the problem lays with the absorber this alteration will influence the moment where the simulation stops working.

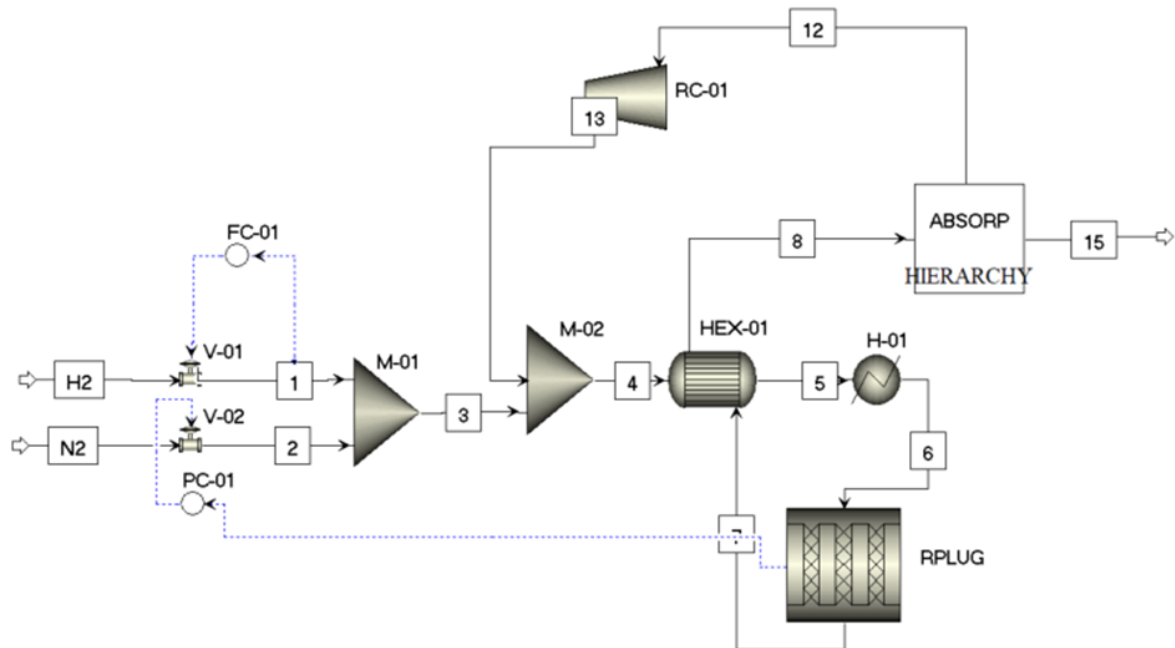


Figure D.6: Reduction of the absorber volume

An error still occurs with the 30% hydrogen feed reduction at the exact same point as before ($H_2 = 157 \text{ kmol/hr}$). Resizing the absorber vessel only quickened the response but not the point at which the simulation fails. Therefore, the absorber alone is also not the cause of this simulation failure.

Conclusion It was tried to find the precise cause of the simulation error by isolating and testing individual equipment units or subtracting them from the original simulation. Using this method, no clear cause has been established.

The error log of Aspen Plus Dynamics seemed to indicate that the problem lays with the vapor valve of the absorber, however more detail or certainty on the simulation failure could not be gained.

With the information available, it was concluded that the increased density of the recycle stream (Hydrogen is replaced with Nitrogen) in combination with the simulation dynamics poses this limitation. It sounds reasonable that in reality equipment in the system would also experience issues when the mass flow rate is increased.



Model 3: Additional results ramp-down 25% scenario

E.1. Control Structure 1

E.1.1. System pressures & temperatures

Control structure 1 – initial steady state

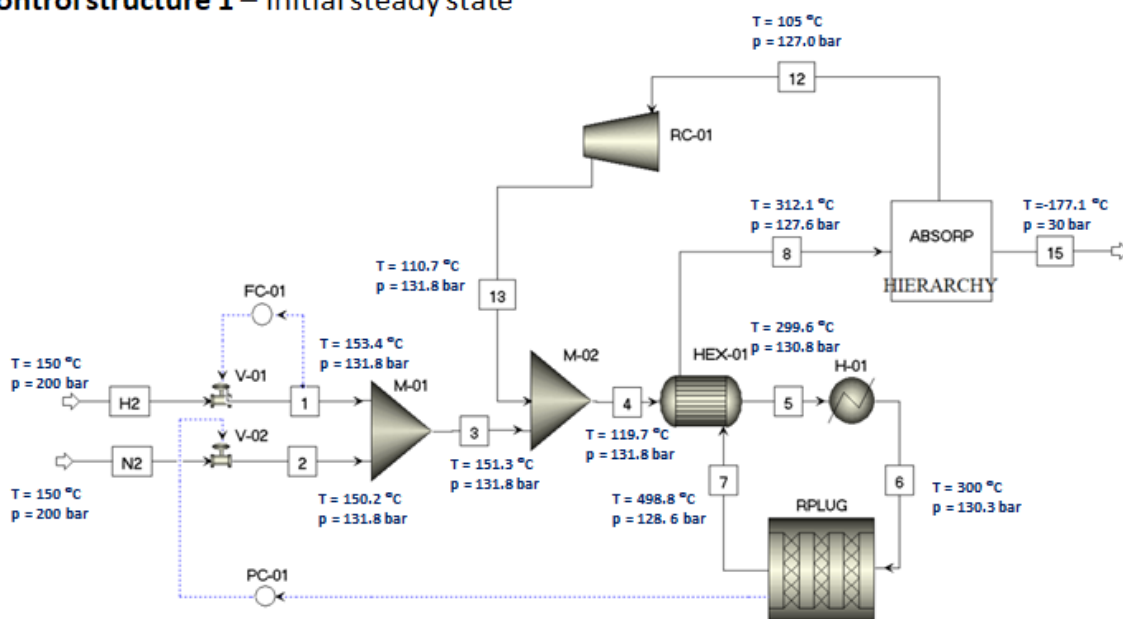


Figure E.1: Control Structure 1 - initial state

Control structure 1 – 25% ramp down (steady state)

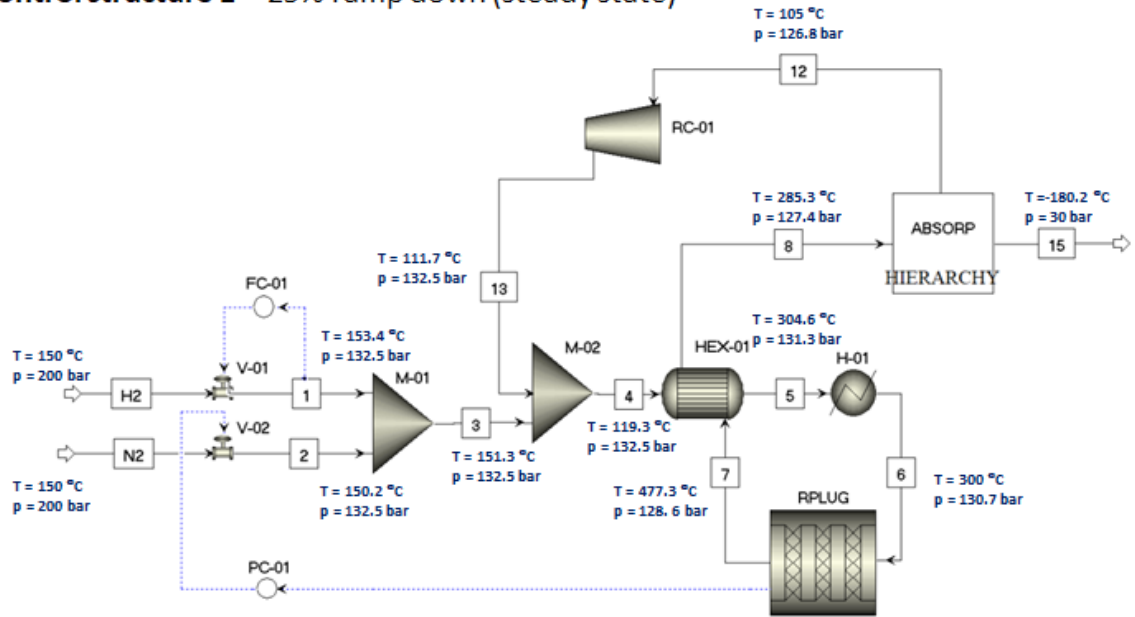
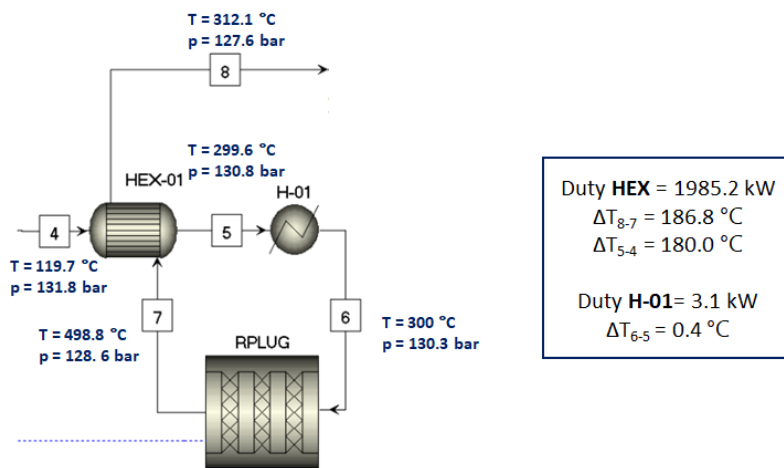
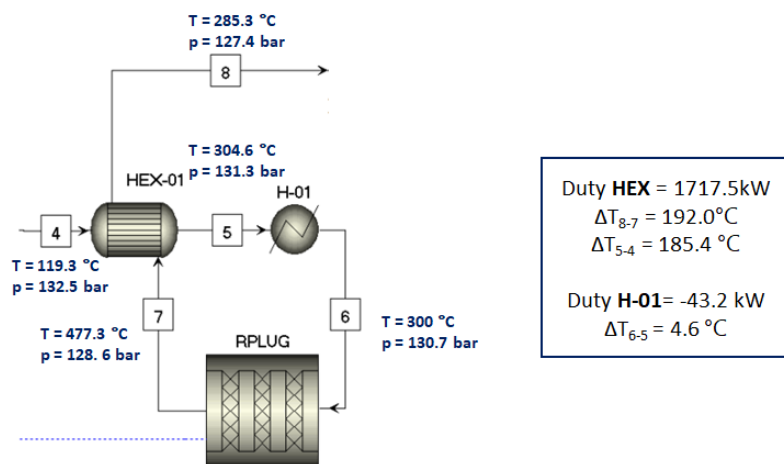


Figure E.2: Control Structure 1 - steady state after 25% H₂ ramp-down

E.1.2. Reactor loop heat duties



(a) Initial steady state



(b) Steady state after 25% H₂ ramp-down

Figure E.3: Reactor loop heat duties (*Control structure 1*)

E.1.3. Heat-exchanger (HEX-01) specifics

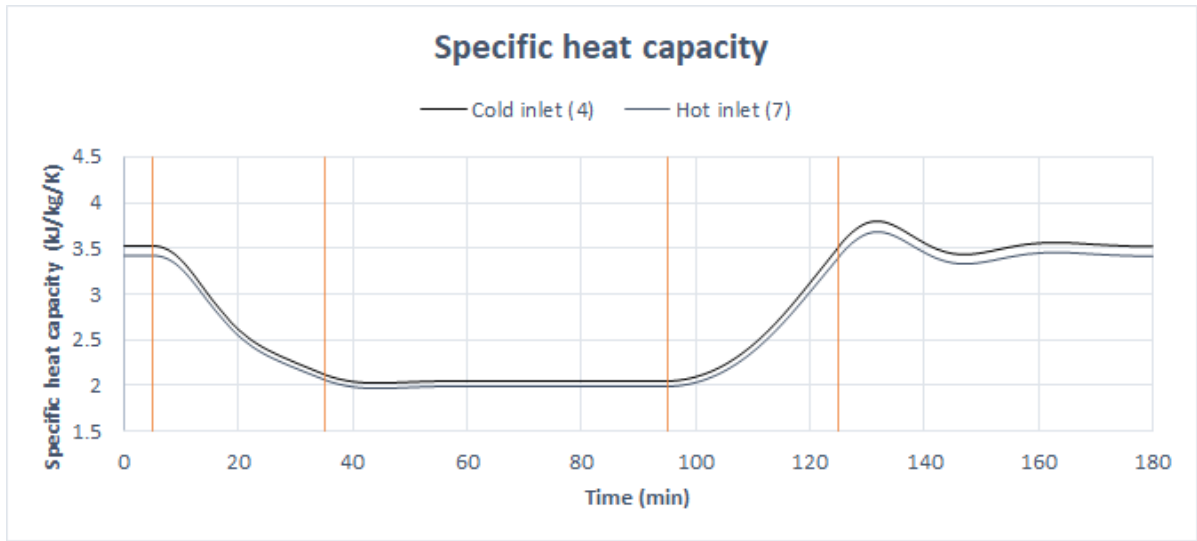
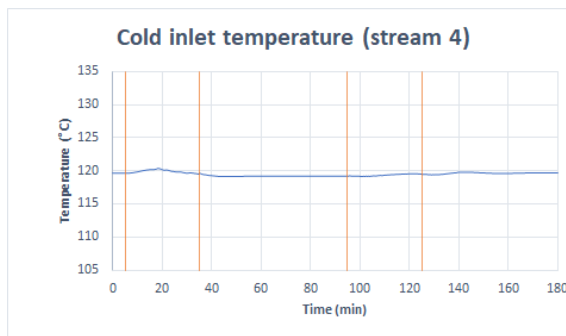
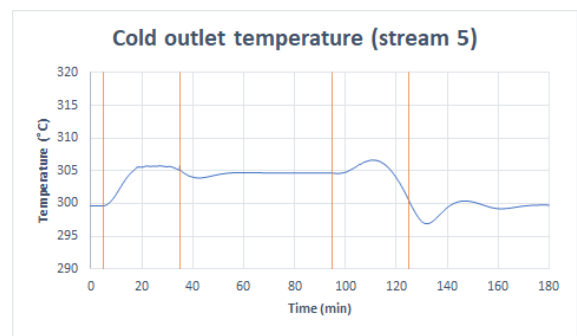


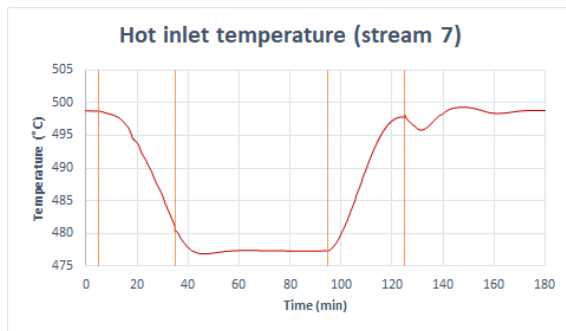
Figure E.4: Specific heat capacity of the in-going hot and cold streams



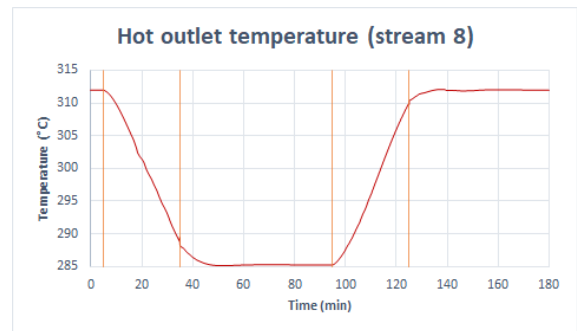
(a)



(b)



(c) Temperature of the hot inlet stream



(d) Temperature of the hot outlet stream

Figure E.5: temperatures around the heat-exchanger (HEX-01) - 25% ramp-down/up scenario

E.2. Control Structure 2

E.2.1. System pressures & temperatures

Control structure 2 – initial steady state

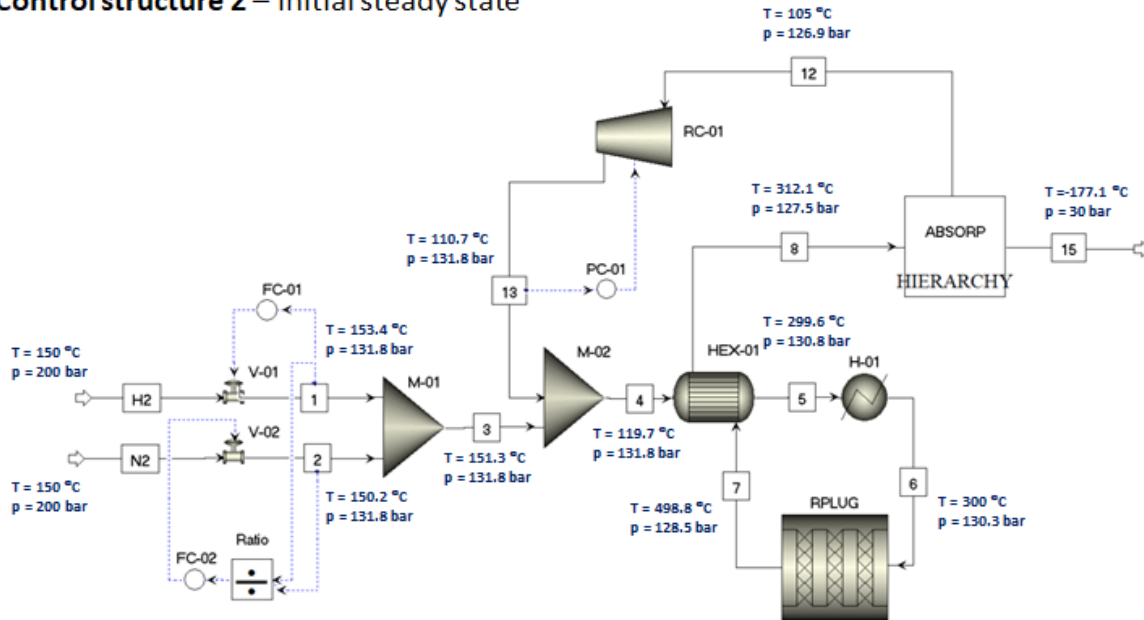


Figure E.6: Control Structure 2 - initial state

Control structure 2 – 25% ramp down (steady state)

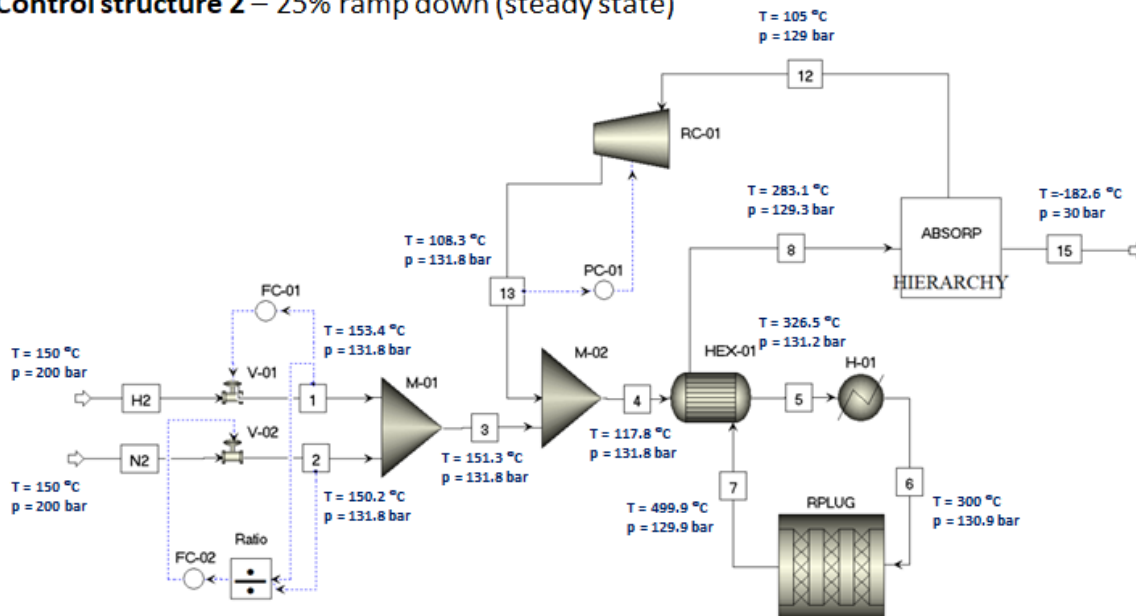
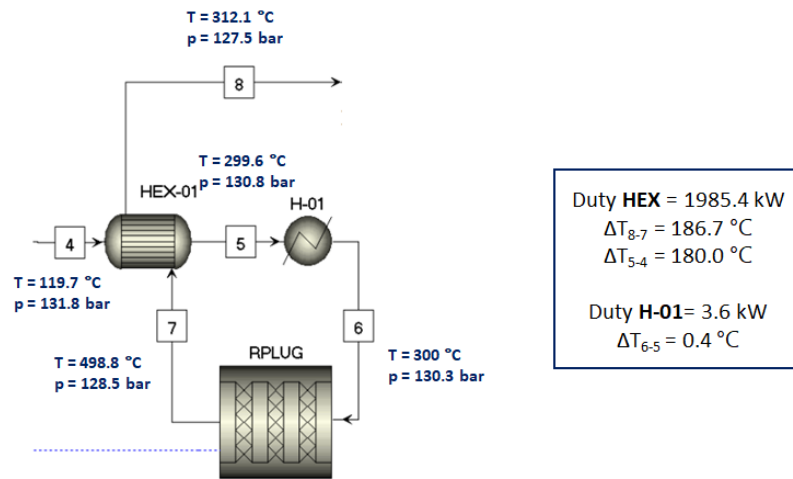
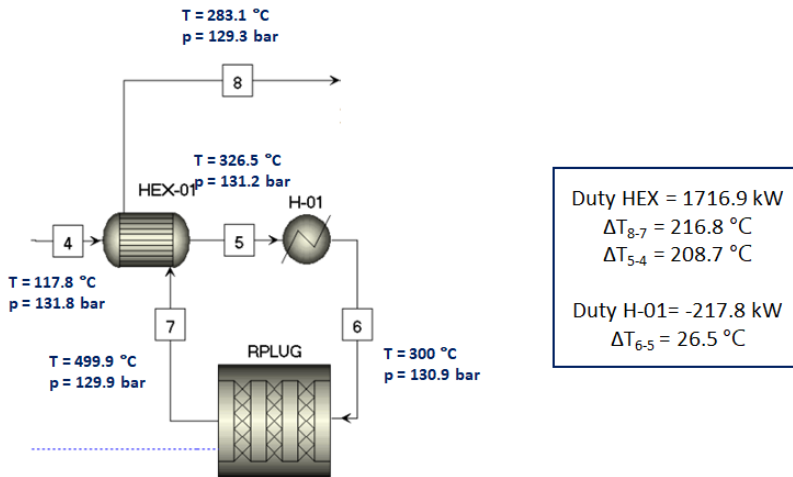


Figure E.7: Control Structure 2 - steady state after 25% H₂ ramp-down

Reactor loop heat duties



(a) Initial steady state



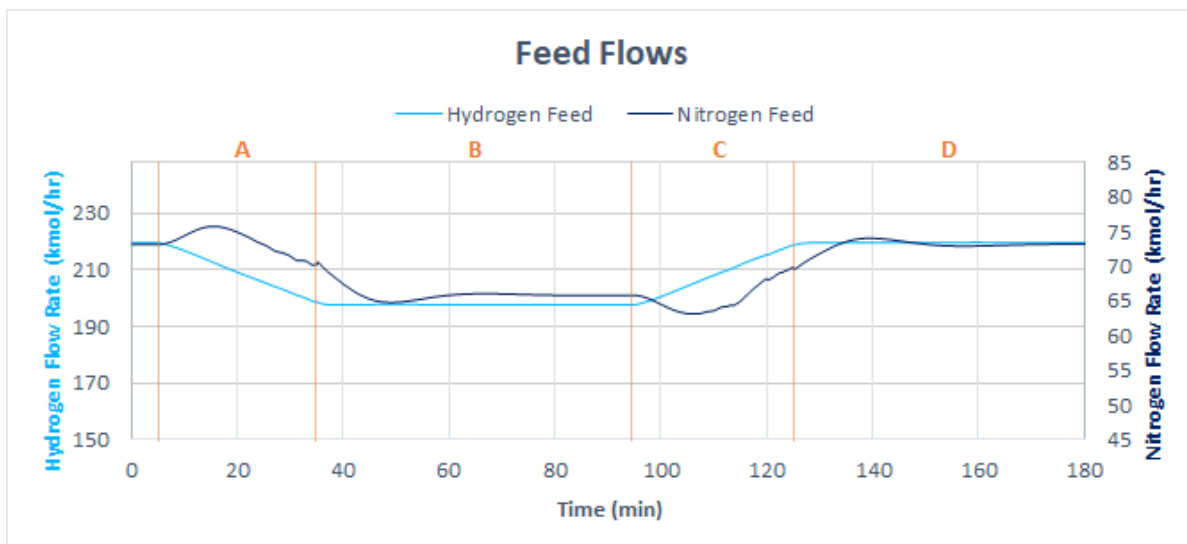
(b) Steady state after 25% H₂ ramp-down

Figure E.8: Reactor loop heat duties (*Control structure 2*)

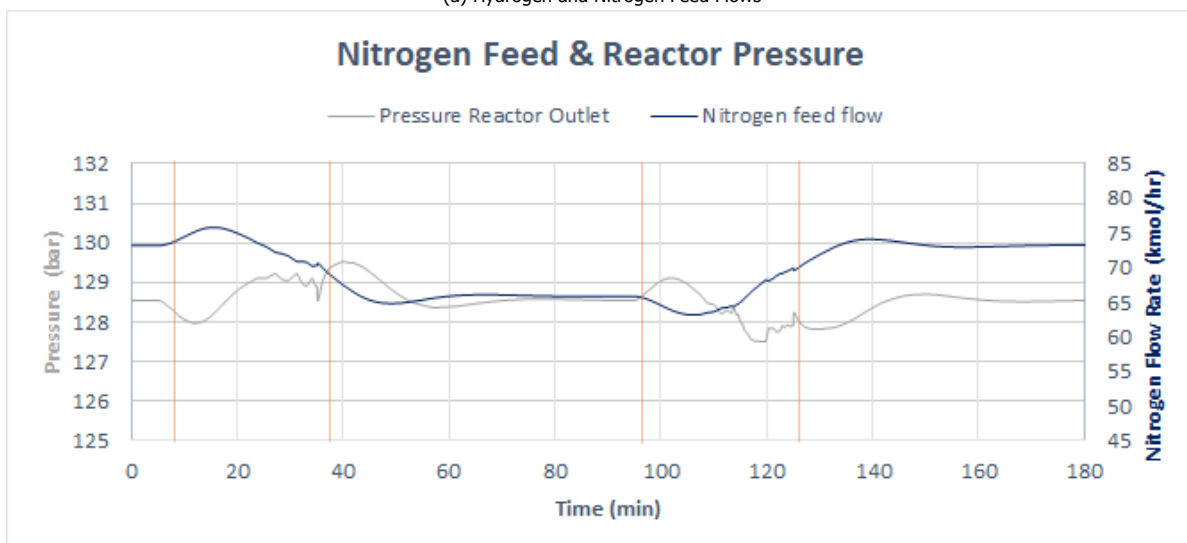
F

Model 3: Additional results

F.1. Control Philosophy 1 - Gradual reduction in hydrogen feed flow

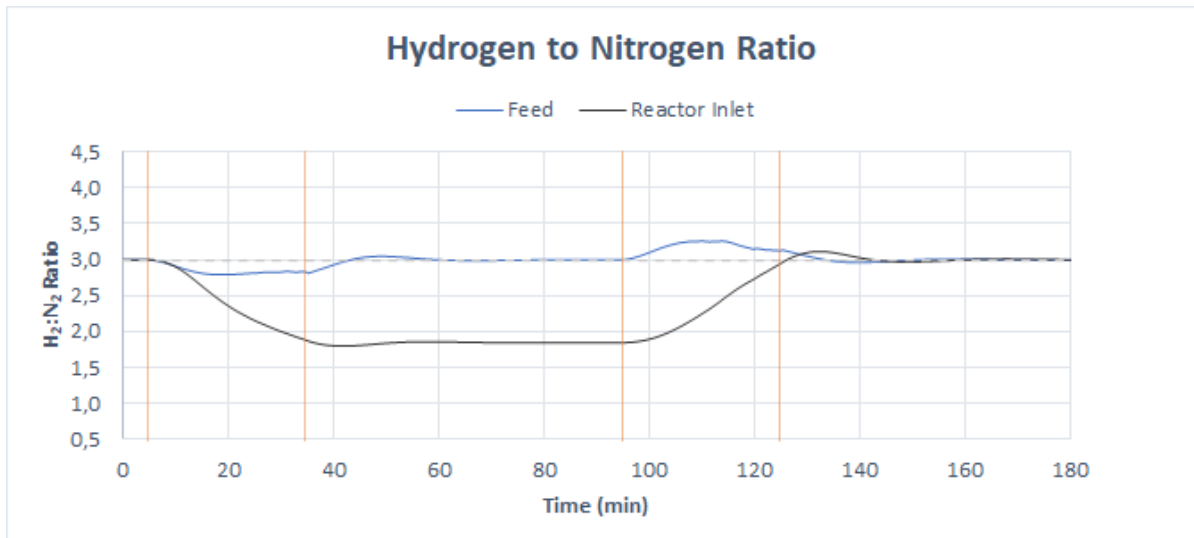
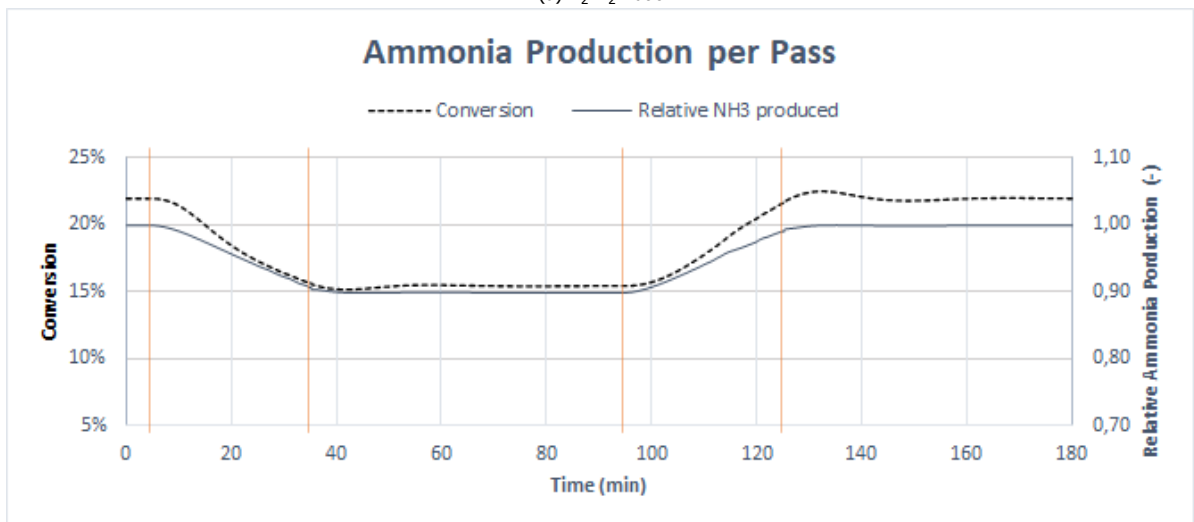


(a) Hydrogen and Nitrogen Feed Flows



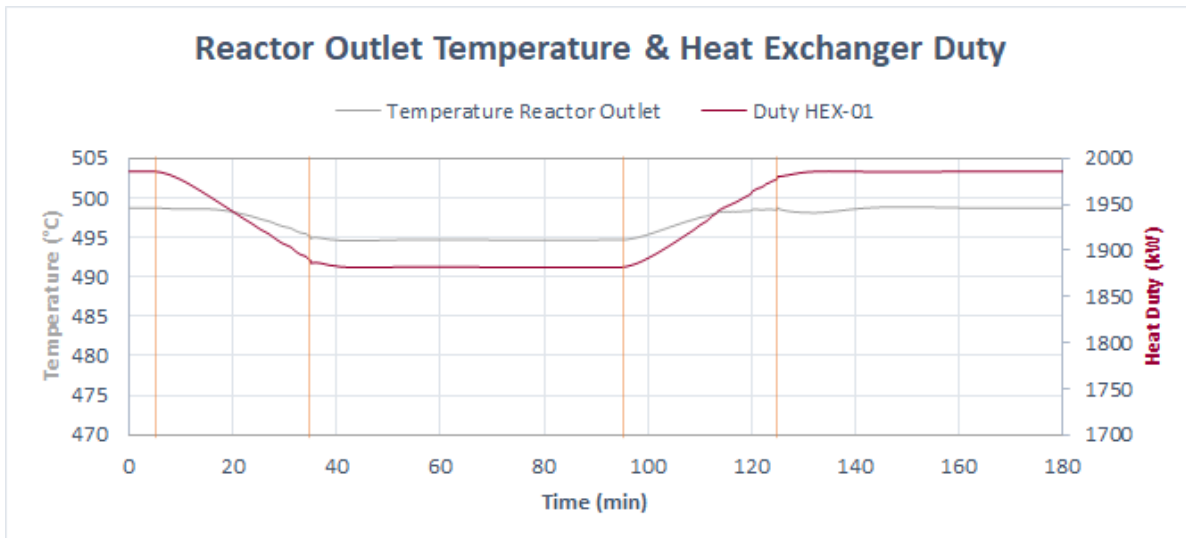
(b) Pressure at Reactor Outlet (bar) and Nitrogen Feed Flows

Figure F.1: Time series for 10% Ramp-down/up scenario - Control Structure 1

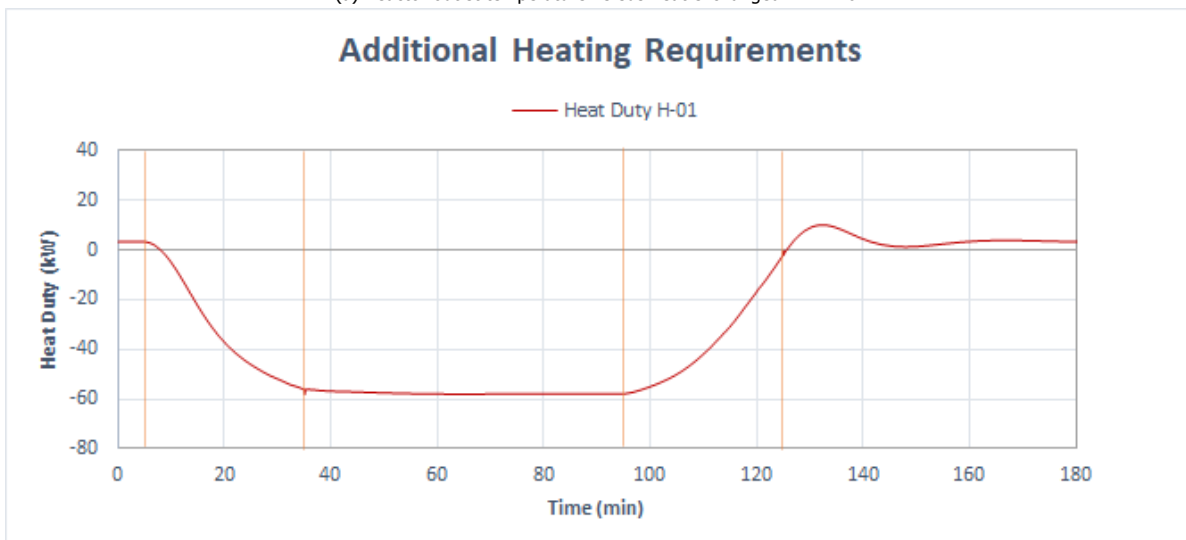
(a) $H_2:N_2$ Ratio

(b) Conversion vs. relative ammonia production

Figure F.2: Time series for 10% Ramp-down/up scenario - *Control Structure 1*



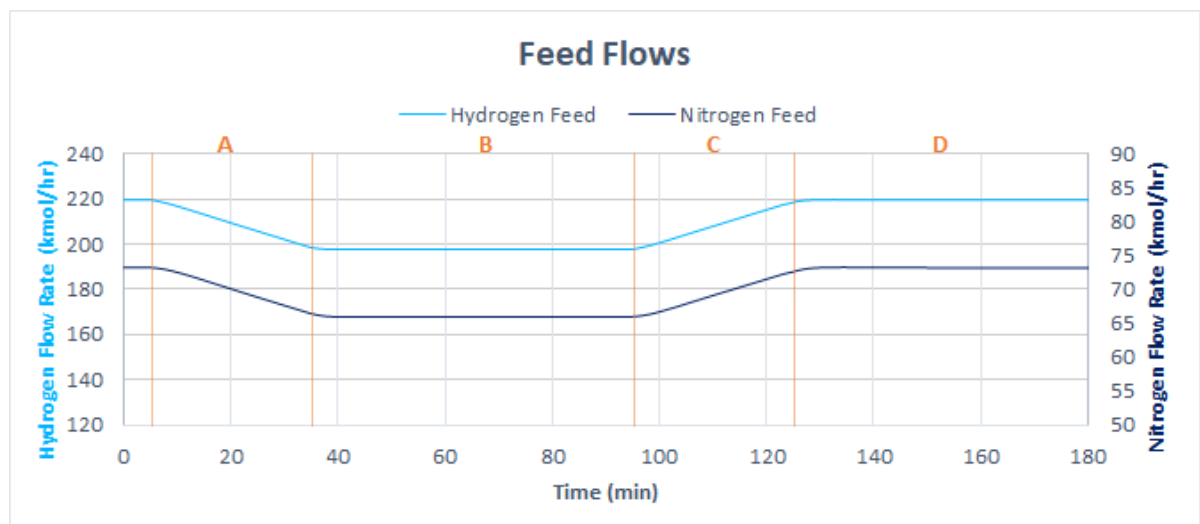
(a) Reactor outlet temperature versus heat exchanged in HEX-01



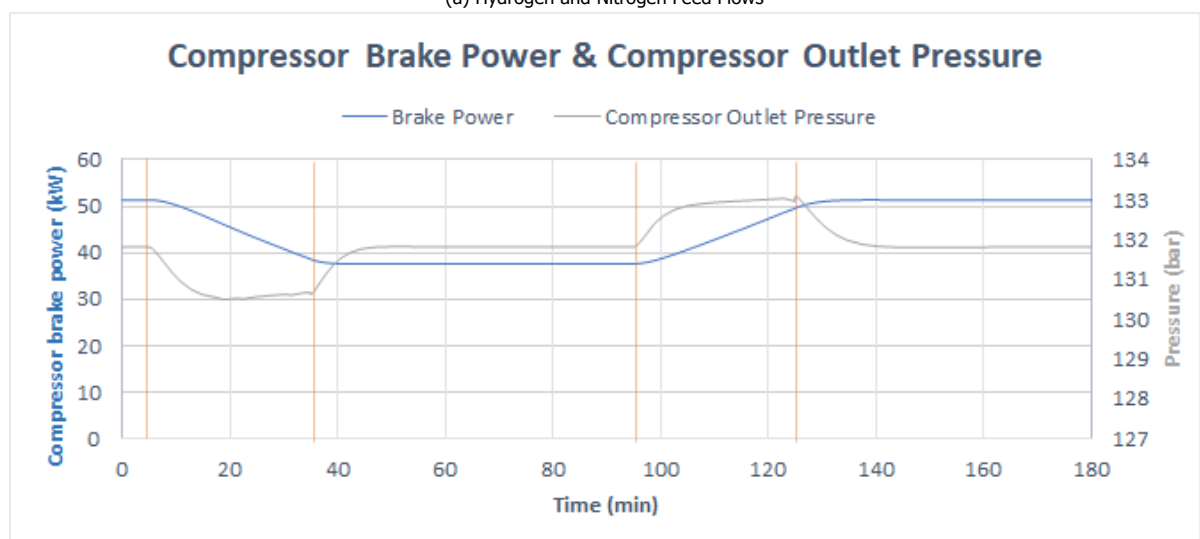
(b) Additional heat requirement provided by heater H-01

Figure F.3: Time series for 10% Ramp-down/up scenario - Control Structure 1

F.2. Control Philosophy 2 - Gradual reduction in hydrogen feed flow



(a) Hydrogen and Nitrogen Feed Flows



(b) Recycle compressor brake power vs. Pressure at the compressor outlet

Figure F.4: Time series for 10% Ramp-down/up scenario - Control Structure 2

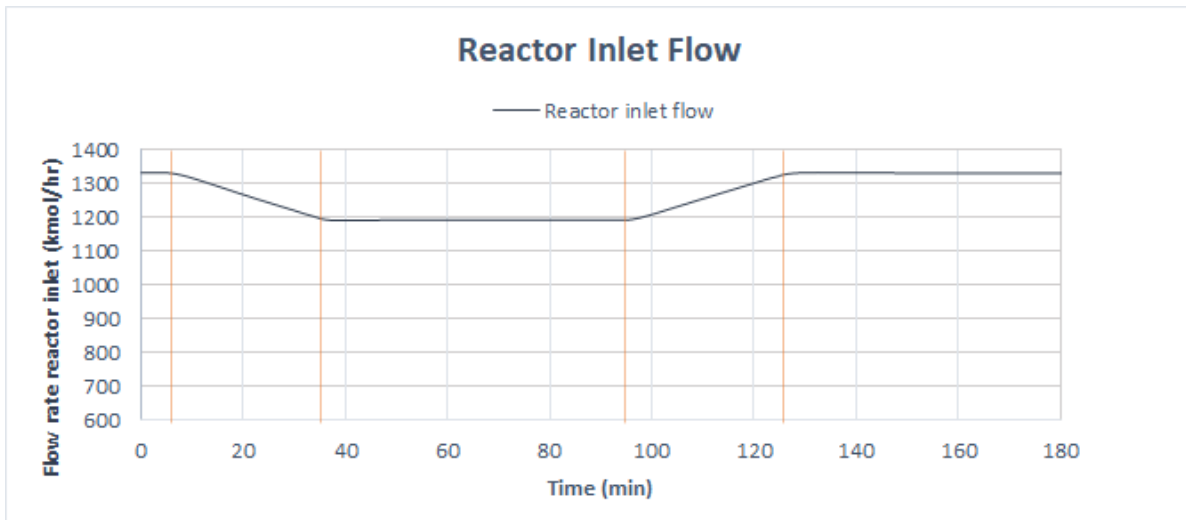
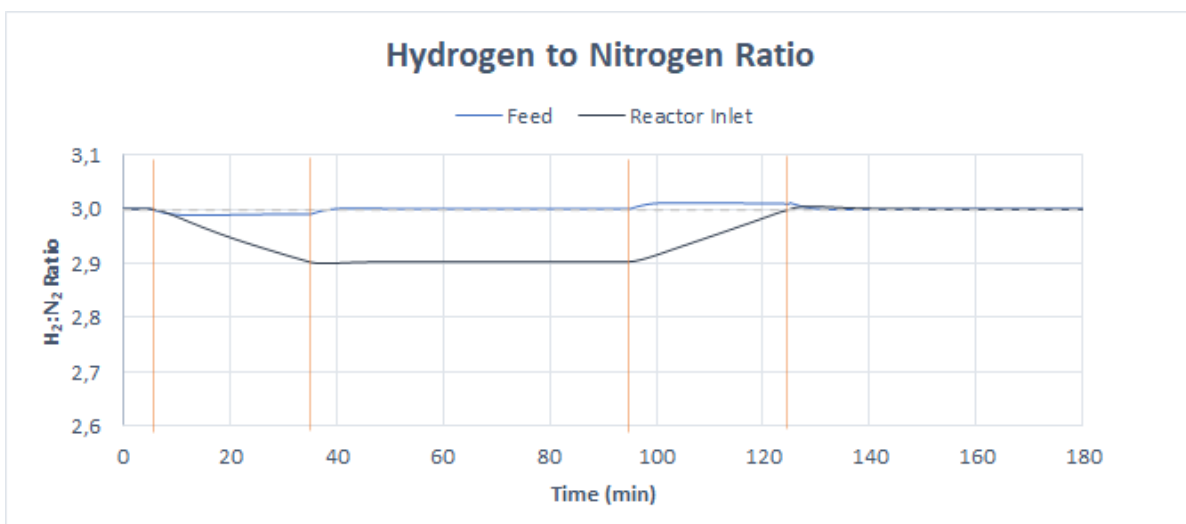
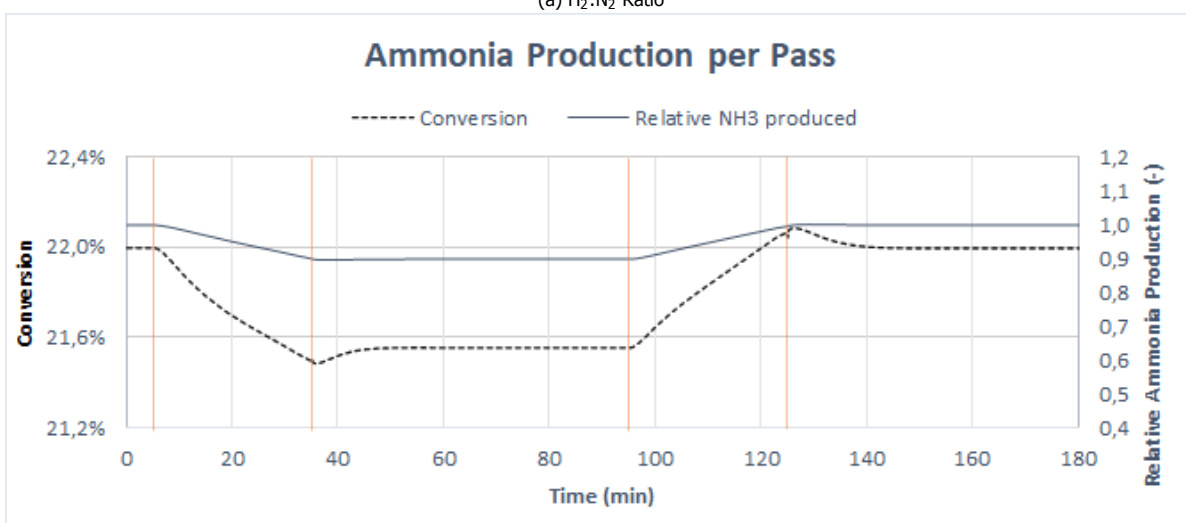


Figure F.5: Residence time vs. inlet flow rate reactor (10% Ramp-down/up scenario - Control Structure 2)

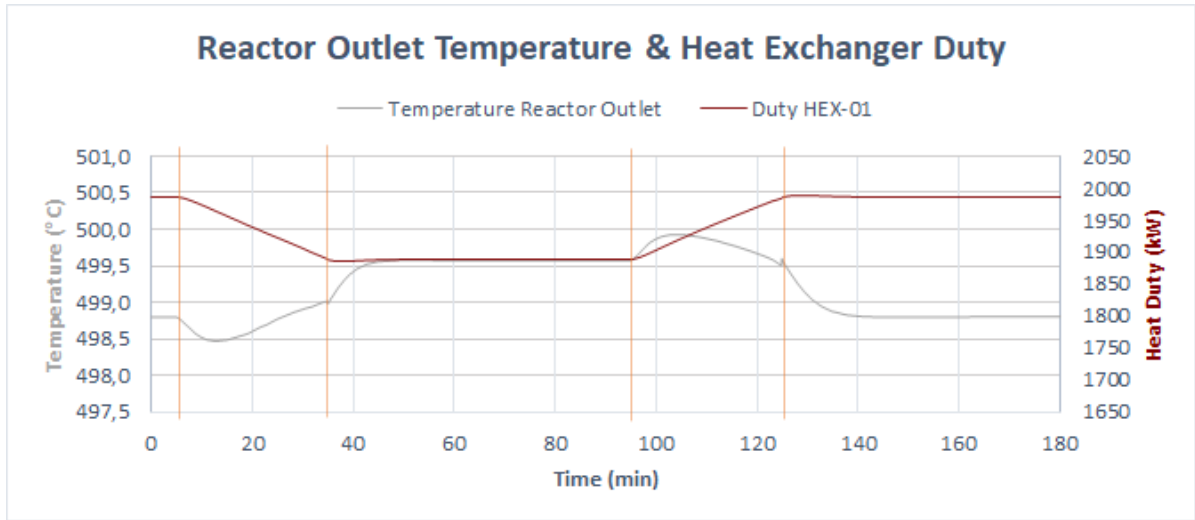


(a) H₂:N₂ Ratio

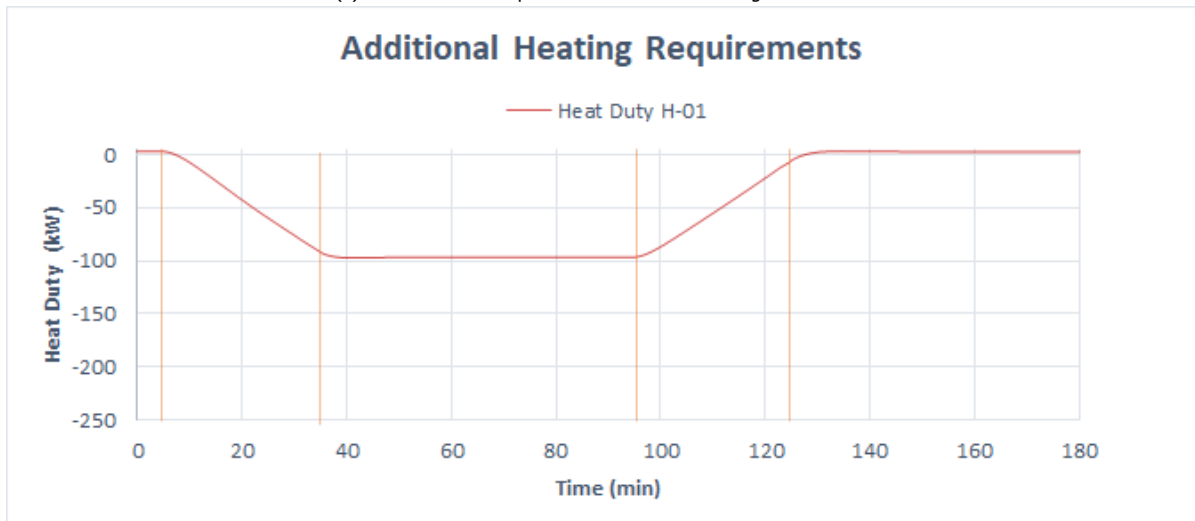


(b) Conversion vs. relative ammonia production

Figure F.6: Time series for 10% Ramp-down/up scenario - Control Structure 2

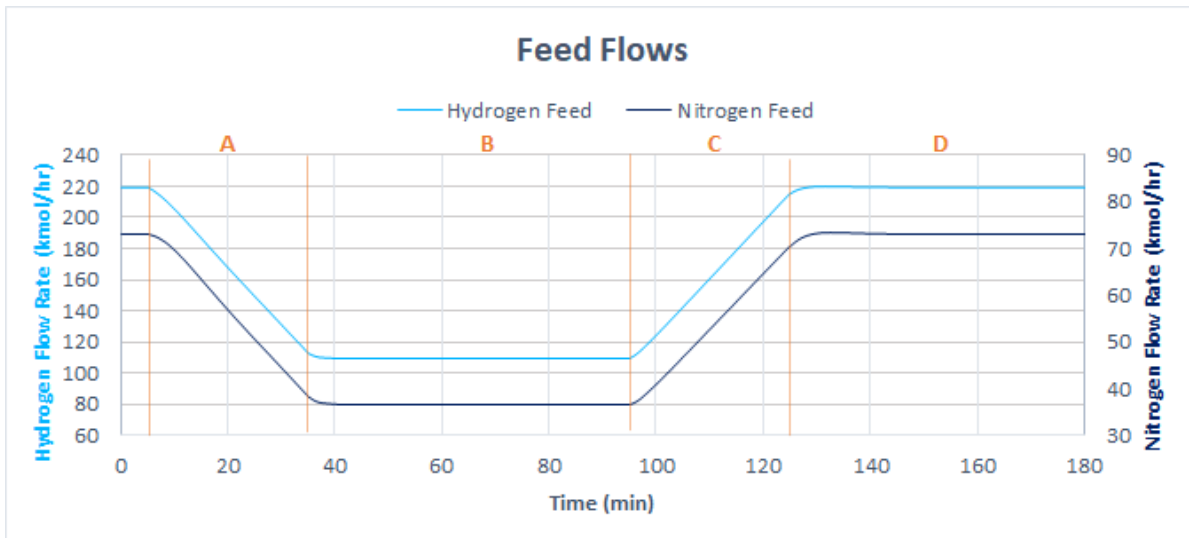


(a) Reactor outlet temperature versus heat exchanged in HEX-01

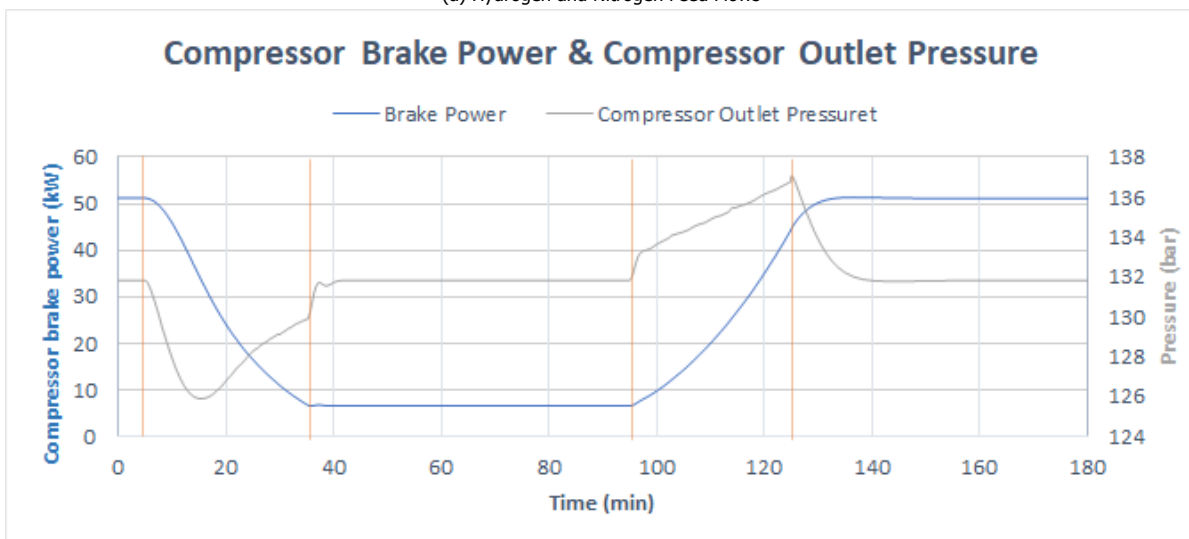


(b) Additional heat requirement provided by heater H-01

Figure F.7: Time series for 10% Ramp-down/up scenario - Control Structure 2



(a) Hydrogen and Nitrogen Feed Flows



(b) Recycle compressor brake power vs. Pressure at the compressor outlet

Figure F.8: Time series for 50% Ramp-down/up scenario - Control Structure 2

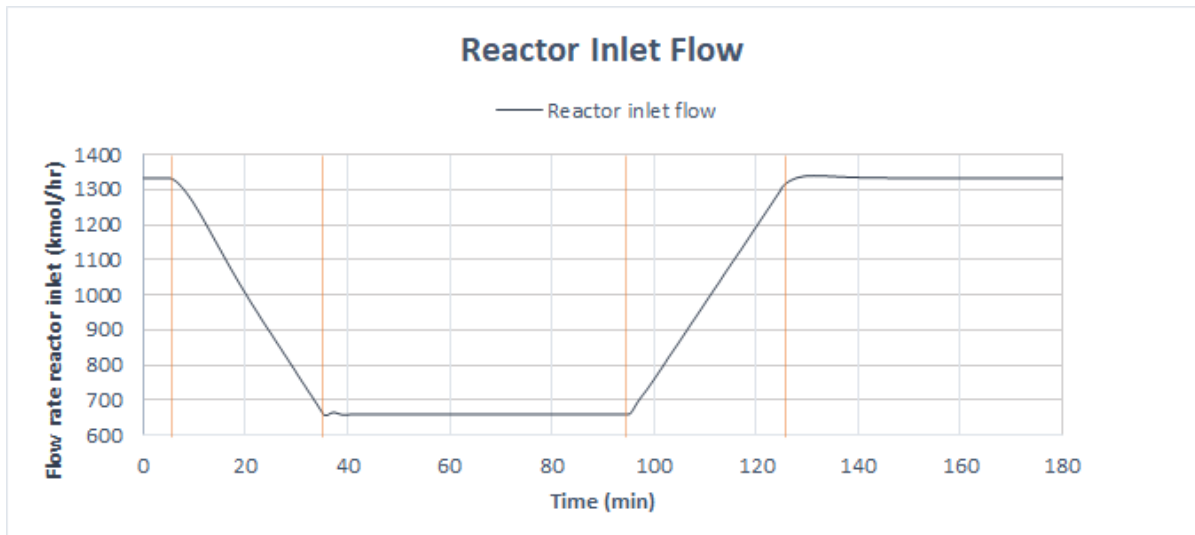
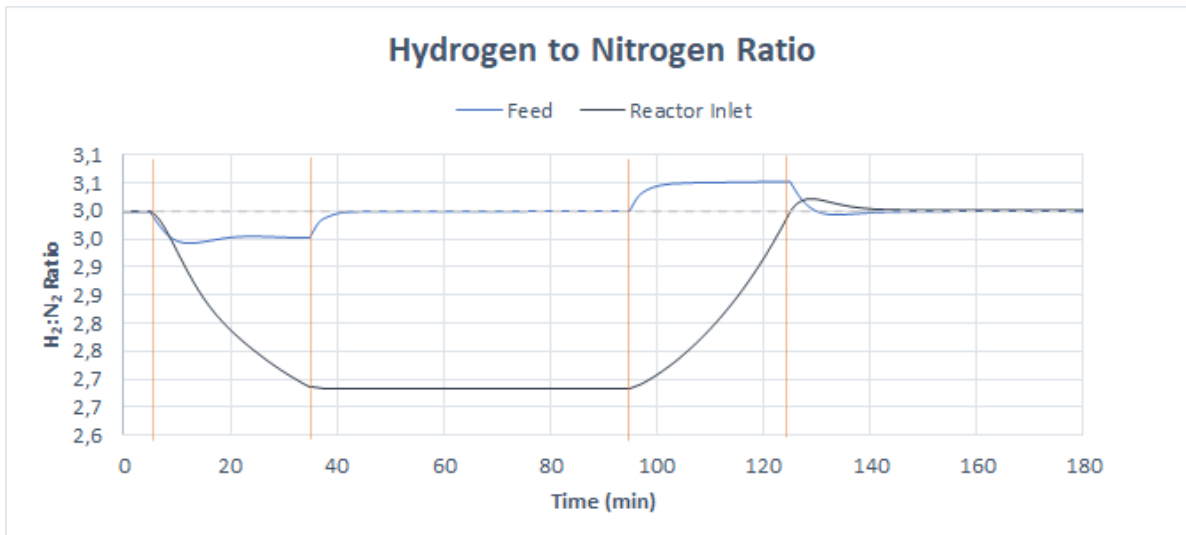
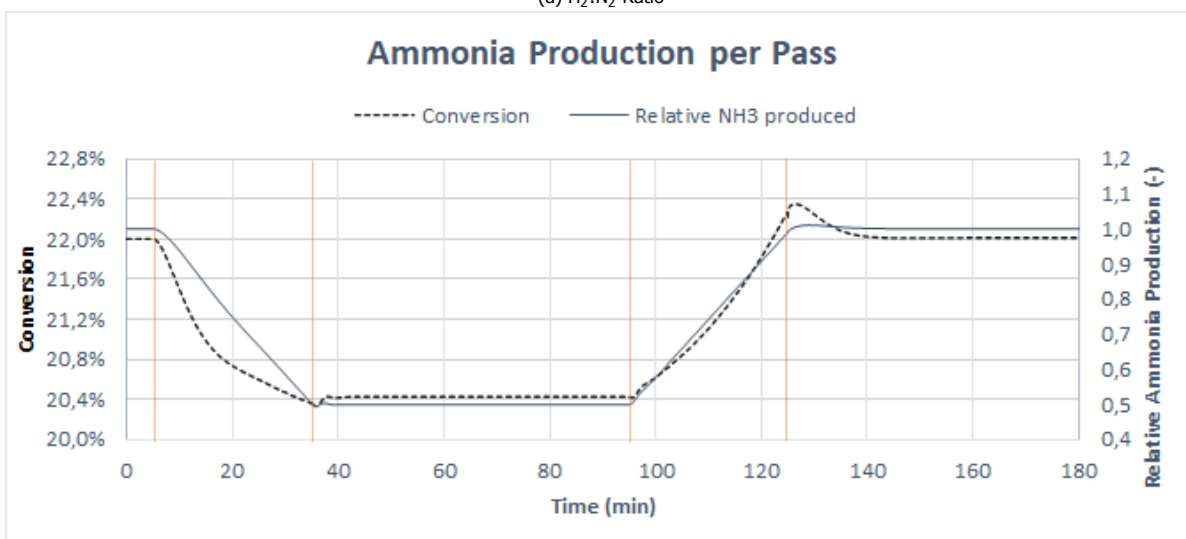


Figure F.9: Residence time vs. inlet flow rate reactor (50% Ramp-down/up scenario - *Control Structure 2*)

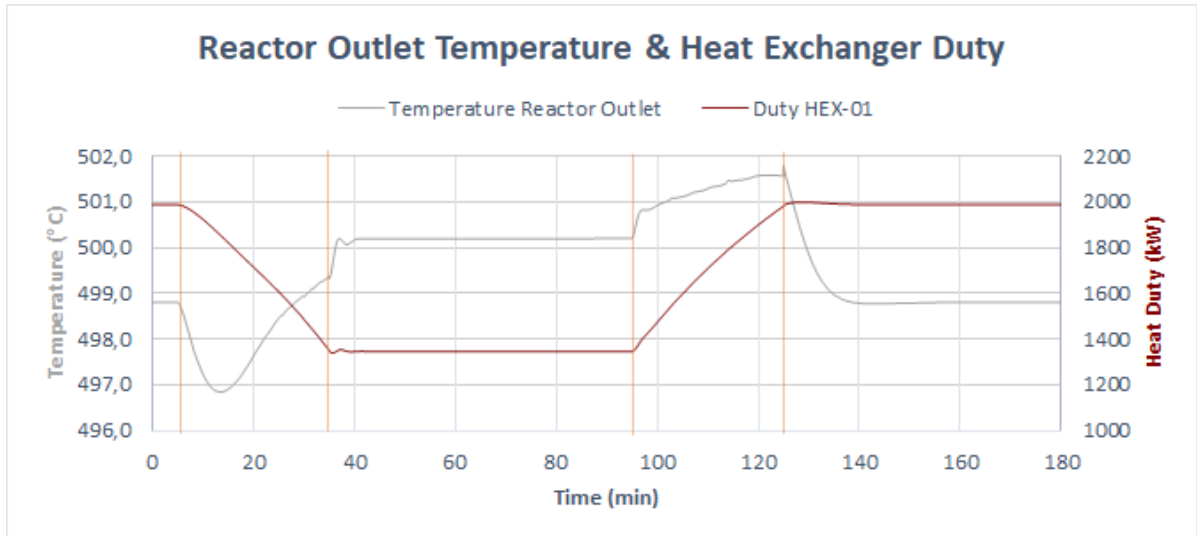


(a) H₂:N₂ Ratio

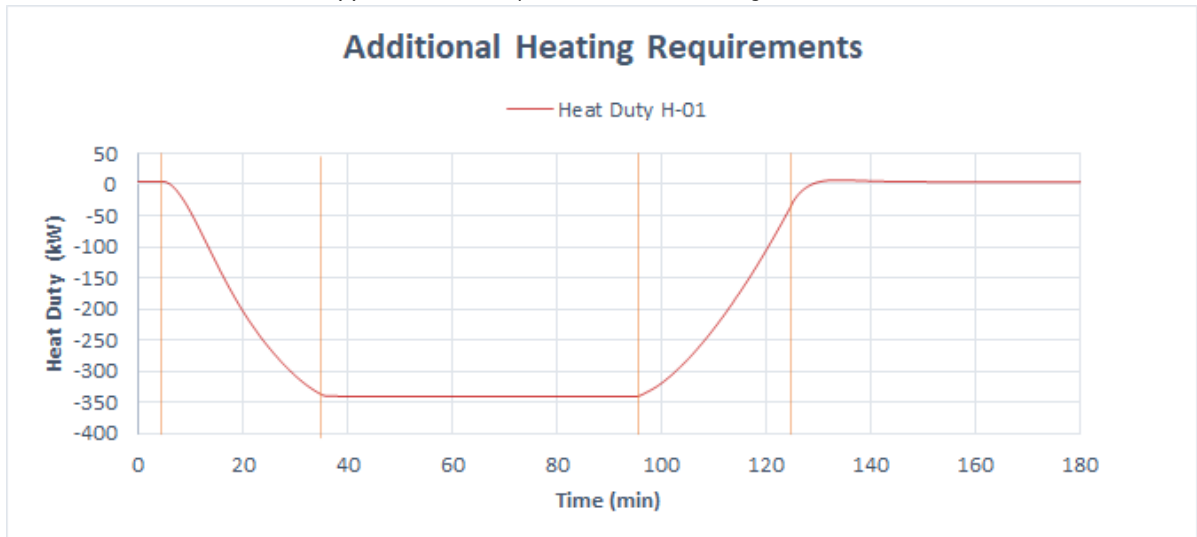


(b) Conversion vs. relative ammonia production

Figure F.10: Time series for 50% Ramp-down/up scenario - Control Structure 2



(a) Reactor outlet temperature versus heat exchanged in HEX-01



(b) Additional heat requirement provided by heater H-01

Figure F.11: Time series for 50% Ramp-down/up scenario - Control Structure 2

Bibliography

- [1] I. E. A. (IEA), *Renewable electricity growth is accelerating faster than ever worldwide, supporting the emergence of the new global energy economy*, (2021), <https://www.iea.org/news/renewable-electricity-growth-is-accelerating-faster-than-ever-worldwide-supporting-the-emergence-of-the-new-global-energy-economy> Accessed on: 20-08-2022.
- [2] I. E. A. (IEA), *Net zero by 2050: A roadmap for the global energy sector*, (2021), <https://www.iea.org/reports/net-zero-by-2050> Accessed on: 23-09-2022.
- [3] M. A. Mac Kinnon, J. Brouwer, and S. Samuelsen, *The role of natural gas and its infrastructure in mitigating greenhouse gas emissions, improving regional air quality, and renewable resource integration*, *Progress in Energy and Combustion science* **64**, 62 (2018).
- [4] S. Martinez Romero and W. Hughes, *Bringing variable renewable energy up to scale: options for grid integration using natural gas and energy storage*, (2015).
- [5] InnoEnergy, *Collaboration is key to win the race to reach net zero*, (2022), <https://tbb.innoenergy.com/collaboration-is-key-to-win-the-race-to-reach-net-zero/> Accessed on: 26-10-2022.
- [6] A. S. Strub and G. Imarisio, *Hydrogen as an Energy Vector: Proceedings of the International Seminar, Held in Brussels, 12–14 February 1980* (Springer Science & Business Media, 1980).
- [7] IRENA, *Global hydrogen trade to meet the 1.5c climate goal: Part iii – green hydrogen cost and potential*, (2022).
- [8] A. Valera Medina, S. Morris, J. Runyon, D. G. Pugh, R. Marsh, P. Beasley, and T. Hughes, *Ammonia, methane and hydrogen for gas turbines*, *Energy Procedia* **75**, 118 (2015).
- [9] S. Global, *Unpacking ammonia's market landscape and its role in the energy transition*, (2022), <https://www.spglobal.com/commodityinsights/en/market-insights/blogs/energy-transition/091622-ammonia-prices-supply-demand-hydrogen-power-bunker-fuel#article0> Accessed on: 28-09-2022.
- [10] W. Mackenzie, *What role will ammonia play in global hydrogen trade?* (2022), <https://www.woodmac.com/news/opinion/what-role-will-ammonia-play-in-global-hydrogen-trade/> Accessed on: 03-10-2022.
- [11] G. Soloveichik and U. D. of Energy, *Ammonia as virtual hydrogen carrier*, in *H2@ Scale Workshop* (2016) p. 19.
- [12] C. Makhloufi, P. Olivier, N. Kezibri, and A. Lienes, *Ammonia as hydrogen carrier to unlock the full potential of green renewables*, in *2019 AIChE Annual Meeting* (AIChE, 2019).
- [13] L. K. Boerner, *Industrial ammonia production emits more CO₂ than any other chemical-making reaction. Chemists want to change that*, *Chemical & Engineering News* **97**, 1 (2019).
- [14] I. E. A. (IEA), *Ammonia technology roadmap - towards a more sustainable nitrogen fertiliser production*, Report (2021), <https://www.iea.org/reports/ammonia-technology-roadmap> Accessed on: 08-10-2021.
- [15] D. Liu, M. Chen, X. Du, H. Ai, K. H. Lo, S. Wang, S. Chen, G. Xing, X. Wang, and H. Pan, *Development of electrocatalysts for efficient nitrogen reduction reaction under ambient condition*, *Advanced Functional Materials* **31**, 2008983 (2021).
- [16] S. Z. Andersen, V. Čolić, S. Yang, J. A. Schwalbe, A. C. Nielander, J. M. McEnaney, K. Enemark-Rasmussen, J. G. Baker, A. R. Singh, B. A. Rohr, *et al.*, *A rigorous electrochemical ammonia synthesis protocol with quantitative isotope measurements*, *Nature* **570**, 504 (2019).

- [17] K. H. Rouwenhorst, P. M. Krzywda, N. E. Benes, G. Mul, and L. Lefferts, *Ammonia*, 4. *green ammonia production*, Ullmann's Encyclopedia of Industrial Chemistry, 1 (2000).
- [18] J. S. Cardoso, V. Silva, R. C. Rocha, M. J. Hall, M. Costa, and D. Eusébio, *Ammonia as an energy vector: Current and future prospects for low-carbon fuel applications in internal combustion engines*, Journal of Cleaner Production **296**, 126562 (2021).
- [19] Y. Bennani, A. Perl, A. Patil, C. van Someren, L. Heijne, and M. van Steenis, *Power-to-Ammonia: Rethinking the role of ammonia—from a value product to a flexible energy carrier (FlexNH3)*, (2016).
- [20] P. Worldwide, *Small in japan: Decentralizing ammonia-production*, (2022), <https://www.process-worldwide.com/small-in-japan-decentralizing-ammonia-production-a-d3481965a22aa989862e7998867d8a60/> Accessed on: 12-10-2022.
- [21] R. voor Ondernemend Nederland, *Decentralized production of green ammonia*, (2015), <https://data.rvo.nl/subsidies-regelingen/projecten/decentralized-production-green-ammonia> Accessed on: 28-08-2022.
- [22] M. Pfennig, D. Böttger, B. Häckner, D. Geiger, C. Zink, A. Bisevic, and L. Jansen, *Global gis-based potential analysis and cost assessment of power-to-x fuels in 2050*, arXiv preprint arXiv:2208.14887 (2022).
- [23] A. K. Hill, C. Smith, and L. Torrente-Murciano, *Current and future role of Haber-Bosch ammonia in a carbon-free energy landscape*, Energy & Environmental Science (2020).
- [24] E. Cussler, A. McCormick, M. Reese, and M. Malmali, *Ammonia synthesis at low pressure*, JoVE (Journal of Visualized Experiments), e55691 (2017).
- [25] H. Liu, *Ammonia synthesis catalysts: innovation and practice* (World Scientific, 2013).
- [26] G. Ertl, *Surface science and catalysis—studies on the mechanism of ammonia synthesis: the ph emmett award address*, Catalysis Reviews Science and Engineering **21**, 201 (1980).
- [27] P. Emmett and J. Kummer, *Kinetics of ammonia synthesis*, Industrial & Engineering Chemistry **35**, 677 (1943).
- [28] F. Haber and G. Van Oordt, *Über die bildung von ammoniak den elementen*, Zeitschrift für anorganische Chemie **44**, 341 (1905).
- [29] A. Larson and R. Dodge, *The ammonia equilibrium*, Journal of the American Chemical Society **45**, 2918 (1923).
- [30] A. T. Larson, *The ammonia equilibrium at high pressures*, Journal of the American Chemical Society **46**, 367 (1924).
- [31] L. J. Gillespie and J. A. Beattie, *The thermodynamic treatment of chemical equilibria in systems composed of real gases. i. an approximate equation for the mass action function applied to the existing data on the haber equilibrium*, Physical review **36**, 743 (1930).
- [32] J. M. Modak, *Haber process for ammonia synthesis*, Resonance **7**, 69 (2002).
- [33] B. R. W. P. University), *Le chatelier's principle*, <https://chemed.chem.purdue.edu/genchem/topicreview/bp/ch16/lechat.php> Accessed on: 16-04-2020.
- [34] T. H. Rod, A. Logadottir, and J. K. Nørskov, *Ammonia synthesis at low temperatures*, The Journal of Chemical Physics **112**, 5343 (2000).
- [35] H. Liu, *Ammonia synthesis catalyst 100 years: Practice, enlightenment and challenge*, Chinese journal of catalysis **35**, 1619 (2014).
- [36] BASF, *History 1902-1924*, (2016), <https://www.basf.com/ca/en/who-we-are/history/1902-1924.html> Accessed on: 07-08-2020.
- [37] J. W. Erisman, M. A. Sutton, J. Galloway, Z. Klimont, and W. Winiwarer, *How a century of ammonia synthesis changed the world*, Nature Geoscience **1**, 636 (2008).

- [38] J. G. Chen, R. M. Crooks, L. C. Seefeldt, K. L. Bren, R. M. Bullock, M. Y. Darensbourg, P. L. Holland, B. Hoffman, M. J. Janik, A. K. Jones, *et al.*, *Beyond fossil fuel-driven nitrogen transformations*, *Science* **360**, eaar6611 (2018).
- [39] J. Guo and P. Chen, *Catalyst: Nh₃ as an energy carrier*, *Chem* **3**, 709 (2017).
- [40] S. Klinsrisuk, S. Tao, and J. Irvine, *Membrane reactors for ammonia production*, in *Membrane Reactors for Energy Applications and Basic Chemical Production* (Elsevier, 2015) pp. 543–563.
- [41] A. Ekejiuba, *Evaluation of the exact production quantity of nitrogen fertilizer in real-time from any particular associated gas flare volume in nigeria*, *International Journal of Applied* **7** (2017).
- [42] V. Pattabathula and J. Richardson, *Introduction to ammonia production*, *Chem. Eng. Prog* **112** (2016).
- [43] L. Group, *LAC™ linde ammonia concept*, Company brochure (2019), https://www.linde-engineering.com/en/images/40479_LE_HS_Ammonia_brochure_modified_RZ3_VIEW_tcm19-569093.pdf.
- [44] C. J. Van der Ham, M. T. Koper, and D. G. Hetterscheid, *Challenges in reduction of dinitrogen by proton and electron transfer*, *Chemical Society Reviews* **43**, 5183 (2014).
- [45] G. Ertl, *Primary steps in catalytic synthesis of ammonia*, *Journal of Vacuum Science & Technology A: Vacuum, Surfaces, and Films* **1**, 1247 (1983).
- [46] M. Appl, *Ammonia*, *Ullmann's encyclopedia of industrial Chemistry* (2000).
- [47] J. R. Jennings, *Catalytic ammonia synthesis: fundamentals and practice* (Springer Science & Business Media, 2013).
- [48] A. J. Medford, A. Vojvodic, J. S. Hummelshøj, J. Voss, F. Abild-Pedersen, F. Studt, T. Bligaard, A. Nilsson, and J. K. Nørskov, *From the Sabatier principle to a predictive theory of transition-metal heterogeneous catalysis*, *Journal of Catalysis* **328**, 36 (2015).
- [49] C. J. Jacobsen, S. Dahl, B. S. Clausen, S. Bahn, A. Logadottir, and J. K. Nørskov, *Catalyst design by interpolation in the periodic table: bimetallic ammonia synthesis catalysts*, *Journal of the American Chemical Society* **123**, 8404 (2001).
- [50] A. Logadottir, T. H. Rod, J. K. Nørskov, B. Hammer, S. Dahl, and C. Jacobsen, *The Brønsted–Evans–Polanyi relation and the volcano plot for ammonia synthesis over transition metal catalysts*, *Journal of Catalysis* **197**, 229 (2001).
- [51] J. Bronsted, *Acid and Basic Catalysis*. *Chemical Reviews* **5**, 231 (1928).
- [52] C. J. Jacobsen, *Novel class of ammonia synthesis catalysts*, *Chemical Communications* , 1057 (2000).
- [53] L. Huazhang and L. Xiaonian, *Relationship between precursor phase composition and performance of catalyst for ammonia synthesis*, *Industrial & engineering chemistry research* **36**, 335 (1997).
- [54] A. Ozaki, *Development of alkali-promoted ruthenium as a novel catalyst for ammonia synthesis*, *Accounts of Chemical Research* **14**, 16 (1981).
- [55] K.-i. Aika, H. Hori, and A. Ozaki, *Activation of nitrogen by alkali metal promoted transition metal I. Ammonia synthesis over ruthenium promoted by alkali metal*, *Journal of Catalysis* **27**, 424 (1972).
- [56] KAAPplus™, *Ammonia kaapplus™ ammonia process*, (2005), <https://halliburtoncontracts.theyesmen.org/kbr/hydroChem/fertSynGas/kaapPlusAmmoniaProcess.html>.
- [57] A. Tripodi, M. Compagnoni, E. Bahadori, and I. Rossetti, *Process simulation of ammonia synthesis over optimized ru/c catalyst and multibed fe+ ru configurations*, *Journal of Industrial and Engineering Chemistry* **66**, 176 (2018).
- [58] A. Tripodi, F. Conte, and I. Rossetti, *Process intensification for ammonia synthesis in multibed reactors with fe-wustite and ru/c catalysts*, *Industrial & Engineering Chemistry Research* **60**, 908 (2021).

- [59] M. Temkin, *Kinetics of ammonia synthesis on promoted iron catalysts*, Acta physiochim. URSS **12**, 327 (1940).
- [60] K. J. Laidler, *The development of the Arrhenius equation*, Journal of Chemical Education **61**, 494 (1984).
- [61] A. Nielsen, J. Kjaer, and B. Hansen, *Rate equation and mechanism of ammonia synthesis at industrial conditions*, Journal of Catalysis **3**, 68 (1964).
- [62] L. M. Aparicio and J. A. Dumesic, *Ammonia synthesis kinetics: surface chemistry, rate expressions, and kinetic analysis*, Topics in Catalysis **1**, 233 (1994).
- [63] K.-i. Aika, *Role of alkali promoter in ammonia synthesis over ruthenium catalysts — Effect on reaction mechanism*, Catalysis Today **286**, 14 (2017).
- [64] M. Temkin, *The kinetics of some industrial heterogeneous catalytic reactions*, in *Advances in Catalysis*, Vol. 28 (Elsevier, 1979) pp. 173–291.
- [65] A. Ozaki, H. S. Taylor, and M. Boudart, *Kinetics and mechanism of the ammonia synthesis*, Proceedings of the Royal Society of London. Series A. Mathematical and Physical Sciences **258**, 47 (1960).
- [66] D. Dyson and J. Simon, *Kinetic expression with diffusion correction for ammonia synthesis on industrial catalyst*, Industrial & engineering chemistry fundamentals **7**, 605 (1968).
- [67] G. B. Ferraris, G. Donati, F. Rejna, and S. Carra, *An investigation on kinetic models for ammonia synthesis*, Chemical engineering science **29**, 1621 (1974).
- [68] I. Rossetti, N. Pernicone, F. Ferrero, and L. Forni, *Kinetic study of ammonia synthesis on a promoted Ru/C catalyst*, Industrial & engineering chemistry research **45**, 4150 (2006).
- [69] K.-I. Aika and A. Ozaki, *Kinetics and isotope effect of ammonia synthesis over ruthenium*, Journal of Catalysis **16**, 97 (1970).
- [70] M. J. Kale, D. K. Ojha, S. Biswas, J. I. Militti, A. V. McCormick, J. H. Schott, P. J. Dauenhauer, and E. Cussler, *Optimizing ammonia separation via reactive absorption for sustainable ammonia synthesis*, ACS Applied Energy Materials **3**, 2576 (2020).
- [71] T. Vegge, R. Z. Sørensen, A. Klerke, J. S. Hummelshøj, T. Johannessen, J. K. Nørskov, and C. Christensen, *Indirect hydrogen storage in metal ammines*, in *Solid-State Hydrogen Storage* (Elsevier, 2008) pp. 533–564.
- [72] C. H. Christensen, R. Z. Sørensen, T. Johannessen, U. J. Quaade, K. Honkala, T. D. Elmøe, R. Køhler, and J. K. Nørskov, *Metal ammine complexes for hydrogen storage*, Journal of Materials Chemistry **15**, 4106 (2005).
- [73] A. Klerke, C. H. Christensen, J. K. Nørskov, and T. Vegge, *Ammonia for hydrogen storage: challenges and opportunities*, Journal of Materials Chemistry **18**, 2304 (2008).
- [74] T. Yan, Z. Kuai, and S. Wu, *Experimental investigation on a $\text{mnc}l_2\text{-srcl}_2/\text{nh}_3$ thermochemical resorption heat storage system*, Renewable Energy **147**, 874 (2020).
- [75] A. L. Ammitzbøll, S. Lysgaard, A. Klukowska, T. Vegge, and U. J. Quaade, *Surface adsorption in strontium chloride ammines*, The Journal of chemical physics **138**, 164701 (2013).
- [76] R. Iwata, T. Yamauchi, Y. Hirota, M. Aoki, and T. Shimazu, *Reaction kinetics of ammonia absorption/desorption of metal salts*, Applied thermal engineering **72**, 244 (2014).
- [77] *Ammonia - Thermophysical Properties*, The Engineering Toolbox (2008), https://www.engineeringtoolbox.com/ammonia-d_1413.html Accessed on: 20-11-2020.
- [78] S. N. Gunasekara, M. Laios, A. Karabanova, V. Martin, and D. Blanchard, *Design of a bench-scale ammonia-srcl₂ thermochemical storage system using numerical modelling*, in *Eurotherm Seminar# 112: Advances in thermal energy storage, 15-17 May 2019, University of Lleida, Spain* (2019).
- [79] S. Soprani, *Modeling-tes system based on srcl₂-nh₃*, Technical University of Denmark (DTU), Lyngby (2017).

- [80] I. Graabak and M. Korpås, *Variability characteristics of european wind and solar power resources—a review*, *Energies* **9**, 449 (2016).
- [81] A. Mills, M. Ahlstrom, M. Brower, A. Ellis, R. George, T. Hoff, B. Kroposki, C. Lenox, N. Miller, M. Milligan, *et al.*, *Dark shadows*, *IEEE Power and Energy Magazine* **9**, 33 (2011).
- [82] A. Tripodi, M. Compagnoni, R. Martinazzo, G. Ramis, and I. Rossetti, *Kinetic Modelling at the Basis of Process Simulation for Heterogeneous Catalytic Process Design*, (2017).
- [83] Dr. YA Hussain, *Thermodynamic models & physical properties*, Jordan University of Science & Technology, <https://www.just.edu.jo/~yahussain/files/Thermodynamic%20Models.pdf>.
- [84] A. D. C. Júlio, *Comparison of Chemical Process Simulators: Aspen vs. HYSYS*, Tech. Rep. (Instituto Superior Técnico, Lisboa, Portugal) :<https://fenix.tecnico.ulisboa.pt/downloadFile/395137861652/>.
- [85] Aspen Plus Ammonia Model, *Aspen plus*, (2008).
- [86] Al-Malah, Kamal IM, *Aspen plus - Chemical Engineering Applications* (Wiley Online Library, 2016).
- [87] A. J. Gunorubon and R. N. Raphael, *Simulation of an Ammonia Synthesis Converter*, *Canadian Journal of Pure and Applied Sciences* , 2913 (2014).
- [88] I. I. Cheema and U. Krewer, *Supplementary Materials: Optimisation of the Autothermal NH₃ Production Process for Power-to-Ammonia*, .
- [89] J. C. Morud and S. Skogestad, *Analysis of instability in an industrial ammonia reactor*, *AIChE Journal* **44**, 888 (1998).
- [90] M. J. Palys, A. McCormick, E. Cussler, and P. Daoutidis, *Modeling and optimal design of absorbent enhanced ammonia synthesis*, *Processes* **6**, 91 (2018).
- [91] A. Murase, H. L. Roberts, and A. O. Converse, *Optimal thermal design of an autothermal ammonia synthesis reactor*, *Industrial & Engineering Chemistry Process Design and Development* **9**, 503 (1970).
- [92] NC State University Department of Chemical Engineering, *Ammonia Case Study*, (2005), https://projects.ncsu.edu/project/actionagenda/coprotein/amcs/am_prob2.htm accessed on: 25-05-2020.
- [93] W. L. Luyben, *Design and control of a cooled ammonia reactor*, *Plantwide Control, Recent Developments and Applications*. EUA: John Wiley & Sons, Ltda (2012).
- [94] F. Haber and R. Le Rossignol, *Die Lage des Ammoniakgleichgewichtes*, *Zeitschrift für Elektrochemie und angewandte physikalische Chemie* **14**, 513 (1908).
- [95] A. Araújo and S. Skogestad, *Control structure design for the ammonia synthesis process*, *Computers & Chemical Engineering* **32**, 2920 (2008).
- [96] R. Sinnott, *Chemical engineering design*, Vol. 6 (Elsevier, 2014).
- [97] Didier Blanchard, Denmark Technical University, *Personal communication*, (September 2020).
- [98] T. S. . Contributors, *Compressor choke*, *Turbomachinery International* (2019), <https://www.turbomachinerymag.com/compressor-choke/> Accessed on: 24-11-2020.
- [99] C. for Chemical Process Safety, *Guidelines for initiating events and independent protection layers in layer of protection analysis*, (2014).
- [100] D. T. I. o. C. E. I. Cameron Milne, *Emergency depressurisation: 690 kpa or 50% in 15 minutes?* https://www.icheme.org/media/11408/h11b_thu_1155_talbert.pdf Accessed on: 05-10-2022.
- [101] *AspenTech Support Center*, Aspen (), https://esupport.aspentech.com/apex/S_Homepage.
- [102] *Getting Started with Aspen Dynamics*, Aspen ONE AspenTech (), https://aspentechsupport.blob.core.windows.net/cbt/135831%20Getting%20Started%20with%20Aspen%20Dynamics/presentation_html5.html.

